理學博士學位論文

Streptomyces coelicolor 에서 니켈에 반응하는 Nur에 의한 슈퍼옥사이드 디스뮤타제 유전자발현의 조절

Regulation of gene expression for Fe-SOD and Ni-SOD by nickel-responsive Nur in *Streptomyces coelicolor*

2014年 2月

서울大學校 大學院

生命科學部

金 慧 美

Regulation of gene expression for Fe-SOD and Ni-SOD by nickel-responsive Nur in *Streptomyces coelicolor*

by

Hae Mi Kim

under the supervision of

Professor Jung-Hye Roe, Ph.D.

A Thesis Submitted in Partial Fulfillment
of the Requirements for the Degree of
Doctor of Philosophy

February, 2014

School of Biological Sciences
Graduate School
Seoul National University

ABSTRACT

Nur (Nickel uptake regulator) is a nickel-responsive transcription factor the regulates nickel homeostasis and anti-oxidative response in *S. coelicolor.* Nur is a unique nickel-specific Fur-family regulator. In *S. coelicolor,* expression of the *sodF* and *sodN* genes is inversely regulated by Nur. Superoxide dismutases (SODs) are widely distributed enzymes that convert superoxides to hydrogen peroxide and molecular oxygen, using various metals as cofactors. Many actinobacteria contain genes for both Ni-containing (*sodN*) and Fe-containing (*sodF*) SODs. With sufficient nickel, Nur directly represses *sodF* transcription, while inducing *sodN* indirectly. Bioinformatic search revealed that a conserved 19 nt stretch upstream of *sodN* matches perfectly with the *sodF* downstream sequence. So we estimated that Nur could activates *sodN* gene through *sodF* transcripts, double repression mechanism. First we checked the existence of transcripts containing anti-*sodN* region by S1 mapping. We found that the *sodF* gene produced a stable small-sized RNA species (s-SodF) that harbors the anti-*sodN* sequence complementary to *sodN* mRNA from the 5′ end up to the ribosome binding site and s-SodF is approximately ~90 nt confirmed by northern blotting. We could not detect any Nur box in nearby 5′ end of s-SodF and s-SodF is sensitive to 5′-monophosphate-specific exonuclease. These data strongly indicated that the s-SodF RNA is a likely processed product of *sodF* mRNA. In order to check the s-SodF effect on *sodN* expression, we introduced to *ΔsodF* mutant an overexpression plasmid for s-SodF RNA whose expression was driven by a strong ermE* promoter. In *ΔsodF* mutant, half-life of *sodN* is delayed to about 16min compared to WT (3min). But, in s-SodF overexpression strain, delayed half-life of *sodN* is restored to 7min. This result indicated that the s-SodF RNA caused a significant decrease in the half-life of the *sodN* mRNA. Therefore, Nur activates *sodN* expression through inhibiting

the synthesis of *sodF* mRNA, from which inhibitory s-SodF RNA is generated. This reveals a novel mechanism by which antagonistic regulation of one gene is achieved by small RNA processed from the 3'UTR of another gene's mRNA.

Recently, we reported crystal structure of Nur and Nur is homodimer and two DNA binding domains (DB-domain) are attached to the dimeric core constructed by two dimerization domains (D-domain). It contains a unique nickel-specific metal site (Ni-site) and nonspecific common metal site (M-site) per each monomer. Nur also has two Cys-X–X Cys motif but no zinc coordination is shown in crystal structure. Electrophoretic mobility shift assay (EMSA) using Nur overexpression cell extract by PET system in *E. coli* showed that Ni-site and M-site not Cys4 site are both important for DNA binding activity of Nur. This result coincide with Crystal structure of Nur. In order to confirm the critical residues of Nur in vivo, we introduced to *⊿nur* mutant an integration vector for *pnur*::*nur* variants expression and we checked the *sodF* repression activity of Nur by S1 mapping. We found that Ni-site was still important for Nur in vivo but mutations of M-site residues could not affect repression activity of Nur. Interestingly, Cys96S, Cys133S and Cys136 which consist of two Cys-X–X Cys motif were confirmed as critical residues of Nur. So we tried to do EMSA using *S. coelicolor* cell extract and result showed that Ni-site and two Cys-X–X Cys motif not M-site are both important for Nur in vivo. This result match with S1 mapping data. These experiment suggest the possibility that Nur coordinate zinc in two Cys-X–X Cys motif and this Cys4-Zn site will be critical structural metal binding site like BsuPerR in vivo

Keywords: *Streptomyces coelicolor*, Fur, Nur, nickel, structure, metal binding site, small RNA, superoxide dismutase(SOD)

CONTENTS

LIST OF FIGURES

LIST OF TABLES

ABBREVIATIONS

bp	base pair
BSA	bovine serum albumin
DTT	dithiothreitol
EDTA	ethylenediamietetraacetate
nt	nucleotide
OD	optical density
PAGE	polyacrylamide gel electrophoresis
PCR	polymerase chain reaction
SDS	sodium dodecyl sulfate
DEPC	diethyl pyrocarbonate
EMSA	electrophoretic mobility shift assay
Fur	ferric uptake regulator
hr	hour
ICP-MS	inductively coupled plasma-mass spectrometry
IPTG	isopropyl-β-D-thiogalactopyranoside
min	minute
aa	amino acid
WT	wild type
Nur	nickel uptake regulator

CHAPTER I.

INTRODUCTION

I.1. Biology of *Streptomyces coelicolor*

Streptomycetes are the most widely studied and well-known genus of the actinomycete family and ubiquitous Gram-positive soil bacteria with a unique capacity for the production of varied and complex secondary metabolites. They are crucial in soil environment because of their broad range of metabolic processes and biotransformations. The importance of Streptomycetes to medicine results from their production of over two-thirds of naturally derived antibiotics in current use (Bentley et al. 2002).

Unusually for bacteria, Streptomycetes undergo complex multicellular developm ental life cycle. *Streptomyces* life cycle starts from germination of spore and format ion of highly branched vegetative mycelium. The hyphae are divided into mul tigenomic compartments by the infrequent formation of vegetative sept a. After a period of active growth, aerial mycelium develops from substrate myce lium on the surface of colony, and eventually differentiates into unigenomic spor es.

Streptomyces species have been the subject of genetic investigation for over 50 years, with many studies focusing on the developmental cycle and the production of secondary metabolites. Among them, *S. coelicolor* is genetically the best known representative of the genus. The complete DNA sequence of *S. coelicolor* M145 has been published recently, with others expected to follow soon (Bentley et al. 2002). The linear chromosome is 8,667,507 bp long and is predicted to contain 7,825 genes, about twice as many as typical free-living bacteria, making it the largest bacterial genome yet sequenced. The genome shows a strong emphasis on regulation, with 965 proteins (12.3%) predicted to have regulatory function. This is not only attractive feature but also for a challenging puzzle for future investigation to elucidate gene regulation in this organism.

I.2. Superoxide dismutase (SOD) system

Superoxide dismutases (SODs) are ubiquitous enzymes that catalyze conversion of superoxide to molecular oxygen and hydrogen peroxide, using catalytic metal ions. Depending on their structure and metal cofactors, three classes of SODs have been reported; Cu/Zn-SOD found in eukaryotes and some bacteria, Fe- or Mn-containing SOD present in bacteria, mitochondria, and chloroplasts, and Ni-containing SOD found in some bacteria (Fridovich 1997; Miller 2004; Perry et al. 2010; Miller 2012). They are present both in aerobes as well anaerobes, protecting and preparing cells against superoxide toxicity in the presence of O_2 (Storz and Imlay 1999). Cells usually contain more than two types of SODs in diverse combinations, whose production is regulated tightly in response to metabolic and environmental cues.

NiSOD and its encoding gene (*sodN)* were first discovered in *Streptomyces* spp. (Youn et al. 1996). The *sodN* gene was subsequently found in the genome of nearly all streptomycetes, various actinomycetes (Dupont et al. 2008; Schmidt et al. 2009), diverse marine cyanobacteria (Dufresne et al. 2003; Palenik et al. 2003; Rocap et al. 2003; Venter et al. 2004), and some distantly related proteobacteria and eukaryotic green algae (Schmidt et al. 2009). The SodN protein is processed at its N-terminal region by its cognate peptidase to produce active Ni-SOD (Eitinger 2004), which consists of homohexameric polypeptides with bound nickel at the N-terminal hook of each monomer (Barondeau et al. 2004; Wuerges et al. 2004). Bioinformatic analyses predicted the presence of NiSOD either alone in some actinobacteria and marine cyanobacteria, or in combination with FeSOD, MnSOD, or CuZnSOD (Priya et al. 2007; Dupont et al. 2008).

I.2.1. Regulation of SOD system in bacteria

In *E. coli*, where *sodA*, *sodB,* and *sodC* genes encode Mn-SOD, Fe-SOD, and Cu,Zn-

SOD, respectively, the presence of metal, oxygen, and redox-active compounds, as well as growth phase regulate their gene expression via transcriptional regulators such as Fur, Fnr, ArcA, SoxR, and RpoS (Hassan and Schrum 1994; Gort et al. 1999). Regulation of *sodA* and *sodB* genes encoding cytoplasmic SODs is intricately inter-connected by a global regulator Fur in response to iron availability. In the presence of iron, Fur represses transcription of *sodA* and small regulatory RNA RyhB that inhibits translation and stability of *sodB* RNA, allowing the production of Fe-SOD. In the absence of iron, expression of *sodA* and RyhB is induced, resulting in the production of MnSOD (Tardat and Touati 1991; Dubrac and Touati 2000; Masse and Gottesman 2002). This mode of regulation is conserved in Pseudomonads, where the inverse regulation of *sodA* and *sodB* genes in response to iron is exerted by Fur, and *sodB* is activated by Fur through inhibiting the transcription of small regulatory RNA PrrF1 and PrrF2, functional homologs of RyhB (Polack et al. 1996; Hassett et al. 1997; Wilderman et al. 2004). In *Bacillus subtilis*, production of Fe-containing proteins is activated by Fur through repressing transcription of yet another small RNA FsrA (Gaballa et al. 2008). These examples support the presence of an evolutionarily robust regulatory circuit mediated by an iron-specific regulator Fur and small RNAs in coordinated synthesis of iron-requiring proteins across distantly related bacteria.

I.3. Bacterial Metalloregulators

There are currently seven major families of metal-sensing transcriptional regulators that have been identified in prokaryotes (Giedroc and Arunkumar 2007) (Fig. I-1). These seven sensor families span the detection of the six primary biologically essential first row transition elements Mn, Fe, Co, Ni, Cu and Zn, as well as heavymetals Ag/Au and Cd/Hg, respectively (Giedroc and Arunkumar 2007). In addition, ArsR and MerR family sensors have been identified the Pb as

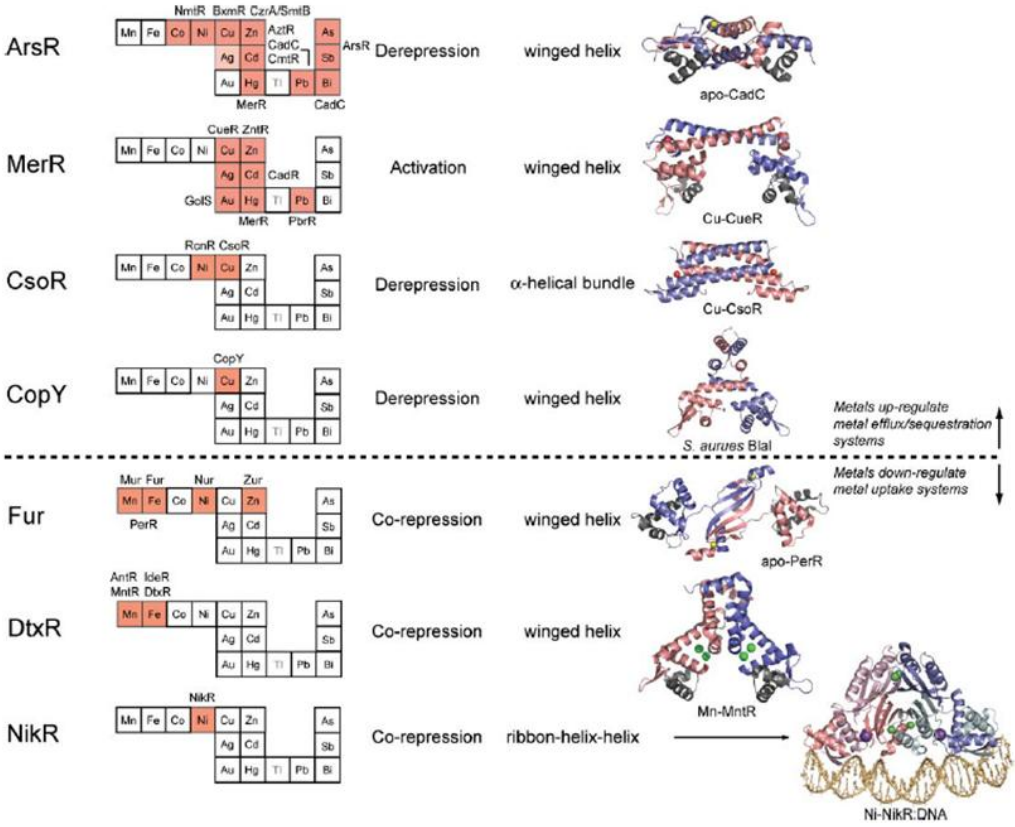

Fig. I-1. Structural families of metal sensor proteins

Metals sensed in each case are shaded red, with individual metal sensor proteins that sense the particular metal(s) indicated. The mechanism of gene expression is indicated as is the structural unit that mediates operator–promoter DNA binding. Ribbon representations of selected representative members are shown with individual protomers shaded *red* and *blue*.

well as As/Sb and Bi. Metal sensor families regulate metal import, efflux, storage and detoxification. The direct binding of a specific metal to a repressor either allosterically inhibits DNA binding, leading to de-repression of regulated genes (ArsR, CsoR and CopY), or allosterically activates transcription initiation by RNA polymerase by remodeling the promoter structure (MerR) (Giedroc and Arunkumar 2007) (Fig. I-1). On the other hand, the Fur, DtxR and NikR families turn down the expression of uptake systems in response to metal excess (Fig. I-1).

I.3.1. Fur family regulators

Fur (Fe uptake regulator) was first characterized as an iron-responsive repressor of iron-transport systems in *Escherichia coli* (Hantke 1981; Bagg and Neilands 1987b; Bagg and Neilands 1987a). The studies of the *E. coli* Fur and its role have been summarized in several reviews (Bagg and Neilands 1987b; Bagg and Neilands 1987a; Escolar et al. 1998; Hantke 2001; Braun 2003). Together, these studies led to a clear and compelling model for Fur mediated repression of target genes under iron-replete conditions. This regulation model posits that the coordination of one Fe^{2+} per monomer enables the dimeric Fur protein to bind a specific 19 bp DNA sequence, called the "Fur box", within the promoter of the regulated genes. The affinity of Fur protein for Fe^{2+} is poised to allow accumulation of sufficient intracellular Fe to activate essential iron-containing and iron-utilizing enzymes (e.g. enzymes for heme and Fe-S cluster synthesis). However, when iron levels exceed those needed for metalloenzyme function, Fur protein represses further uptake and thereby helps prevent iron overload. Typically, the binding of iron-loaded Fur hinders the access of RNA polymerase resulting in the repression of downstream genes. Numerous studies support the validity of this general model and it likely accounts for a significant fraction of the iron-dependent regulation effected by Fur. On the other hand, Fur upregulates those genes that encode proteins with iron-binding capacity

(bacterioferritin, superoxide dismutases, fumarase, etc.) by repressing transcription of small RNAs that inhibit the expression of these genes (Masse and Gottesman 2002). Recent results indicate the regulation by Fur, and Fur-like proteins, can be much more complex (Lee and Helmann 2007).

Fur family members show an extraordinary diversity in sensing different type of metals (Fe, Zn, Mn, Ni, and Heme-Fe) in addition to controlling a wide range of regulated genes (Fig. I-2). Current knowledge on Fur subfamilies, in terms of selective metals, gene regulatory role, and representative functions of their target genes, is summarized in extreme simplicity in Fig. I-2 (Storz and Hengge 2011).

I.3.2. Structural features of Fur family members

Cystal structures of several Fur family regulators were reported. The first, publication of the crystal structure of *Pseudomonas aeruginosa* (Fur_{PA}) solved in complex with Zn^{2+} provided the first detailed view of the metal-binding sites in a Fur protein (Pohl et al. 2003). The basic fold of the protein consists of two domains: an N-terminal DNA-binding domain and a C-terminal dimerization domain (Fig. I-3A). The structure of PA-Fur clearly identifies two metal-binding sites (Fig. I-3B and C.). Site 1 is located in the dimerization domain and the Zn^{2+} ion is coordinated by the side chains of His86, Asp88, Glu107, His124, and by a water molecule showing a distorted octahedral geometry. Site 2 connects the DNA-binding domain and the dimerization domain, and comprises the side chains of His32, Glu80, His89, and Glu100 in a tetrahedral geometry. Fe^{2+} exchange experiments followed by XAS suggested that the Zn^{2+} ion at site 1, but not at site 2, is readily exchanged by Fe^{2+}. This led to the assignment of site 1 as the regulatory metal binding site and site 2 as a structural Zn^{2+}-binding site (Pohl et al. 2003).

The second, crystal structure of apo-PerR-Zn protein from *Bacillus subtilis* was resolved in 2006 (Traore et al. 2006). This crystal structure was built as oxidized

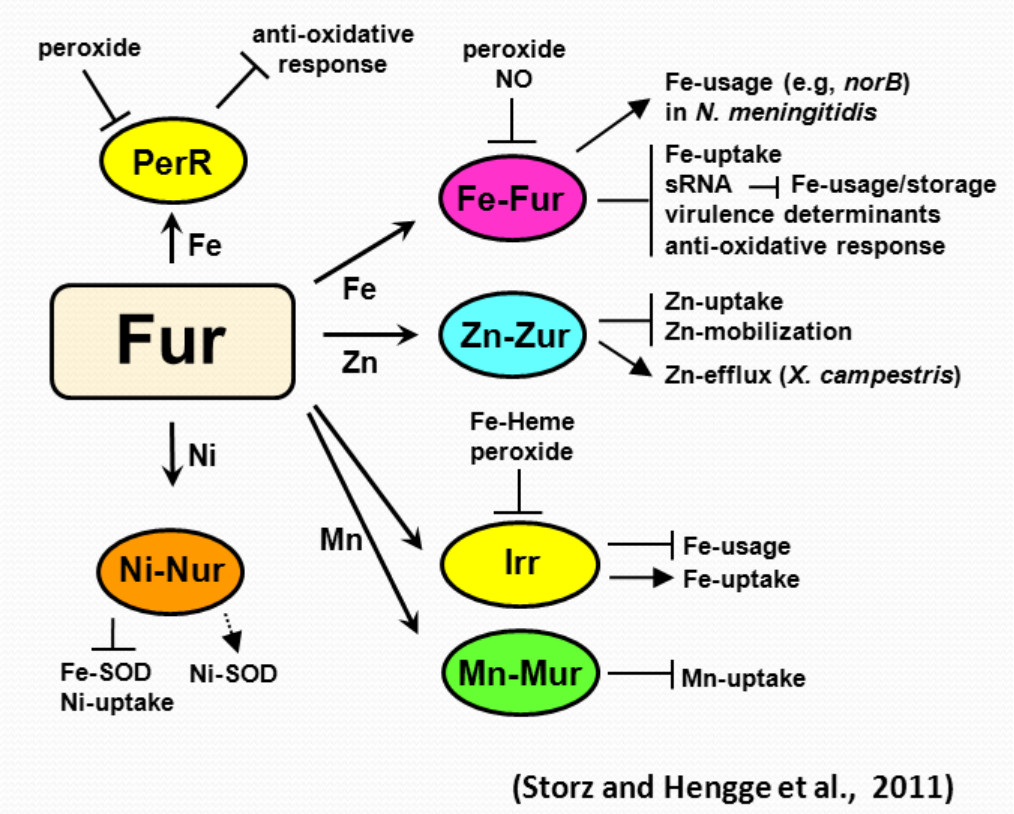

Fig. I-2. Diversity of Fur subfamilies.

Specialized Fur subfamilies with respect to their activity modulators (specific metals, peroxide, heme, etc.) are presented with representative gene functions they regulate and mode of regulation

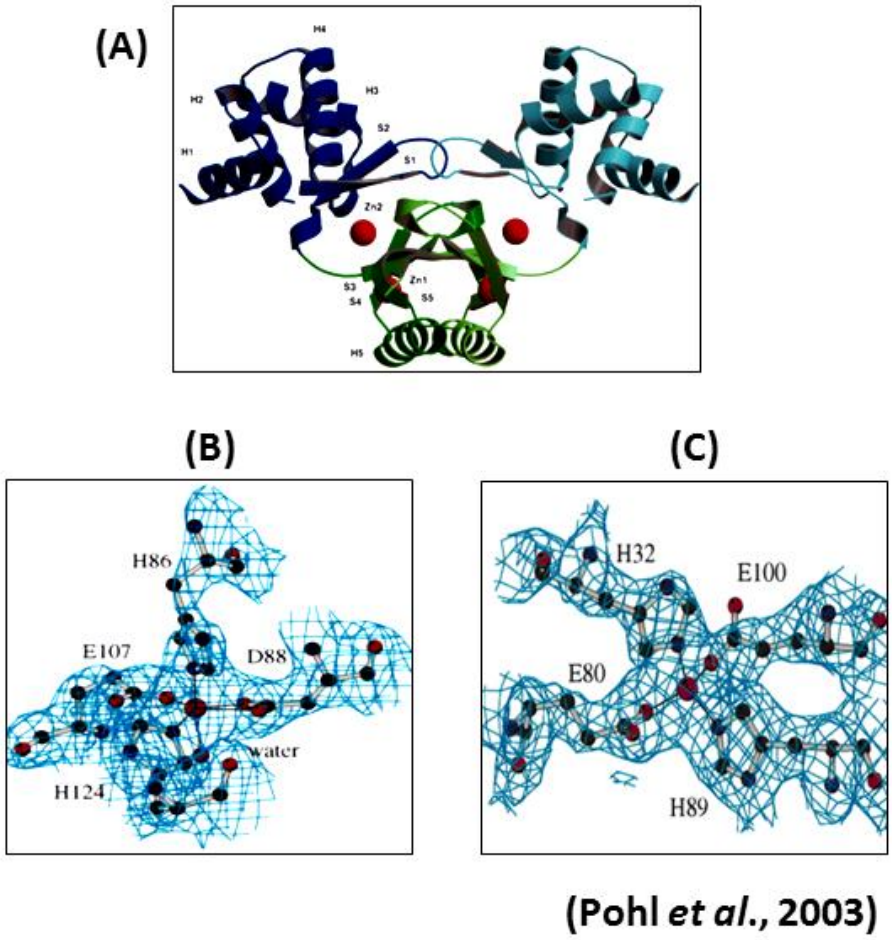

Fig. I-3. Ribbon diagram of the crystal structure of the PA-Fur dimer with secondary structural elements.

A. The view shown is approximately perpendicular to the crystallographic twofold axis. The DNA-binding domains are depicted in blue and the dimerization domain in green. The symmetry-related second monomer is shown in light blue and green. **B**. Stereoview of the experimental electron density of the Zn binding site 1. **C**. Stereoview of the Zn binding site 2.

apo-PerR which containing the one zinc ion per monomer. And then, metal binding sites and structure of the *B. subtilis* Fur paralog, PerR were analyzed with in vivo experiments (Lee and Helmann 2006). Like other Fur family members, PerR contains two metal binding sites per monomer (Herbig and Helmann 2001): one site binds Zn (II); 4 Cys (C96, 99, 136, and 139) and may play a largely structural role, whereas the second site binds a regulatory metal (H37, D85, H91, H93, and D104) and among the residues, H37 and H91 play a role for H_2O_2-mediated oxidation (Fig. I-4). Purified PerR contains both zinc and iron and can be readily dissociated from DNA by low levels of H_2O_2. The addition of Mn (II), which binds competitively with Fe(II), yields a form of the protein that is not readily dissociated from DNA by peroxide (Herbig and Helmann 2001). Together, these results suggest that PerR in the ferrous form may mediate most peroxide induction.

The other resolved crystal structure is FurB (Zur) protein of *Mycobacterium tuberculosis*. *M. tuberculosis* FurB is Zn (II)-dependent and is likely to control genes involved in the bacterial zinc uptake (Lucarelli et al. 2007). Interestingly, FurB protein has three zinc binding sites; site I (Asp 62, Cys 76, His 81, and His 83), site II-4Cys (Cys 86, 89, 126, and 129), and site III (His 80, 82, 118, and Glu 101) (Fig. I-5). As a result, according to the preceding crystal structures of *Pseudomonas aeruginosa* Fur (*Pa*Fur), PA-Fur has two zinc ions (Fig. I-3), *Bs*PerR with the regulatory metal site empty (Traore et al. 2006) and *Mycobacterium tuberculosis* FurB (*Mt*FurB) with three zinc ions (Fig. I-5), the Fur family members are homodimer and each monomer consists of an N-terminal DNA-binding domain (DB-domain), a C-terminal dimerization domain (D-domain), and a hinge region between the two domains. According to the structural comparison between *Pa*Fur and apo-*Bs*PerR, which represent the DNA-binding competent and the DNA-binding incompetent conformations, respectively, DB-domain seems to swing around the hinge region with respect to D-domain on metal association

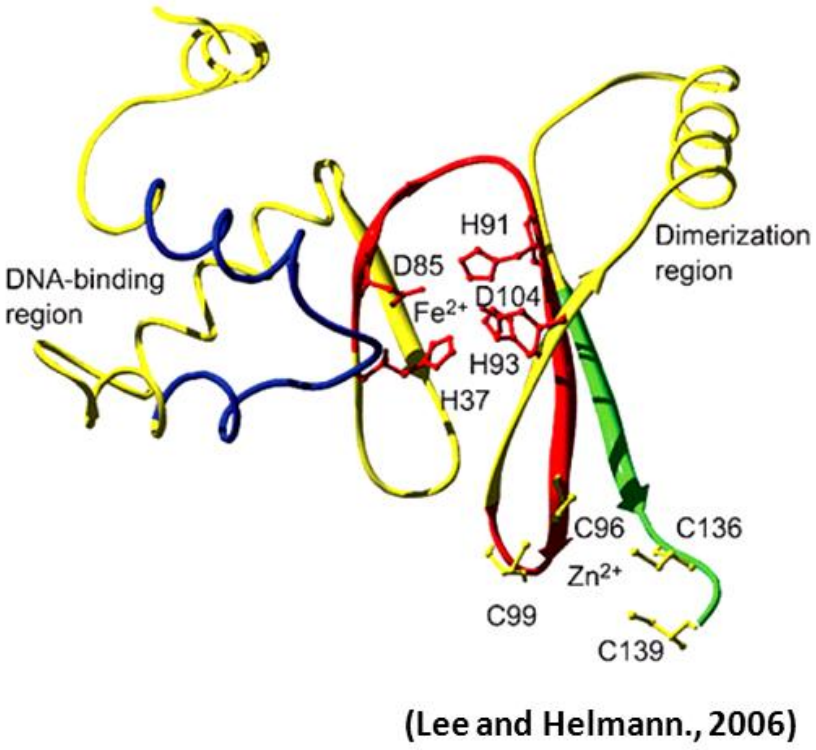

Fig. I-4. PerR contains two metal-binding sites.

A monomer of PerR was modeled on the *Pseudomonas aeruginosa* Fur (FurPA) structure using SwissModel. Candidate amino acid ligands for Fe^{2+} (red) and Zn^{2+} (yellow) are conserved in PerR family members. The sites of H_2O_2-mediated oxidation (H37 and H91) are in tryptic peptides 1 (T1, shown in blue) and 2 (T2, red) and are positioned to bind Fe^{2+} (corresponding to FurPA metal site 2). The four cysteine residues are in peptides T2 (red) and T3 (green) (Lee and Helmann., 2006).

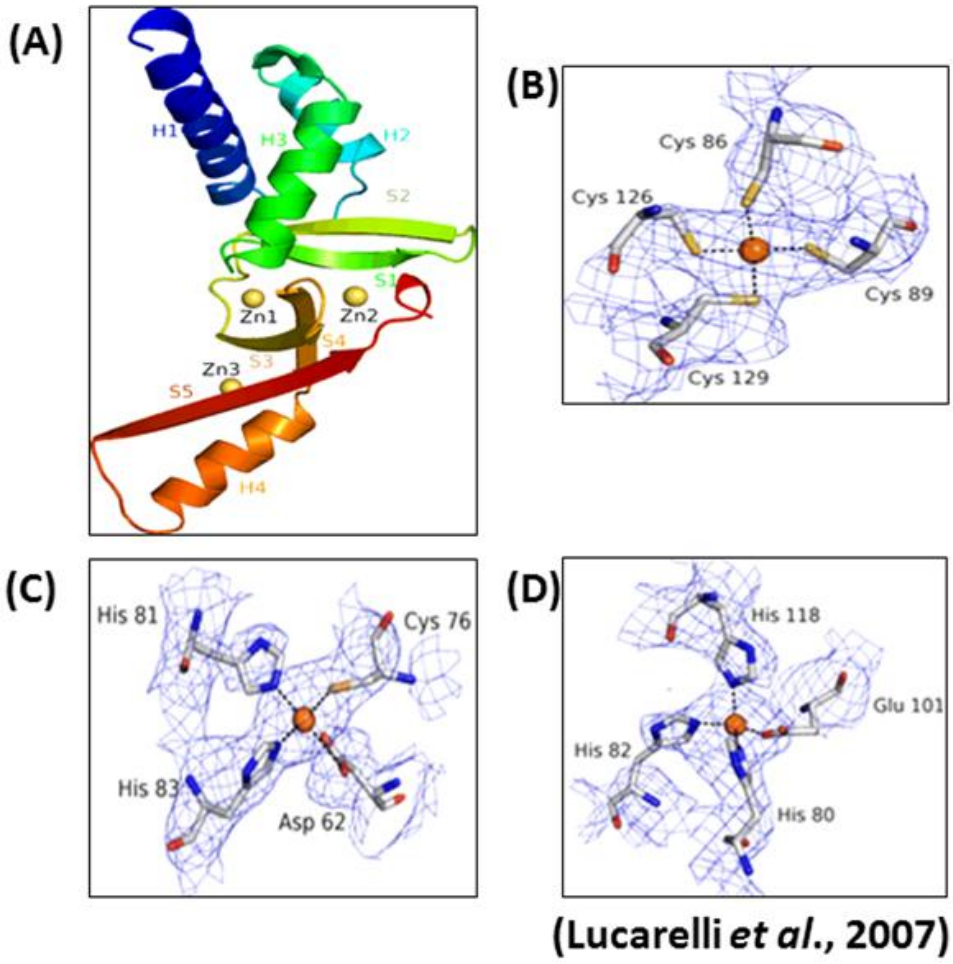

Fig. I-5. Ribbon diagram of the *M. tuberculosis* FurB monomer with secondary structural elements annotated.

A. The metal sites are shown as *yellow spheres*. The DNA binding domain is shown with colors changing from the N terminus in *blue* to *green*, and the dimerization domain from *yellow* to the C terminus in *red*. **B**. Stereoview of the zinc site 1. **C**. The zinc site 2. **D**. The zinc site 3 (Lucarelli *et al*., 2007).

(Traore et al. 2006).

I.4. Role and regulation of Nickel

Nickel is the 24th abundant element in earth crust (Hausinger 1993). Since the discovery of nickel-dependent growth of *Ralstonia* (formerly *Hydrogenomonas* or *Alcaligenes*, (Bartha and Ordal 1965), studies on the role of nickel in living organisms have expanded. In addition, nickel was found to enhance the microbial fixation of dinitrogen into biological material. At physiological concentrations in the cell, nickel serves as an essential cofactor for several microbial and plant enzymes (Mulrooney and Hausinger 2003). When in excess, it is toxic to cells by generating reactive oxygen species (Stohs and Bagchi 1995), and acts as a potent human carcinogen (Denkhaus and Salnikow 2002). Therefore, it is critical for cells to keep homeostatic control of its level through sensing and transport systems, and to maintain protective measures against its potentially harmful effects.

The best-characterized ABC-type transporter for nickel is that found in *E. coli*. This multicomponent system consists of five proteins, NikABCDE, that carry out the ATP-dependent transport of nickel (Navarro et al. 1993). NikA is a soluble, periplasmic, Ni-binding protein; NikB and NikC form a transmembrane pore for passage of nickel; and NikD and NikE hydrolyze ATP and couple this energy to nickel transport. Nickel represses expression of the *nik* operon, therefore blocking the entrance of metal ion by the high-affinity nickel transport system. A nickel responsive protein encoded by *nikR* gene located downstream of *nikE* is responsible for this regulation.

I.5. Nur in *S. coelicolor*

In *S. coelicolor*, where Fe-SOD and Ni-SOD are present, the two enzymes are

produced in an antagonistic fashion in response to the presence of nickel in the media (Kim et al. 1998a; Kim et al. 1998b). Recently, a nickel-uptake regulator (Nur) was discovered in *S. coelicolor* as a nickel responsive member to the Fur family (Ahn et al. 2006). Expression of the *sodF* gene encoding Fe-SOD is inhibited by nickel through a nickel-specific Fur-family regulator Nur that binds to and inhibits expression from the *sodF* promoter in the presence of nickel (Kim et al. 1998a; Ahn et al. 2006; An et al. 2009) (Fig. I-6). Nur also negatively regulates nickel-uptake genes (*nikA*), justifying its name as nickel-uptake-regulator (Ahn et al. 2006) (Fig. I-7). On the other hand, expression of the *sodN* gene requires Nur as a positive regulator in the presence of nickel (Ahn et al. 2006) (Fig. I-6). However, Nur does not bind to the *sodN* gene, most likely acting via an indirect way that needs to be revealed (Chung et al. 1999a; Ahn et al. 2006).

I.6. Small regulatory RNAs in bacteria

Study on the discovery and investigation of small regulatory RNAs in bacteria has exploded recently. Small regulatory RNAs in bacteria can be divided into several group depending on their form and regulation mechanism.

Riboswitches is the leader sequences of 5′ UTR in mRNA and small molecules like metabolites can bind to that sequences. These binding cause conformational change of riboswitches and result in repression of transcription or translation in general. Commonly, the riboswitches in Gram-negative bacteria inhibit translation, whereas the riboswitches in Gram-positive bacteria cause transcriptional attenuation (Nudler and Mironov 2004).

Some sRNAs can modulate protein activity and these type of sRNAs have binding activity of certain protein. For example, 6S RNA in bacteria mediates cellular response to environmental stress in *Escherichia coli* in nutrients-limited condition. This highly conserved RNA can form stable complex with the s70-

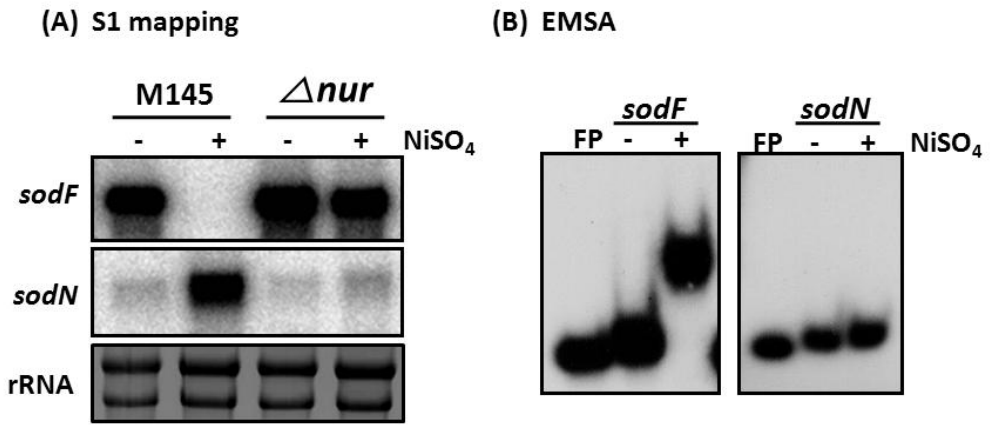

Fig. I-6. Inverse regulation of *sodF* and *sodN* by Nur in *S.coelicolor*

(A) Expression of *sod* genes in wild type and *⊿nur* mutant. *S.coelicolor* cells were grown in YEME medium including either 50uM $NiSO_4$ or not. Cells were harvested and their RNAs were analysed by S1 mapping with 5′ end-labelled probe. (B) Nickel specific binding of purified Nur to *sodF* promoter not *sodN* promoter. Purified Nur proteins were incubated with *sodF* and *sodN* promoter in the presence of 100uM $NiSO_4$.

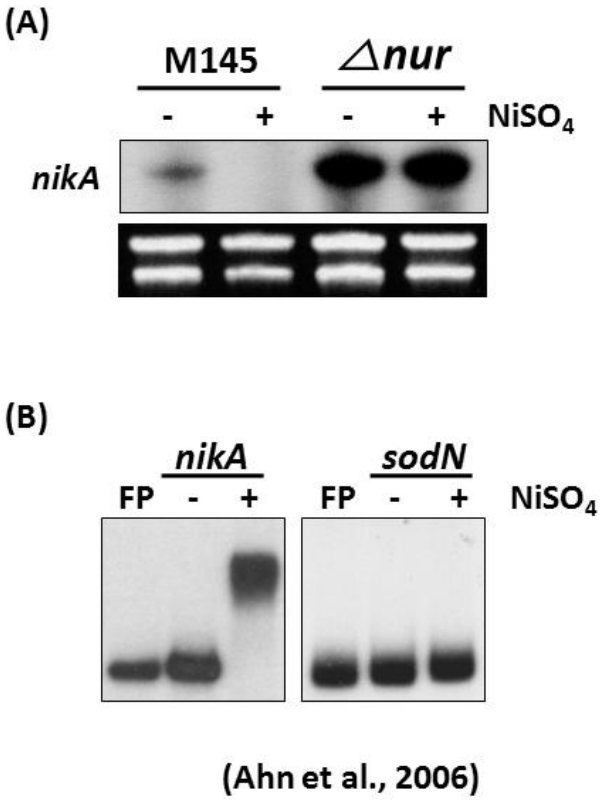

Fig. I-7. Nur-dependent expression of *nikA*

(A) Repression of *nikA* transcription by Nur. RNAs from the wild type and *Δnur* mutant grown in YEME with or without 50 μM $NiSO_4$ were analyzed for *nikA* transcripts by S1 mapping. rRNA of each sample was presented as a control of total amount of RNA. (B) Gel mobility shift assay with *nikA* promoter DNA and Nur protein in the presence or absence of 100 μM $NiSO_4$ in the binding buffer. *sodN* promoter DNA was used as a negative control. FP: free probe.

containing form of RNAP (Es70), inhibiting transcription at many, although not all, s70-dependent promoters (Wassarman and Saecker 2006).

Cis-encoded base pairing sRNAs are produced on the DNA strand opposite the target RNA and share large and perfect complementarity with their target. This type of sRNAs are mostly expressed from plasmid, bacteriophage and transposon to maintain appropriate copy number in cell and some sRNAs acts as antitoxin to repress the expression of toxin molecules.

Trans-encoded base pairing sRNAs are major group of small regulatory RNAs in bacteria. This type of sRNAs has limited complementarity (10-25nt) with their target mRNA, so single sRNA regulates multiple mRNA targets. Generally, these sRNAs regulate mRNA stability by recruiting RNase and repress translation by blocking ribosome binding site.

CRISPR(Clustered Regularly Interspaced Short Palindromic Repeats) RNAs are produced from CRISPR system. CRISPR are found in the genomes of approximately 40% of sequenced bacteria and 90% of sequenced archaea and is a prokaryotic immune system which confers resistance to foreign genetic elements such as plasmids and phages. Processed foreign DNA fragment by CAS protein are incorporated into CRISPR locus and then crRNA containing foreign genetic sequence are produced. Ths crRNA-CAS protein complex binds to foreign DNA target and causes the degradation of the foreign DNA.

I.6.1. In Hfq-containg bacteria

Accumulating lists of small non-coding RNAs have been shown to play a variety of regulatory roles (Waters and Storz 2009; Storz et al. 2011). In many cases, especially in Gram-negative bacteria, these sRNAs function in association with the RNA-binding modulator Hfq to control expression of single to multiple genes, showing a broad range of specificity. The RNA chaperone Hfq is required for trans-encoded sRNA-mediated regulation, to help RNA-RNA interactions due to

limited complementarity between the sRNA and target mRNA (Aiba 2007; Brennan and Link 2007). The hexameric Hfq ring is homologous to Sm and Sm-like proteins involved in splicing and mRNA decay in eukaryotes and it may remodel the RNAs to melt inhibitory secondary structures (Waters and Storz 2009). Hfq also may serve as a platform to allow sRNAs and mRNAs to sample potential complementarity, effectively increasing the local concentrations of sRNAs and mRNAs (Waters and Storz 2009).

Beyond halping base pairing, Hfq contributes to sRNA regulation through modulating sRNA levels (Aiba 2007; Brennan and Link 2007). Somewhat counterintuitively, most *E. coli* sRNAs are unstable in the absence of Hfq, presumably because Hfq protects sRNAs from degradation in the absence of base pairing with mRNAs (Waters and Storz 2009). Once base paired with target mRNAs, many of the known sRNA-mRNA pairs are degraded by RNase E, and Hfq may also serve to recruit RNA degradation machinery through its interactions with RNase E and other components of the degradosome (Waters and Storz 2009).

I.6.2. In Actinobacteria with no Hfq homologs

Actinomycetes, Gram-positive bacteria with high GC content, along with cyanobacteria and deinococci, do not contain any apparent Hfq-homologues (Sun et al. 2002; Swiercz et al. 2008). Quite a number of small RNAs have been identified in actinomycetes, primarily in streptomycetes and mycobacteria, through bioinformatics combined with experimental verifications, cloning of isolated small RNAs, and genome-scale deep sequencing of RNA (Panek et al. 2008; Swiercz et al. 2008; Tezuka et al. 2009; Vockenhuber et al. 2011; Moody et al. 2013). Even though some correlation with growth phases and differentiation have been demonstrated, direct targets and physiological functions of small RNAs from actinomycetes have been identified only in a very limited number of

examples (Vockenhuber et al. 2011; Vockenhuber and Suess 2012). This reflects difficulties not only in identifying functional small regulatory RNAs but also in predicting and/or validating their physiological targets in bacteria with genomes of high GC content.

In *S. coelicolor* an example has been reported for the interaction of a trans-acting small RNA (scr5239) and its target (*dagA* mRNA encoding an agarase), where a base-pairing was suggested to involve a 17 nt-long near-perfect match with a bulge of one nt (Vockenhuber and Suess 2012). For RNAs with GC content of >75%, strict base pairing between sRNA and mRNA may be required to compete with prevalent intra-molecular secondary structures with low ΔG values. The search for relatively long complementary sequence stretches in the genome may increase the possibility of identifying possible interacting partners of sRNAs.

I.7. RNA processing

Most small non-coding RNAs identified so far are transcribed as independent units from their own promoter to the terminator (Sharma and Vogel 2009; Waters and Storz 2009). In some cases, the transcribed small RNA undergoes further processing to result in a more stable and/or functional form (Davis and Waldor 2007; Papenfort et al. 2009). Recently, deep sequencing of Hfq-bound small RNAs in *Salmonella* revealed that a significant proportion of them are produced from the 3′ UTR (downstream of the coding region) of a transcribed gene (Chao et al. 2012). This raised the possibility of finding sRNAs which are transcribed in parallel with the mRNA downstream of the coding region, or are processed from existing mRNA. In one characterized example in *Salmonella*, DapZ was found to be transcribed from its own promoter located downstream of the coding region of *dapB* which encodes a lysine biosynthetic enzyme (Chao et al. 2012). DapZ small RNA expression is independent of *dapB* expression, and it acts to translate

at least two mRNAs encoding ABC transporters. A few sRNAs were suggested to be processed from existing mRNAs, based on the lack of promoters and the presence of 5′ monophosphate ends. However, all the cleavages sites occurred in the coding region, making the parental mRNAs inactive (Chao et al. 2012).

CHAPTER II.

MATERIALS AND METHODS

II.1. Strains and growth conditions

II.1.1. *Streptomyces coelicolor*

Streptomyces coelicolor A3(2) M145 strain and its derivatives were grown and maintained according to standard procedures (Kieser 2000). For liquid culture, YEME medium (0.3% yeast extract, 0.3% malt extract, 0.5% peptone, 1% glucose, 10 or 34% sucrose, 5 mM $MgCl_2$ separately autoclaved) was used. For nickel treatment, 50 μM $NiSO_4$ was added to the culture when inoculating seed culture. For surface culture, NA (nutrient agar plate; 8 % nutrient broth, 2.2 % agar) was used. The *Δnur, ΔsodF* and *ΔsodF2* strains had been previously generated in our laboratory (Chung et al. 1999b; Ahn et al. 2006; Han 2007).

II.1.2. *Escherichia coli*

E. coli strain DH5α was routinely used for manipulation of DNA. For overexpression of recombinant proteins using T7 polymerase-based system, *E. coli* BL21(DE3)pLysS was used according to the manufacturer's recommendations (Novagen). To gain methylation-negative DNA, *E. coli* ET12567 (*dam dcm hsdS*; (MacNeil et al. 1992)) was used, and for direct transformation of *S. coelicolor*, DNA was introduced into *E. coli* ET12567 harboring pUZ8002 (lab collection) to supply the donor (*trans*-) function when having a compatible *oriT*-containing plasmid. *E. coli* BW25113 (Datsenko and Wanner 2000) was used to propagate the recombination plasmid pIJ790 and *S. coelicolor* cosmids (Redenbach et al. 1996). *E. coli* strains were grown at 37 ℃ in LB (1% tryptone, 0.5% yeast extract, 1% NaCl) or SOB (2 % tryptone, 0.5 % yeast extract, 0.05% NaCl, 2.5mM KCl) containing 20 mM MgSO4 under aeration at 37℃ or 30℃. Carbenicillin (Carb, 100ug/ml), apramycin (Apr, 50ug/ml), chloramphenicol (Cm, 25 ug/ml), or kanamycin (Kan, 50ug/ml) were added to growth media when required. L-arabinose (10mM final concentration) was

added as indicated to SOB medium to induce genes under control of the pBAD promoter (Datsenko and Wanner 2000).

II.2. DNA manipulations

Purification of plasmid DNA from *E. coli*, digestion with restriction enzymes, gel electrophoresis, ligation, and transformation of *E. coli* competent cells were carried out as described previously (Joseph Sambrook 2001). Purification of genomic or plasmid DNA from *S. coelicolor* were done following the method described by (Kieser 2000).

II.3. Polymerase Chain Reaction (PCR)

Each 100μL reaction mixture contained the followings; 1×Taq polymerase reaction buffer, 150 μM MgCl2, 200 μM dNTP, 500 nM each of 5′ and 3′ primers, 100 ng of template DNA, and 5 U of *Taq* polymerase. Reaction was done in thermal cycler (Thermo) by denaturing at 94 ℃, annealing at different temperature for different samples, and extending at 72 ℃ and cycle is 26-30 cycle.

II.4. Construction of *sodF* transcript overproducing strain

The *sodF* whole fragment (from -680 to +142 relative to the end of the *sodF* stop codon) and *sodF* downstream fragment (from +10 to +142 nt from the end of the *sodF* stop codon) were generated from M145 chromosomal DNA by PCR using primer pairs as described in Table II-1. The PCR products were fused by overlapping PCR to another 240 bp PCR-generated fragment containing the strong *ermE** promoter (Bibb et al. 1985). 1086bp for *sodF* whole fragment and 399 bp for *sodF* downstream fragment final PCR product were cut with EcoRI/XbaI

Table II-1. Oligonucleotides used in this study

Primer / Probe name	Sequence (5' - 3')	Description
nur forward	GACTCGTCATATGGTGAGCACCGA	forward primer for *nur* ORF fragment
nur reverse	CATAGCCGGATCCTACGACTCGCT	reverse primer for *nur* ORF fragment
ermE*p-EcoR1_F	GTAAAACGACGGCCAGTGAATTCGAGCTCGGTACCAGCCCGACCCGAGCA	forward primer for ermE* promoter fragment
sodF-ermE*p_R	CGGCCTCTTATTGCAAAAGCCTTGCGTCAGATCCTCCCCGCACCTCTCGC	*sodF*-ermE* fused primer for overlapping PCR
s-SodF-ermE*p_R	GAAGACGATCACGAGGCGGGACGACGTCAGATCCTCCCCGCACCTCTCGC	s-SodF-ermE* fused primer for overlapping PCR
ermE*-*sodF* STOP -680_F	GCGAGAGGTGCGGGGAGGATCTGACGCAAGGCTTTTGCAATAAGAGGCCG	ermE*-*sodF* fused primer for overlapping PCR
ermE*-s-SodF STOP +10_F	GCGAGAGGTGCGGGGAGGATCTGACGTCGTCCCGCCTCGTGATCGTCTTC	ermE*-s-SodF fused primer for overlapping PCR
sodF STOP+142-XbaI_R	TCTACGAGATCAAGCGGACCCTCTAGAAGGGCCCGGACTTCAGCAACCTG	reverse primer for sodF overlapping PCR
sodN S1_F	CTCGGTCTCCTGCGACAGTTGCTC	forward primer for *sodN* S1 probe
sodN S1_R	CATCTTCTCCTGGACGGCCTTCAC	reverse primer for *sodN* S1 probe
sodF STOP-140_F	AGCACGCCTTCTACCTGC	forward primer for construction of pGEM-sodF200
sodF STOP+60_R	CATTCCGCCCGCCCGGTGAAGG	reverse primer for construction of pGEM-sodF200 and S1 probe to detect *sodF* and s-sodF
sodF STOP-205_F	GATCTACGACCACCAGGGCAAC	forward primer for construction of pGEM-sodF346
sodF STOP+78_R	CCTCGCGGGGGCCTTCCTCA	reverse primer for construction of pGEM-sodF346 and 5' end mapping of s-SodF
sodF 5' RACE	GTTGATCGAGCCCCACGTCT	*sodF* gene specific primer for 5' RACE
sodN 5' RACE	CTGCTCCTTGATGACCGTGG	*sodN* gene specific primer for 5' RACE
5' RACE Outer Primer	GCTGATGGCGATGAATGAACACTG	adaptor specific primer for 5' RACE outer PCR
5' RACE Inner Primer	CGCGGATCCGAACACTGCGTTTGCTGGCTTTGATG	adaptor specific primer for 5' RACE inner PCR
s-SodF_22nt	GTTGAGAAGACGATCACGAGGC	Northern probe to detect s-sodF
anti-*sodN*_V1_F	CCCGCCTCGTGATCGTACCACACACCTTCACCGGGCGGG	forward primer for V1 variant
anti-*sodN*_V1_R	CCCGCCCGGTGAAGGTGTGTGGTACGATCACGAGGCGGG	reverse primer for V1 variant
anti-*sodN*_V2_F	TCGTCCCGCCTCGCTCCATCCTTCTCAACCTTC	forward primer for V2 variant
anti-*sodN*_V2_R	GAAGGTTGAGAAGGATGGAGCGAGGCGGGACGA	reverse primer for V2 variant
anti-*sodN*_V3_F	TGACGTCGTCCCGAACATTGATCGTCTTCTC	forward primer for V3 variant
anti-*sodN*_V3_R	GAGAAGACGATCAATGTTCGGGACGACGTCA	reverse primer for V3 variant

restriction enzymes and were cloned into pSET162, an integration vector containing thiostrepton marker (Kim et al. 2009). The recombinant plasmids were confirmed by nucleotide sequencing and were then transformed into the *ΔsodF* strain. As a negative control, the parental vector pSET162 was introduced to *ΔsodF* in parallel.

II.5. RNA analysis

II.5.1. S1 mapping and northern analyses

RNAs were isolated from wild type (M145) and various mutant cells grown in YEME to OD_{600} of 0.2 to 1.5. Harvested cells were disrupted in modified Kirby mixture (Kieser 2000) using an ultrasonicator with a microtip at 20% of the maximum amplitude (600 W, 20 kHz). Following extraction with phenol/chloroform, the supernatant was precipitated with isopropanol. The RNA pellet was dissolved in DEPC-treated distilled water and quantified by measuring its absorbance at 260 nm. To visualize rRNAs and check for contamination by genomic DNA, RNA samples (10 μg each) were electrophoresed in 1.3 % agarose gel in MOPS buffer. For S1 mapping, DNA probes for *sodN* and *sodF* transcripts were generated by PCR using M145 chromosomal DNA as a template. The PCR-generated *sodN* probe spans from -175 to +127 nt relative to the start codon of the *sodN* coding region. To generate S1 probes for *sodF* RNA, the PCR-generated *sodF* fragments (-140 to +60 nt and -205 to +141 nt relative to the end of the *sodF* stop codon) were cloned into the pGEM-T easy vector (Promega), generating pGEM-sodF200 and pGEM-sodF346, respectively. From pGEM-sodF200, the probe DNA was generated by second PCR, using a T7 forward primer and *sodF* (+60) reverse primer (Table II-1), generating a 278 bp DNA fragment containing the *sodF* gene (-140 to +60) linked to 78 bp of vector sequence (see Fig. 2). From pGEM-sodF346, the probe DNA

was generated by PCR, using a SP6 forward primer and sodF(+78) reverse primer (Table II-1), generating a 383 bp DNA fragment containing the *sodF* gene (-205 to +78) linked to 100 bp of vector sequence. The probe DNAs were radio-labeled at their 5′ ends with [γ-^{32}P]-ATP by T4 polynucleotide kinase. For each RNA sample (25 µg), probe DNA was hybridized and digested with S1 nuclease according to standard procedures. For 3′ end mapping of the *sodF* RNA, the probe was generated by PCR from pGEM-sodF346 as a template, using T7 and SP6 primer. BssSI-cut PCR product (199 bp) containing the *sodF* gene (+21 to +141) and 78 bp of vector sequence was labeled with [α-^{32}P]-dATP. The protected fragments were analyzed on a 6% polyacrylamide gel containing 7 M urea. For high resolution S1 mapping, a sequencing ladder was generated using sequenase version 2.0 as recommended by the manufacturer (USB corporation), using the sodF(+78) oligonucleotide primer and the template pGEM-sodF346 DNA in a labeling mix with [α-^{35}S]-dATP. For northern analysis of *sodF* RNAs, a 22 nt single-stranded DNA probe (+18 to +39 nt relative to the end of the *sodF* stop codon; Table II-1) was synthesized, and labeled with [γ-^{32}P]-ATP by T4 polynucleotide kinase. Each sample of 70 µg total RNA was resolved on 12.5% polyacrylamide gel containing 7 M urea, and transferred to a Zetaprobe-GT-membrane (Bio-Rad). Radioactive signals were detected and quantified by phosphor screen and image analyzer (FLA-2000; Fuji).

II.5.2. 5' RACE

5′-rapid amplification of cDNA ends (RACE) was carried out using the FirstChoice® RLM-RACE kit (Ambion), following the manufacturer's instructions with modifications for bacterial RNA (Swiercz et al. 2008). Briefly, 10 µg of total RNA, extracted from *S. coelicolor* M145 was treated with tobacco acid pyrophosphatase (TAP) before being ligated to a 5′-RACE adapter using T4 RNA ligase. This ligated product was then used as template for reverse transcription

using primers complementary to *sodF* and *sodN*, together with SuperScript™ III reverse transcriptase (Invitrogen). The resulting cDNA then served as template for 5′-end PCR amplification, using an adaptor-specific outer primer (Table II-1) and the same oligonucleotide used to prime the reverse transcription reaction. The second PCR was done with a pair of inner primer specific for adaptor and RNA, respectively. The final PCR products were separated on an agarose gel, excised, and purified using the Qiagen® Gel extraction kit, and then sequenced.

II.5.3. Exonuclease digestion of RNA

RNA samples were prepared from the wild type and *Δnur* cells grown exponentially in YEME. Treatment of RNA samples with tobacco acid pyrophosphatase (TAP) and the terminator 5′-phosphate-dependent exonuclease (5′-exo) was done as described previously (Celesnik et al. 2008). Total RNAs (5 µg per each sample) were incubated in 10 µl reaction volume containing 1 µl of 10X TAP reaction buffer (0.5 M sodium acetate [pH 6.0], 10 mM EDTA, 1% ß-mercaptoethanol, 0.1% Triton X-100), 0.5 ul of TAP (5 µ; Epicentre) or water, and 1 µl of RNasin (40 µ; Promega) for 3 h at 37°C. The reaction mixture was extracted with phenol/chloroform, and the RNA was precipitated by ethanol. Further digestion with Terminator Exonuclease (Epicenter) was carried out in 20 µl reaction volume containing 2 µl of 10X reaction buffer (500 mM Tris Cl [pH 8.0], 20 mM $MgCl_2$, 1 M NaCl), 1 µl of RNasin (40 U; Promega), and 1 µl of either Terminator Exonuclease (1 U; Epicentre) or water, for 3 h at 30 °C. The reaction mixture was extracted with phenol/chloroform, ethanol precipitated in the presence of glycogen, and analyzed by northern blotting as described above.

II.6. Overproduction of *S. coelicolor* Nur variants from

E. coli

The coding region of the nur gene was amplified from *S. coelicolor* M145 genomic DNA using primers; *nur* forward , *nur* reverse (Table II-1). The PCR product was digested with NdeI and BamHI and inserted into pET3a (Novagen) digested with the same enzymes. Site-directed mutagenesis of residues in Nur was carried out using mutagenic primers (Table II-2) and pET3a-based plasmid (Novagen) that contains the cloned *nur* gene was used as a template. Mutated clones were selected and confirmed by nucleotide sequencing. The resulting recombinant plasmid (pET3aNur) was transformed into *E. coli* BL21 (DE3). For overexpression of Nur, an overnight culture from a single colony was used to inoculate 3ml of LB media. Cells were grown with vigorous shaking at 37℃ to OD600 of 0.5 and were induced with 1mM (final concentration) isopropyl-β-D-galactopyranoside (IPTG) for 2hrs at 37℃. Harvested cells were resuspended with in vitro Nur binding buffer (4mM Tris-HCl , 1mM EDTA, 4mM DTT, 5mM MgCl2. 20mM KCl, 0.3mg/ml BSA, 10% Glycerol) and were disrupted using an ultrasonicator with a microtip at 20% of the maximum amplitude (600 W, 20 kHz). Disrupted cells are centrifuged in 20,000g for 30min and cell-free extracts were prepared.

II.7. Complementation and expression of *S. coelicolor* Nur variants in vivo

In order to construct a complementation plasmid for WT *nur* and *nur* variants, DNA fragments containing *nur* promoter was amplified by PCR and cloned into pGEM-T (Promega) generating pGEM-T:: p*nur*. ORF of WT *nur* and *nur* variants from pET3aNur were cloned into pGEM-T::p*nur* generating pGEM-T::p*nur-nur. Pnur-nur* fragment of pGEM-T::p*nur-nur* were ligated into pSET162 generating pSET162::p*nur-nur.* Various complementation plasmids were verified by

Table II-2. Primers for mutagenesis

Primer name	Sequence (5' - 3')
H33A_F	GAC ACG CTG GAG GCC GCG ACC CCG GAC
H33A_R	GTC CGG GGT CGC GGC CTC CAG CGT GTC
H70A_F	GGG CTG GTC AGC GCC GCC CAT CTC GGG
H70A_R	CCC GAG ATG GGC GGC GCT GAC CAG CCC
H72A_F	GTC AGC CAC GCC GCC CTC GGG CAC GGT
H72A_R	ACC GTG CCC GAG GGC GGC GTG GCT GAC
H75A_F	GCC CAT CTC GGG GCC GGT GCG CCC ACC
H75A_R	GGT GGG CGC ACC GGC CCC GAG ATG GGC
H86A_F	CTG GCC GAC CGG GCC CAC CAC ATC CAC
H86A_R	GTG GAT GTG GTG GGC CCG GTC GGC CAG
H88A_F	GAC CGG CAC CAC GCC ATC CAC CTG GTC
H88A_R	GAC CAG GTG GAT GGC GTG GTG CCG GTC
H90A_F	CAC CAC CAC ATC GCC CTG GTC TGC CGG
H90A_R	CCG GCA GAC CAG GGC GAT GTG GTG GTG
C93S_F	ATC CAC CTG GTC TCC CGG GAC TGC ACC
C93S_R	GGT GCA GTC CCG GGA GAC CAG GTG GAT
C96S_F	GTC TGC CGG GAC TCC ACC AAC GTG ATC
C96S_R	GAT CAC GTT GGT GGA GTC CCG GCA GAC
H126A_F	ACC GAC ATG AAG GCC TTC GCG ATC TTC
H126A_F	GAA GAT CGC GAA GGC CTT CAT GTC GGT
C133S_F	ATC TTC GGC CGG TCC GAG AGC TGT TCC
C133S_R	GGA ACA GCT CTC GGA CCG GCC GAA GAT
C136S_F	CGG TGC GAG AGC TCT TCC CTG AAG GGT
C136S_R	ACC CTT CAG GGA AGA GCT CTC GCA CCG

nucleotide sequencing. The complementation constructs were introduced into methylation negative, conjugal host strain ET12567/pUZ8002 and were integrated into the chromosomal DNA of the *nur* deletion mutant by bacterial conjugation. The proper integration exoconjugants showing the apramycin^R and thiostrepton^R phenotypes were verified by genomic PCR analysis using their chromosomal DNA as a template. *S. coelicolor* cell extracts expressing WT *nur* and *nur* variants were obtained in 50uM NiSO4 treated YEME. Harvested cells were resuspended with in vivo Nur binding buffer (4mM Tris-HCl , 1mM DTT, 5mM MgCl2. 20mM KCl, 0.3mg/ml BSA, 5% Glycerol) and were disrupted using an ultrasonicator with a microtip at 20% of the maximum amplitude (600 W, 20 kHz). Disrupted cells are centrifuged in 20,000g for 30min and cell-free extracts were prepared.

II.8. Electrophoretic mobility shift assay (EMSA)

Binding reactions were performed with 90bp *sodF* promoter DNA fragment and cell extracts of *E. coli* or *S. coelicolor* in 20-40ul of the reaction buffer; in vitro Nur binding buffer or in vivo Nur binding buffer (above). Following incubation at room temperature for 10min, the binding mixture was subjected to electrophoresis at 4℃ or room temperature on a 5% polyacrylamide gel at 130 V in TBE buffer (for *E. coli* cell extract) or TB buffer (for *S. coelicolor* cell extract). After electrophoresis, the gel was dried and radioactive signals were detected and quantified by phosphor screen and image analyzer (FLA-2000; Fuji).

II.9. Western blotting

In order to assess the amount of Nur proteins in each binding reaction, we performed western blot analysis of cell extracts used for binding assay. Following SDS–PAGE (15%), the gel was electrotransferred to nitrocellulose

membrane (GE healthcare) at 60 V for 60min in Trans-Blot Cell (Bio-Rad). Membrane was blocked in Tris-buffered saline buffer containing 0.1% Triton X-100 (TBST) supplemented with 0.5% BSA, for more than 1hr. The blocked membrane was incubated with polyclonal antibody raised against wild type Nur protein in mice diluted in the same buffer for 1hr. The membrane was washed with TBST for 10min twice. Washed membrane was incubated with anti-mouse IgG secondary antibody 1:10.000 diluted in TBST, and washed with TBST for 10min twice. Detection of the signal was done using ECL detection system (Amersham).

CHAPTER III.

RESULTS

III.1. Inverse Regulation of Fe-SOD and Ni-SOD by Nur

III.1.1. Presence of complementarity between the sense strands of *sodF* and *sodN* genes

The intergenic region between the *sodN* (SCO5254) gene and the *sodX* (SCO5255) gene, where SodX encodes a cognate peptidase for SodN, is highly conserved among streptomycetes (Fig. III-1). A 19 bp sequence stretch within this conserved region also appears in the downstream of the *sodF* gene (Schmidt et al. 2009). This 19 nt stretch is complementary between the sense strands of *sodF* and *sodN* genes (Fig. III-2). Previously mapped 3′ and 5′ ends of *sodF* and *sodN* mRNAs, respectively, in *S. coelicolor* Müller (Kim et al. 1998a; Kim et al. 1998b), led us to hypothesize that a significant fraction of the complementary sequence can actually form base pairs between the 3′ UTR of *sodF* and 5′ UTR of *sodN* transcripts in the *S. coelicolor* A3(2) M145 strain that we used in this study. We determined the 5′ end of *sodN* mRNA in *S. coelicolor* by 5′ RACE. First we extracted M145 RNA from 50uM $NiSO_4$-treated YEME to induce *sodN* gene and DNase-treated RNA as a template for cDNA synthesis. We found that *sodN* mRNA starts at the same G nucleotide as determined for the Müller strain (Kim et al. 1998b) (Fig. III-3). The complementary base-pairing region spanned the first 18 nt of the *sodN* mRNA, encompassing part of the ribosome binding site (Fig. III-2). We investigated whether the complementary base pairing between *sodF* and *sodN* transcripts was responsible for the inverse regulation of the two genes, and if so, how it was mediated.

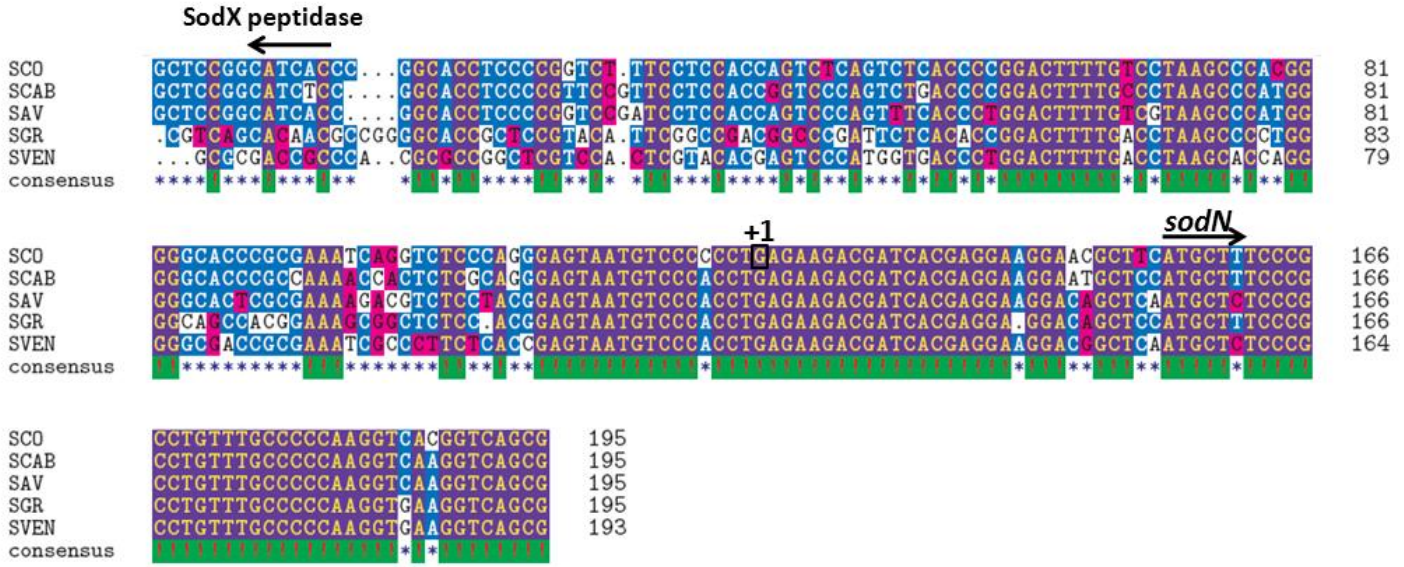

Fig. III-1. Conservation of *sodN* upstream intergenic region in *Streptomyces* species.

Part of *sodN* coding region and its upstream intergenic region in *S. coelicolor* (SCO) was aligned with corresponding sequences from *S. scabies* (SCAB), *S. avermitilis* (SAV), *S. griseus* (SGR) and *S. venezuelae* (SVEN)

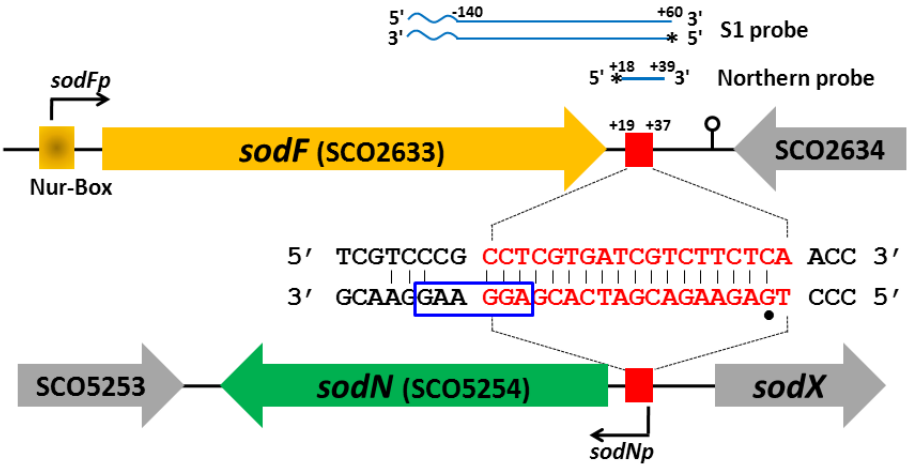

Fig. III-2. Complementarity between sense strands of *sodF* and *sodN* genes

Gene structures around *sodF* and *sodN* genes are schematically shown. The same 19 bp DNA sequence downstream and upstream of *sodF* and *sodN* genes, respectively, are shown as red square. The position of promoters (*sodFp* and *sodNp*) and Nur-binding site (Nur-box) was marked. The complementary sequence in the 3′ and 5′ UTR of *sodF* and *sodN* transcripts, respectively, was shown in the middle. The position of 5′ end and ribosome binding site of *sodN* mRNA was indicated with a dot and square box, respectively. Probes for S1 mapping and northern analysis of *sodF* RNAs were presented with radio-labeled positions (asterisks) along with relative distances from the end of the stop codon of *sodF* ORF. The waved segment of S1 probe indicates non-related vector sequence.

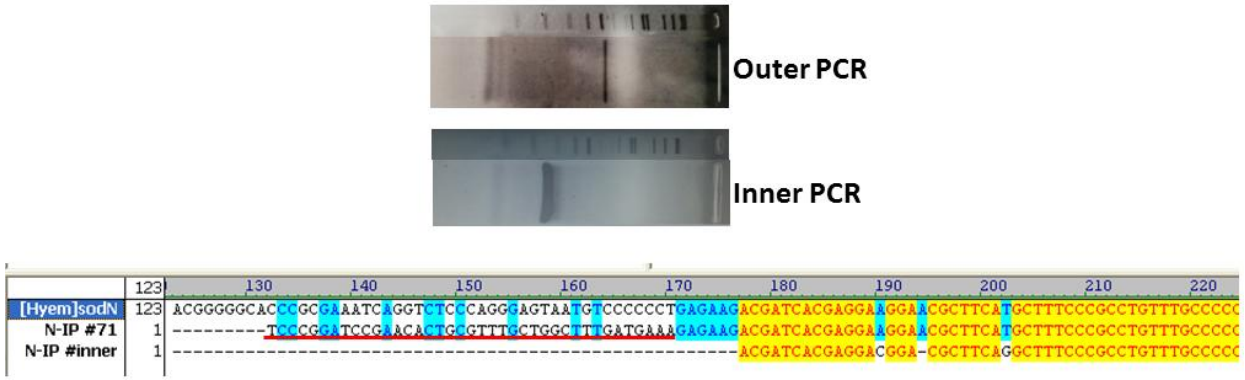

Fig. III-3. 5′ end detection of *sodN* mRNA

5′ end of *sodN* mRNA was determied by 5′ RACE. Red line is 5′ RACE adapter and 5′ end of *sodN* are mapped at equal position in comparison to *S. Muller* strain.

III.1.2. Verification of transcripts existence encompassing the anti-*sodN* sequence

Previously determined positions of the 5′ and 3′ ends of the *sodF* mRNA in *S. coelicolor* Müller strain lay 38 nt upstream from the start codon and 86 nt downstream from the stop codon, respectively (Kim et al. 1998a). The 19 nt *sodN*-complementary (anti-*sodN*) sequence in M145 started 19 nt downstream from the stop codon of the *sodF* ORF (+19 to +37 relative to the end of the stop codon; Fig. III-2). In order to monitor the presence and the boundary of transcripts generated from the *sodF* downstream region, we performed S1 mapping and northern analyses. For S1 mapping, we used a 5′ end-labeled DNA probe that contained part of the *sodF* coding sequence and its downstream region (-140 to +60 relative to the end of the stop codon, Fig. III-2). This probe detected the presence of two kinds of RNA; one producing a fully protected band of ~200 nt (*sodF*) and the other (s-SodF) protecting ~50 nt band (Fig. III-4A). The amount of both RNAs decreased significantly in the wild type (M145) cell when nickel was added to the culture and were produced in a constitutive manner in a *Δnur* mutant. The longer-protecting transcript most likely corresponded to the *sodF* mRNA encoding Fe-SOD, whereas the short-protecting RNA (s-SodF) lacked the *sodF* coding sequence but could contain the anti-*sodN* sequence.

Since S1 mapping detected only the 5′ end point of the s-SodF RNA, we performed northern blot analysis to determine its size. Using a short DNA probe of 22 bp that encompassed the anti-*sodN* sequence, we detected a small RNA of about 90 nt in a 12.5 % polyacrylamide gel specified for resolving small RNAs (Fig. III-4B). The amount of this RNA decreased in the presence of nickel and was constitutively enhanced in *Δnur* mutant, consistent with the observation by S1 mapping. The amount of s-SodF RNA was greatly reduced in a *ΔsodF* mutant. In contrast, deletion of *sodF2,* a paralog of *sodF* in *S. coelicolor* (Chung et al. 1999b),

Fig. III-4. Small-sized *sodF* RNA that contains the 19 nt *sodN*-complementary (anti-*sodN*) sequence is produced in a Nur-dependent manner

(A)S1 mapping of *sodF* RNAs with DNA probe 5′-end labeled at +60 position relative to the stop codon of the *sodF* ORF. RNAs were prepared from the wild type (M145) and *⊿nur* mutant grown in the presence and absence of 50 μM $NiSO_4$. The arrows indicate the presence of *sodF* RNAs that fully protected the probe (*sodF*) and partly protected (s-SodF). FP denotes free probe with plasmid vector sequence attached. (B) Northern blot analysis of *sodF* RNAs. RNAs were prepared from the wild type (M145), *⊿sodF, ⊿sodF2,* and *⊿nur* cells grown in the presence and absence of 50 μM $NiSO_4$. RNAs were run on 12.5% PAG to resolve small sized RNAs and hybridized with 22 nt single-stranded DNA probe (+18 to +39 nt relative to the *sodF* stop codon) labeled at 5′-end by ^{32}P (Fig. 1). 5S rRNA band electrophoresed on agarose gel was shown in parallel to demonstrate the quantity and quality of RNA samples. (C) *sod* transcription pattern in various mutants. RNAs were preparation and S1 mapping are quel to Fig. 4A.

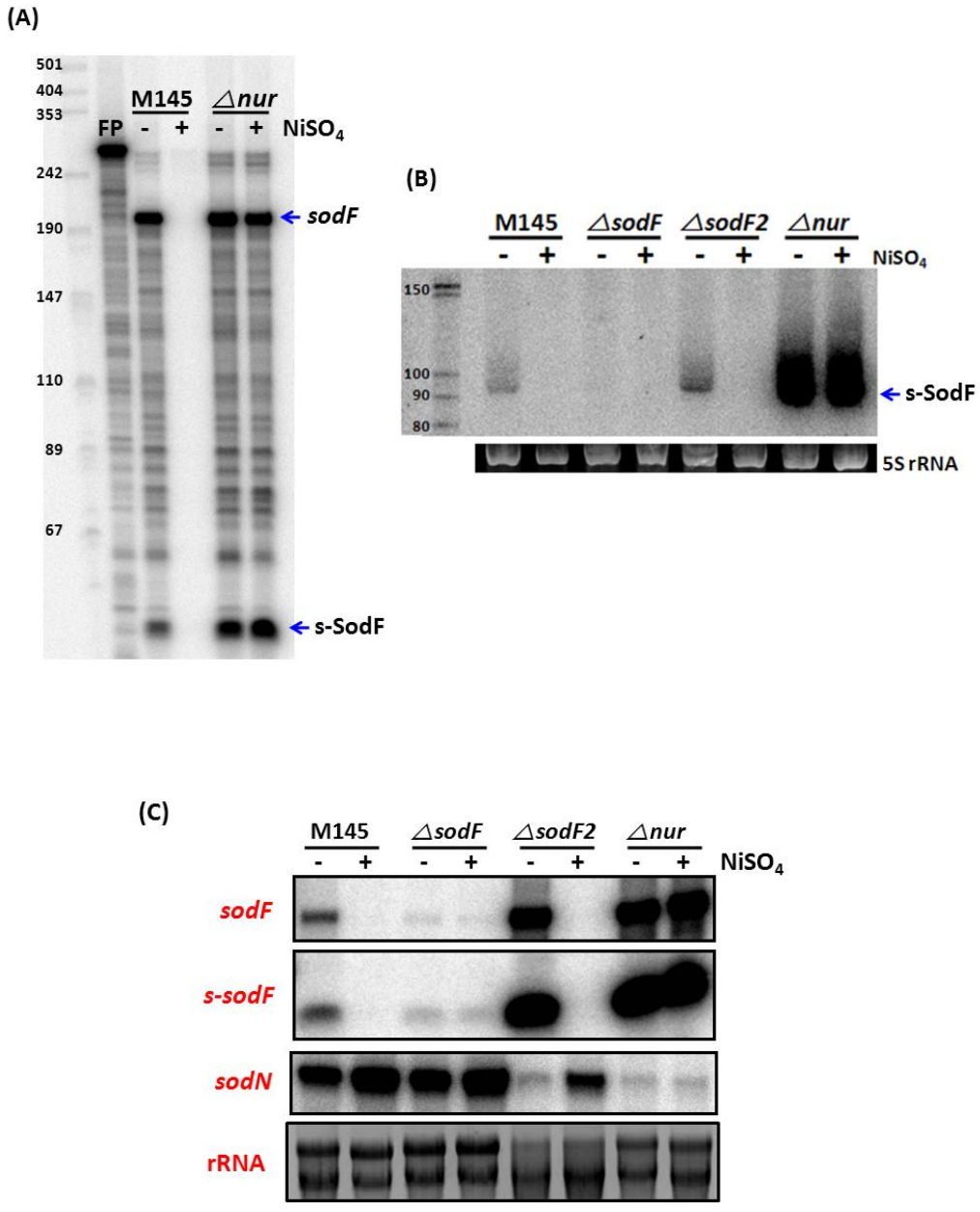
(A)
501
404
353
242
190
147
110
89
67
M145
△nur
FP
-
+
-
+
NiSO4
sodF
s-SodF
(B)
M145
△sodF
△sodF2
△nur
-
+
-
+
-
+
-
+
NiSO4
150
100
90
80
s-SodF
5S rRNA
(C)
M145
△sodF
△sodF2
△nur
-
+
-
+
-
+
-
+
NiSO4
sodF
s-sodF
sodN
rRNA

did not affect the production of s-SodF, suggesting that the s-SodF RNA is primarily produced from the *sodF* gene. Fig. III-4C shows the expression of *sodF* mRNA, s-SodF and *sodN* mRNA in various mutant by S1mapping. These S1 mapping and northern blot analysis clearly revealed that a small RNA species produced from the *sodF* downstream region exists, justifying the name s-SodF. The results also clearly indicated that the production of s-SodF RNA is also inhibited by nickel and Nur, like *sodF* mRNA expression.

III.1.3. Sequence and structure information of s-SodF

III.1.3.1. The 5′ and 3′ boundaries of s-SodF RNA

In order to determine the end points and the exact size of the s-SodF RNA, we performed high resolution S1 mapping. 5′ end mapping was done with the probe labeled at +78. The result showed that the 5′ end of s-SodF was localized at nucleotides T and C (+11 and +12 relative to the end of the stop codon), 7-8 nt upstream of anti-*sodN* sequence (Fig. III-5A). The 3′ end mapping was done with the probe labeled at +21. However, we were not able to localize the exact 3′ end point because the sequencing ladder from the template DNA was compressed severely around the protected band size (Fig. III-5C). This indicated the presence of stable secondary structure near the 3′ end. End-mapping with 3′ RACE was not successful either (data not shown). The presence of an inverted repeat of 15 nt stretch with 80% GC suggested a stable stem and loop structure (ΔG° = - 34.5 kcal), which could hinder nucleotide sequencing ladder (Fig. III-5B). This stem-loop structure likely served as an instrinsic transcription terminator. This coincided with the most prevalent type of intrinsic terminators in actinobacteria, with stem and loop structure of ΔG between -15 and -25 kcal, followed by less than two U residues (Mitra et al. 2009). From the approximate size estimation of s-SodF by S1 mapping and northern analysis, combined with the presence of a

Fig. III-5. Determination of 5′ and 3′ ends of s-SodF RNA.

(A) Determination of 5′ ends by high-resolution S1 analysis. S1 mapping of *sodF* RNAs with a DNA probe 5′-end labeled at +78 nucleotide position relative to the stop codon of the *sodF* ORF. RNAs were prepared from the wild type (M145) and *Δnur* mutant grown in the presence and absence of 50 μM $NiSO_4$. The position of 5′ ends of the transcripts is underlined. The sequencing ladder was obtained with the *sodF* oligonucleotide primer (5′- cct cgc ggg ggc ctt cct ca -3′) and the template pGEM-sodF346. (B) Sequence information of intergenic region between *sodF* (*SCO2633*) and *SCO2634*. The nucleotide position was numbered relative to the end of the stop (TGA) codon of *sodF* ORF. The 5′ end position of s-SodF was marked (bold italic underlined) along with 19 nt anti-*sodN* sequence (red), 15 nt inverted repeats (horizontal arrows), and the possible 3′ end position of *sodF* and s-SodF RNAs. (C) Determination of 3′ ends by high-resolution S1 analysis. S1 mapping of *sodF* RNAs with a DNA probe 3′-end labeled at +21 nucleotide position relative to the stop codon of the *sodF* ORF. RNAs were prepared from the wild type (M145) and *Δnur* mutant grown in the presence and absence of 50 μM $NiSO_4$. Relevant sequence for compressed sequencing ladder from the template DNA is underlined. The sequencing ladder was obtained with the *sodF* oligonucleotide primer (5′- TCG TGA TCG TCT TCT CAA CCT TC -3′) and the template pGEM-sodF346. (D) Predicted secondary structure for s-SodF RNA. The secondary structure of 90 nt long s-SodF RNA (from +11 to +100; Fig. 3B), as well as stability, were predicted by mfold program. The 5′ proximal stem-loop contains the anti-*sodN* sequence.

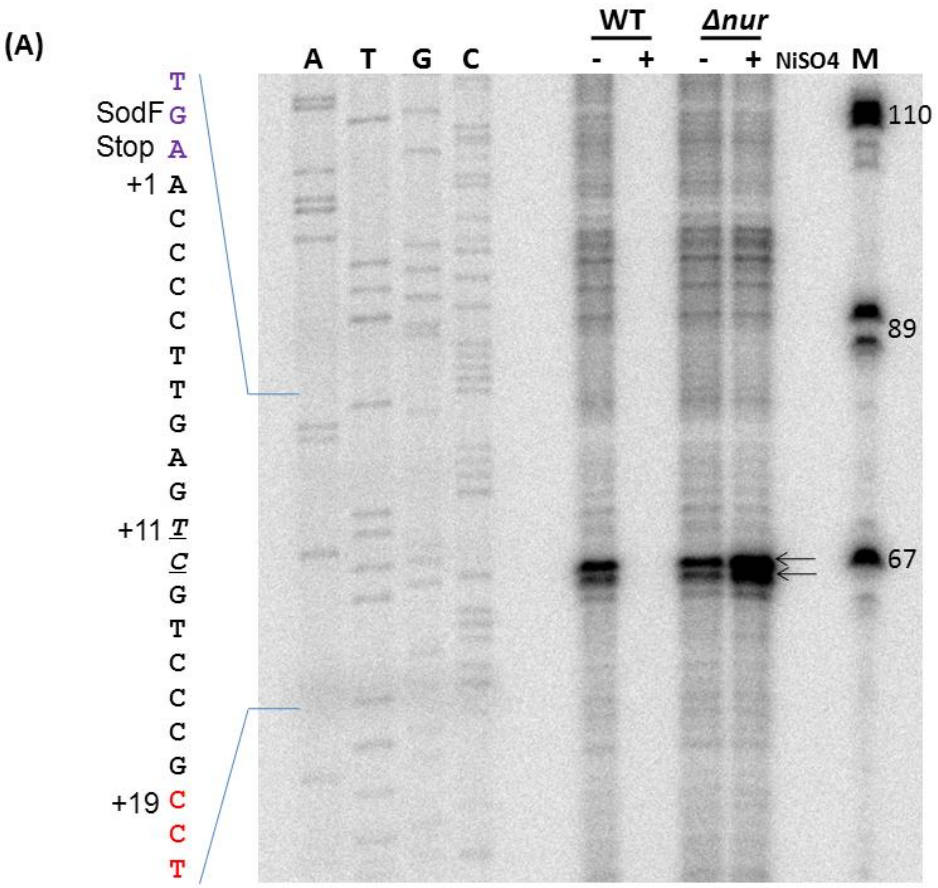
(A)
WT
Δnur
A T G C
- + - + NiSO4 M
SodF
Stop
+1
+11
+19
110
89
67

(B)

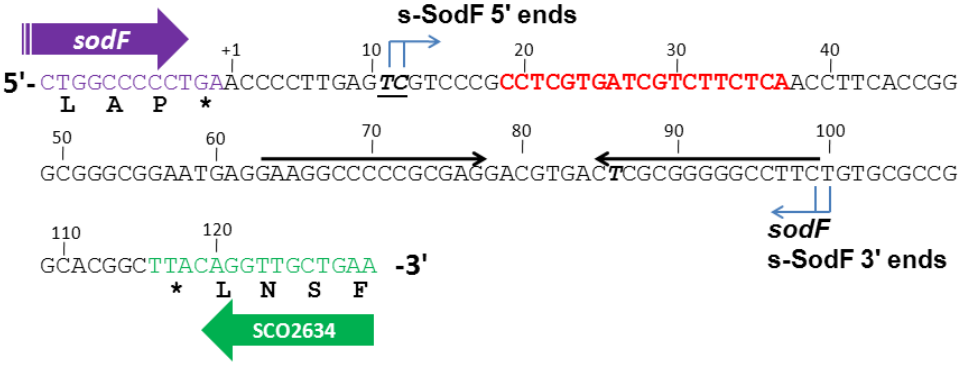
sodF
s-SodF 5' ends
+1
10
20
30
40
5'- CTGGCCCCCTGAACCCCTTGAGTCGTCCCGCCTCGTGATCGTCTTCTCAACCTTCACCGG
L A P *
50
60
70
80
90
100
GCGGGCGGAATGAGGAAGGCCCCCGCGAGGACGTGACTCGCGGGGGCCTTCTGTGCGCCG
sodF
s-SodF 3' ends
110
120
GCACGGCTTACAGGTTGCTGAA -3'
* L N S F
SCO2634

(C)

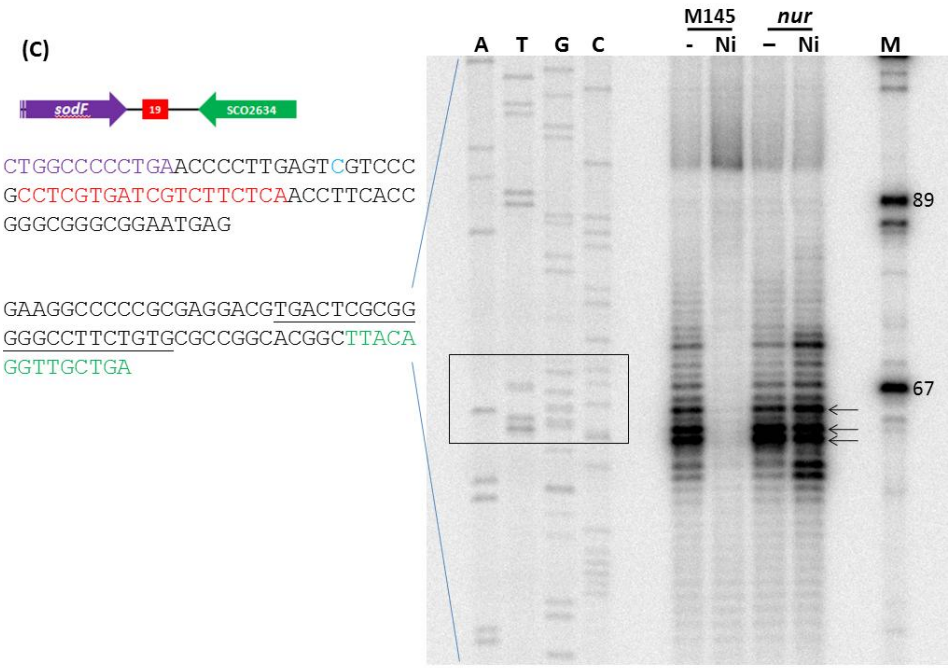
sodF
19
SCO2634
CTGGCCCCCTGAACCCCTTGAGTCGTCCC
GCCTCGTGATCGTCTTCTCAACCTTCACC
GGGCGGGCGGAATGAG
GAAGGCCCCCGCGAGGACGTGACTCGCGG
GGGCCTTCTGTGCGCCGGCACGGCTTACA
GGTTGCTGA
A T G C
M145
- Ni
nur
– Ni
M
89
67

(D)

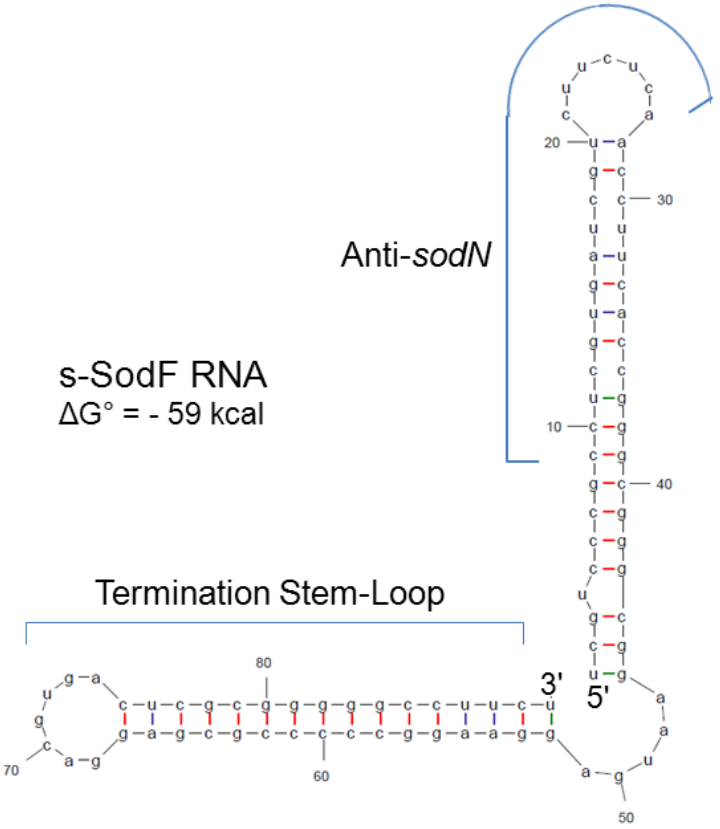
Anti-*sodN*
s-SodF RNA
ΔG° = - 59 kcal
Termination Stem-Loop
3'
5'
10
20
30
40
50
60
70
80

potential intrinsic terminator sequence, we propose that the 3′ boundary of s-SodF RNA lies at the end of the inverted repeat near +100, and thus we estimate s-SodF to be 88-90 nt long (Fig. III-5B).

III.1.3.2. Secondary structure of s-SodF

We predicted the secondary structure of 90 nt s-SodF RNA (+11 to +100; Fig. III-5B) using mfold program (Zuker 2003). Fig. III-5D demonstrated that s-SodF can form a structure with two stem loops; the 5′-proximal one with anti-*sodN* sequence and the termination stem-loop, with an overall ΔG° value of about -59 kcal. The 5'-proximal stem-loop has the anti-*sodN* sequence that spans from the middle of the stem to the entire loop. This stem-loop contains bubbles and a bulge in the stem with an estimated ΔG° of about -22 kcal. The *anti-sodN* sequence was located in such a way that the final 6 nt that could pair with the 5′ terminal residues of *sodN* mRNA is present in the loop region. Therefore, it was plausible to speculate that the seed-pairing between s-SodF and *sodN* mRNA occurs through this single-stranded loop region. The stem region where the rest of the complementary sequence resides consists of relatively weak base-pairing with bubbles, easily breakable to form hydrogen bonds with *sodN* mRNA. The termination stem-loop has a perfectly paired 16 bp stem (including the terminal G-U base pairing) with estimated ΔG° of about -36 kcal.

III.1.4. s-SodF producing mechanism

III.1.4.1. Confirmation of another promoter of s-SodF

The observation that s-SodF RNA is produced in a Nur-dependent manner led us to search for the presence of Nur binding sequence in the genome near the starting position of the small RNA. No sequence matching the proposed Nur-box consensus (tTGCaa-N5-ttGCAA) was found (An et al. 2009).

We performed Electrophoretic mobility shift assay (EMSA) with the 200 bp DNA probe (-140 to +60 relative to the end of the stop codon, Fig. III-2) used for S1 mapping analysis (Fig. III-4) did not detect any binding protein present in cell extracts prepared from wild type cells grown in Ni-supplemented YEME medium (Fig. III-6). The 90bp DNA probe for *sodF* promoter (-740 to -651 relative to the end of the stop codon) is used as a positive control. Therefore, the possibility of initiating transcription from its own Nur-dependent promoter for s-SodF synthesis appeared very low.

III.1.4.2. The 5′ phosphorylation status of s-SodF

The 5' phosphorylation status of s-SodF RNA was then examined using 5′-phosphate-dependent exonuclease. If s-SodF is processed from *sodF* mRNA, 5′ of s-SodF will be monophophorylated. Total RNAs isolated from either wild type (M145) or *Δnur* mutant cells were treated with 5′-monophosphate-dependent exonuclease as described previously (Celesnik et al. 2008), and subjected to 12.5% PAGE and northern analysis. Results in Fig. III-7 (upper panel) demonstrated that 5′ exonuclease digested s-SodF RNA efficiently as it did the bulk of 23S and 16S rRNAs (bottom panel). Treatment with tobacco acid pyrophosphatase (TAP) that removes pyrophosphates from 5' triphosphates of de novo transcribed bacterial mRNA did not make any difference. Therefore, it is highly likely that the 5′-end of s-SodF RNA is monophosphorylated, and hence was generated not by de novo transcription but from the cleavage of a longer RNA. Since the *sodF* mRNA spanned not only the coding region but also the downstream UTR that encompasses the anti-*sodN* sequence, it was most likely that s-SodF is generated from the full-length *sodF* mRNA by cleavage at the 5′ side of T (+11) or C (+12) residues (Fig. III-5).

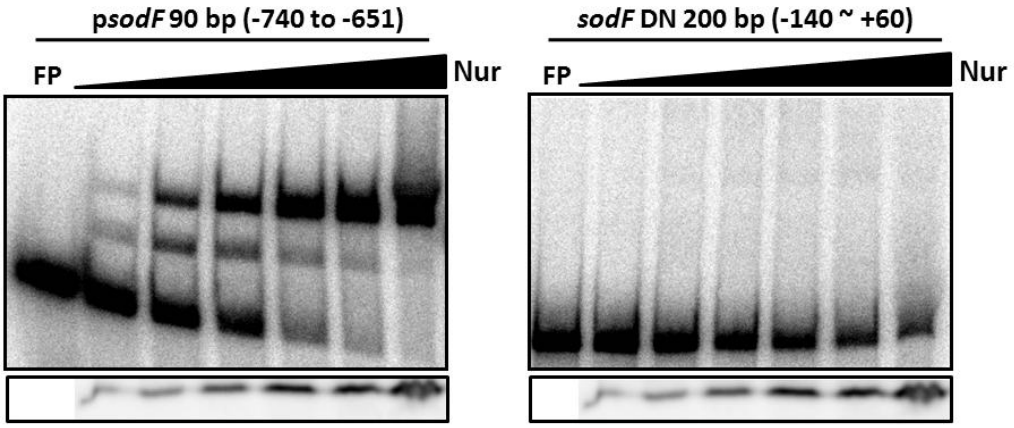

Fig. III-6. Binding activity of WT Nur protein on sodF DNA

Gel mobility shift assay with two *sodF* DNA probe and cell extract from *E. coli* in presence 100uM NiSO4 and 4 ℃. 90 bp promoter region of *sodF* (-740 ~ -651) and *sodF* DN 200 bp probe (-140 ~ + 60) are produced by PCR. Relative amount of Nur protein in cell extract was confirmed by western blotting using Nur antibody.

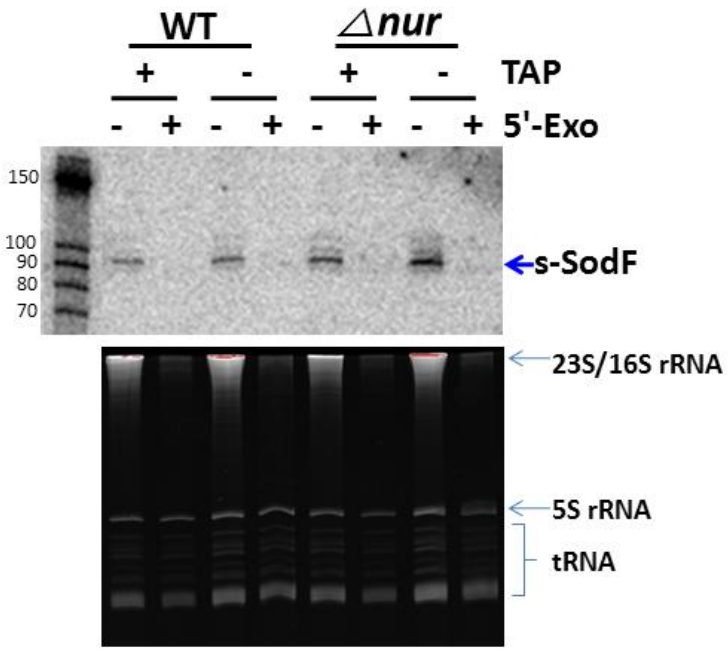

Fig. III-7. Sensitivity of s-SodF RNA toward 5′ monophosphate-dependent exonuclease.

The phosphorylation state of the s-SodF RNA was monitored by treatment with a 5′-monophosphate-dependent exonuclease (5′-Exo). Total RNA isolated from wild type (M145) and *⊿nur* cells were subjected to digestion with 5′-Exo and analyzed by gel electrophoresis (lower panel) and northern blotting with an s-SodF specific radiolabeled probe (upper panel). RNA samples were treated either with or without tobacco acid pyrophosphatase (TAP) that converts 5′-triphosphorylated RNA to 5′-monophosphorylated one prior to 5′-Exo treatment. The status of stable RNAs in each sample is shown in the lower panel.

III.1.4.3. Test for possible RNases related to processing s-SodF

To find out which RNase is in involved in processing s-SodF, we focused on *absB* which is best-known RNase in *S. coelicolor*. *absB* is a member of the RNase III family of endoribonuclease which commonly recognized double strand segment of stem-loop structures and in bacteria carry out the processing of pre-rRNA, tRNA and polycistronic mRNA (Conrad and Rauhut 2002; Drider and Condon 2004). In *S. coelicolor*, *absB* was discovered initially as a global regulator of antibiotic production in this developmentally complex bacterial species and has subsequently also been found to modulate the cellular abundance of multiple messenger RNAs implicated in morphological differentiation (Xu et al. 2010). In *absB* null mutant of J1501 background strain (J-5572), *sodF* mRNA and s-SodF were both still present in S1 mapping (Fig. III-8). So, AbsB might not carry out a processing of s-SodF.

Next, We checked the functional orthologue of *E. coli* RNase E, *rns* (Lee and Cohen 2003). In this paper, *rns* can cleavage the *E. coli* RNase E substrates and *rns* is not essential in *S. coelicolor*, unlike those of *E. coli*. In *rns* mutant strain, *sodF* mRNA and s-SodF were also still present (Fig. III-8). So we knew that processing of s-SodF from long *sodF* mRNA is RNase III (*absB*) & RNase E (*rns*) - independent. This data suggests that other RNases is involved in s-SodF processing and the RNases that are responsible for processing s-SodF RNA and degrading *sodN* mRNA await further investigation.

III.1.5. Function of s-SodF in vivo

III.1.5.1. *sodN* mRNA half life in *sodF* and *sodF2* mutants

We wanted to know that *sodF* transcipts can regulate *sodN* mRNA stability through anti-*sodN* region. In early-stage study, we didn't know that the ratio of *sodF* to *sodN* mRNAs varied depending on growth conditions (see below). So we

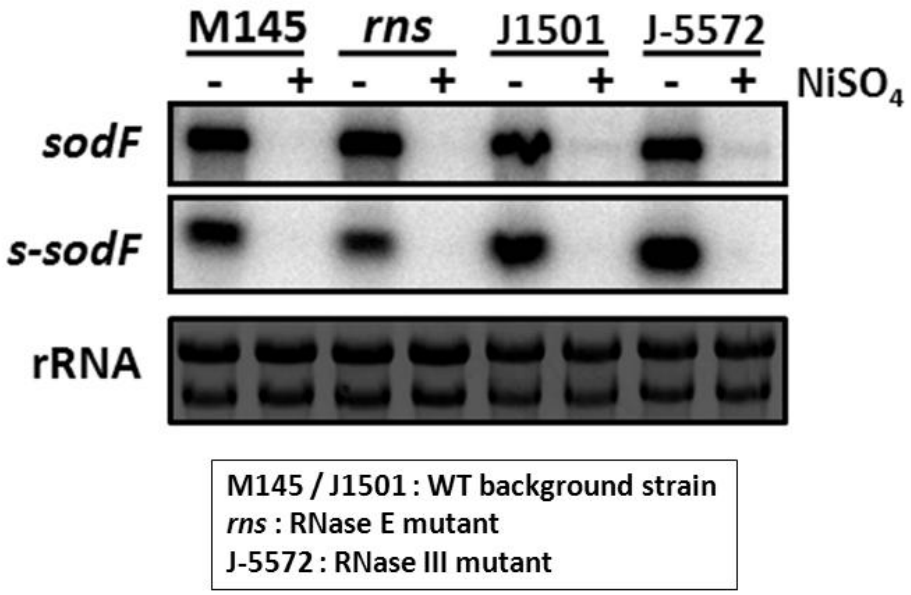

Fig. III-8. *sodF* transcripts in various RNase mutants.

S1 mapping of *sodF* RNAs with DNA probe 5′-end labeled at +60 position relative to the stop codon of the *sodF* ORF. RNAs were prepared from the wild type (M145, J1501), RNase E mutant (*rns*) and RNase III mutant (J-5572) in the presence and absence of 50 μM $NiSO_4$.

tried to capture the moment which *sodF* and *sodN* mRNA level were similar before rifampicin treatment. Finally we set up the experimental condition which cells grown in YEME with 50uM $NiSO_4$ were treated 2mM EDTA for 2hr and then we treated 300ug/ml rifampicin to measure the *sodN* mRNA half life (Fig. III-9). We estimated the half-life of *sodN* mRNA in *sodF* and *sodF2* mutants in this condition. Interestingly, half-life of *sodN* mRNA was delayed to 47 min in *sodF* mutant, compared to WT (13 min) half-life of *sodN* mRNA was a little delayed to 22 min and in *sodF2* mutant (Fig. III-10). This data shows that *sodF* and *sodF2* transtripts can regulate *sodN* mRNA stability and *sodF* could be major role in *sodN* mRNA regulation. It matched the S1 mapping data which s-SodF is mainly produced from *sodF* mRNA not *sodF2* mRNA (Fig. III-4C).

III.1.5.2. s-SodF RNA decreases the stability of *sodN* mRNA

We then explored whether s-SodF RNA really affected *sodN* gene expression. We estimated the half-life of *sodN* mRNA under various genetic background. First, in order to verify the effect of s-SodF RNA alone, we introduced to *ΔsodF* mutant an overexpression plasmid for *sodF* whole RNA (-680 to +142 relative to the end of the stop codon) and s-SodF RNA (+10 to +142 relative to the end of the stop codon) whose expression was driven by a strong *ermE** promoter on the integrating vector pSET162. We checked the stable expression of *sodF* whole RNA and s-SodF RNA by S1 mapping (Fig. III-11).

At this time, We knew that the ratio of *sodF* to *sodN* mRNAs varied depending on growth conditions (see below). So we set up the new experimental condition to detect *sodN* mRNA decay. We measured the RNA decay rates, following inhibition of transcription initiation by rifampicin. Cells grown in YEME to OD_{600} of 0.8 were treated with rifampicin (300 μg/ml), and were harvested at different time points (0 to 20 min) to prepare RNA. S1 mapping of *sodF* mRNA, s-SodF, and *sodN* mRNA in each sample was done with RNA-specific probes in one

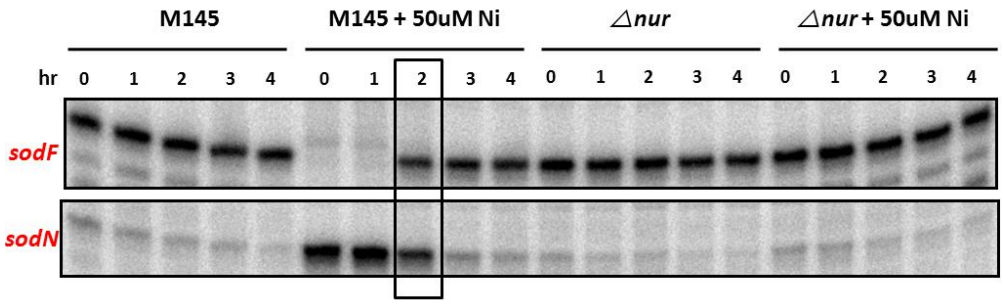

Fig. III-9. Relative expression of *sodF* and *sodN* mRNA response to nickel and EDTA

S.coelicolor cells were grown in YEME medium including either 50uM $NiSO_4$ or not and treated with 2mM EDTA. At 1hr, 2hr, 3hr and 4hr after EDTA treatment, cells were harvested and their RNAs were analysed by S1 mapping with 5′ end-labelled probe. The radioactivity in the S1-protected bands was quantified by Phosphor Imager (Bio-Rad) and presented as relative values.

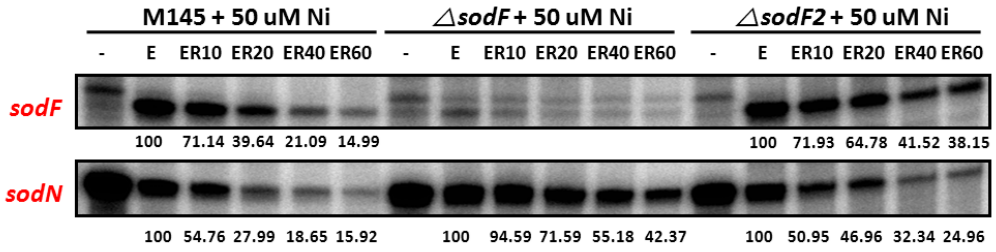

▶ RNA half life (min)

	M145 Ni(+)	*sodF* Ni(+)	*sodF2* Ni(+)
sodF	18	—	36
sodN	13	47	22

Fig. III-10. Measurement of *sodF* and *sodN* mRNA stability in WT and mutant strain.

S.coelicolor cells were grown in YEME medium including 50uM $NiSO_4$ and treated with either 2mM EDTA (E) or nothing(-) for 2hr, followed by treatment with rifampicin (R, 300ug/ml). At 10min (ER10), 20min (ER20), 40min (ER40) and 60min (ER60) after rifampicin treatment, cells were harvested and their RNAs were analysed by S1 mapping with 5′ end-labelled probe. The radioactivity in the S1-protected bands was quantified by Phosphor Imager (Bio-Rad) and presented as relative values.

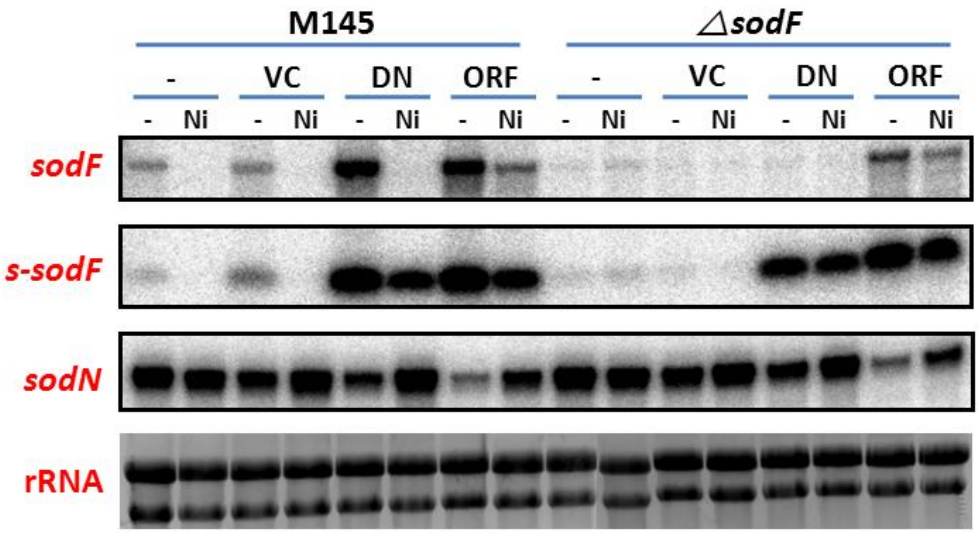

Fig. III-11. Confirmation of various *sodF* transcripts overexpressing mutant by S1 mapping

we introduced to M145 and *ΔsodF* mutant an overexpression plasmid for *sodF* whole RNA (ORF; -680 to +142 relative to the end of the stop codon) and s-SodF RNA (DN; +10 to +142 relative to the end of the stop codon) whose expression was driven by a strong *ermE** promoter on the integrating vector pSET162. *S.coelicolor* cells were grown in YEME medium including either 50uM $NiSO_4$ or not. The radioactivity in the S1-protected bands was quantified by Phosphor Imager (Bio-Rad) and presented as relative values.

reaction tube.

△*sodF* cells with pSET-based recombinant plasmid expressing *sodF* whole RNA (p-*sodF*) express significant level of *sodF* mRNA and s-SodF compared to △*sodF* and in this strain, *sodN* mRNA is barely detected (Fig. III-12). s-SodF RNA expression strain (p-s-SodF) from *ermE** promoter express relative low level of s-SodF compared to p-*sodF* but basal level of *sodN* mRNA is decreased compared to △*sodF* (Fig. III-12). This data shows that *sodF* transcripts directly regulate *sodN* mRNA stability.

As demonstrated in Fig. III-13, the *sodN* mRNA in the wild type strain decayed at $t_{1/2}$ of ~ 3 min. The *sodF* mRNA decayed with half-life of about 10 min, whereas the s-SodF RNA was relatively stable with $t_{1/2}$ of >>20 min. In *ΔsodF* mutant where no *sodF* transcripts are produced, the half-life of *sodN* mRNA increased to about 16 min, suggesting that *sodF* transcripts decrease the stability of *sodN* mRNA. A residual *sodF*-sized band observed in *ΔsodF* mutant is thought to be non-specific, and it is not detectable in the mutant introduced with pSET-derived plasmids (below). Fig. III-13 demonstrated that when s-SodF RNA was stably expressed in the absence of *sodF* mRNA, the half-life of *sodN* mRNA was about ~7 min which was significantly shorter than ~16 min observed in *ΔsodF*. Since the expression level of s-SodF RNA in *ΔsodF* was lower than the level in the wild type, it is thought that the *sodN* half-life was not brought down to the wild type level (~ 3 min). This experiment clearly demonstrated that the production of s-SodF RNA alone was sufficient to decrease the amount of *sodN* mRNA.

III.1.6. Mutations in the anti-*sodN* region of s-SodF inactivate its inhibitory function

In order to test whether the anti-*sodN* sequence in s-SodF was indeed critical to reduce the amount of *sodN* mRNA, we created mutants in this region. Variants

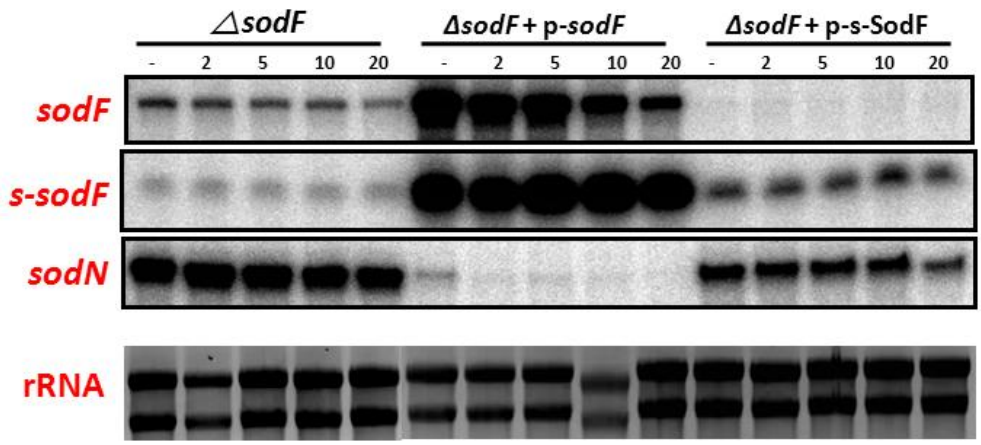

Fig. III-12. Effect of *sodF* transcripts on the stability of *sodN* mRNA

S1 mapping of *sodF* and *sodN* RNAs following rifampicin treatment. *⊿sodF* cells with or without pSET-based recombinant plasmid expressing sodF whole RNA (p-*sodF*) and s-SodF RNA (p-s-SodF) from *ermE** promoter in the chromosome were grown in YEME medium to OD600 of 0.8 and treated with rifampicin (300 μg/ml). At 2, 5, 10, and 20 min after rifampicin treatment, cells were harvested and fixed with methanol. RNA samples were analysed by S1 mapping with 5′ end-labeled probes. A representative result was presented.

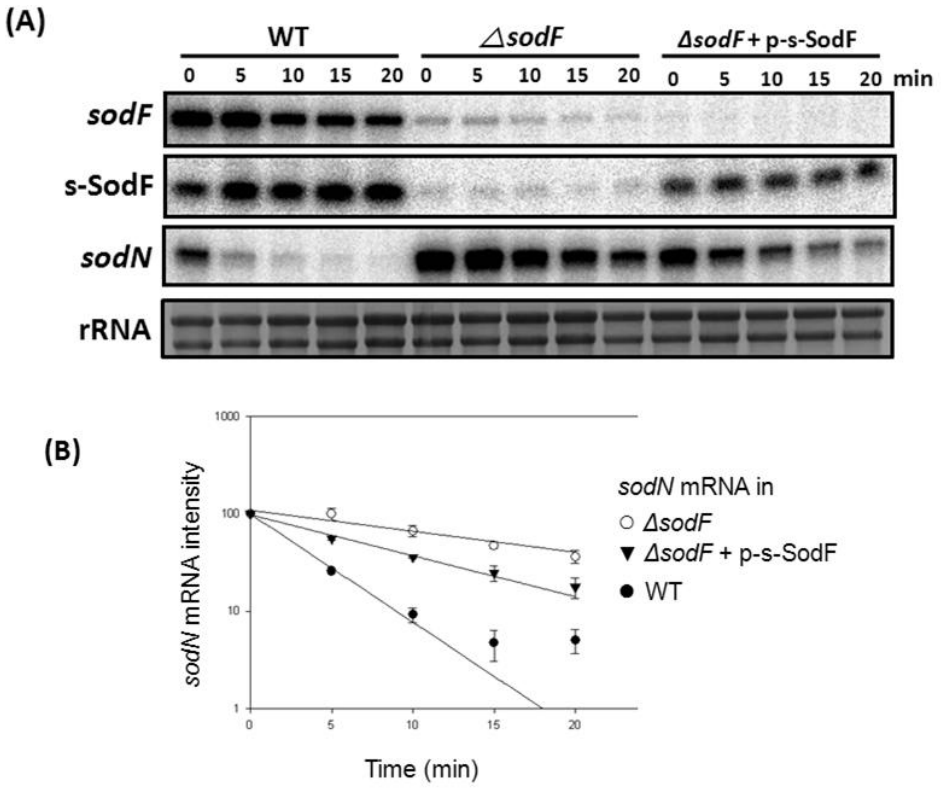

Fig. III-13. Effect of s-SodF RNA on the stability of *sodN* mRNA

(A) S1 mapping of *sodF* and *sodN* RNAs following rifampicin treatment. Wild type (M145) and *ΔsodF* cells with or without pSET-based recombinant plasmid expressing s-SodF RNA from *ermE** promoter (p-s-SodF) in the chromosome were grown in YEME medium to OD600 of 0.8 and treated with rifampicin (300 μg/ml). At 5, 10, 15, and 20 min after rifampicin treatment, cells were harvested and fixed with methanol. RNA samples were analysed by S1 mapping with 5′ end-labeled probes. A representative result was presented. (B) The relative amount of each RNA species was plotted to estimate half-life.

with changes in the predicted 7-nucleotide loop region (V1), and the subsequent seven (V2) five (V3) nucleotides were made by site-directed mutagenesis (Fig. III-14) using mutagenic primers (Table II-1). The secondary structure prediction by mFOLD suggested that V1 would assume almost identical structure to the wild type with ΔG° of -59 kcal, and V2 a similar structure with a larger loop with ΔG° of -55 kcal (Fig. III-14C). We cloned the mutant s-SodF genes in the integration vector (pSET162) and introduced them into the chromosome of *ΔsodF* strain of *S. coelicolor*, in the same way as we made the expression construct for the wild type s-SodF (Fig. III-13). The results demonstrated that the introduction of wild type s-SodF decreased the level of *sodN* mRNA to about 40% of that in the control strain without any s-SodF gene. On the other hand, V1 and V2 variants of s-SodF, even though they were expressed to higher levels than the wild type, did not affect the level of *sodN* mRNA (Fig. III-14B). The levels of V1 and V2 s-SodF RNAs were about 7-fold and 3-fold higher than the wild type level, respectively (Fig. III-14B). This differential expression could arise from the difference in the copy number of incorporated plasmids as well as RNA stability. We tried another stem-variant mutant (V3) that changed the last 5 nucleotides in the anti-*sodN* sequence from CCTCG to AACAT. This variant, however, was expressed too low to examine its effect, presumably due to a dramatic decrease in stability, as expected from the central bulge generated in the stem (Fig. III-14C). All together, these experiments verify that sequences in the *anti-sodN* region of s-SodF, at least the first 14 nt including the predicted loop, were critical for the inhibitory action of s-SodF.

III.1.7. Growth phase-dependent antagonistic expression of *sodN* and *sodF*

III.1.7.1. *sod* genes expression in various growth phase

When we tried to measure the half-life of *sodN* mRNA in the wild type strain, we

Fig. III-14. Sequence-specificity of s-SodF RNA to inhibit *sodN* mRNA.

(A) Variants of s-SodF were created by changing sequences in the anti-*sodN* region. V1 harbor changes of seven nucleotides that correspond to the predicted loop region in anti-*sodN* sequence. V2 and V3 harbor changes in the subsequent seven and five nucleotides, respectively. (B) Effect of s-SodF mutations on the level of *sodN* mRNA. The mutated s-SodF genes were cloned in pSET152-based vector with *ermE** promoter, and incorporated into the chromosome of *ΔsodF* strain through phage attachment site, as done for the wild type s-SodF construct used in Fig. 13. The *ΔsodF* cells with parental vector control (C), wild type (WT) and mutated variants (V1, V2, V3) of s-SodF genes were grown in YEME to OD of 0.8. RNA samples were obtained from cells as in Fig. 13, without rifampicin chase. A representative gel from three independent experiments was presented, and marked with the quantified values of the average ± SD for *sodN* mRNA. (C) Predicted secondary structure for s-SodF RNA variants. The secondary structure of 90 nt long s-SodF RNA (from +11 to +100; Fig. 5B), as well as stability, were predicted by mfold program.

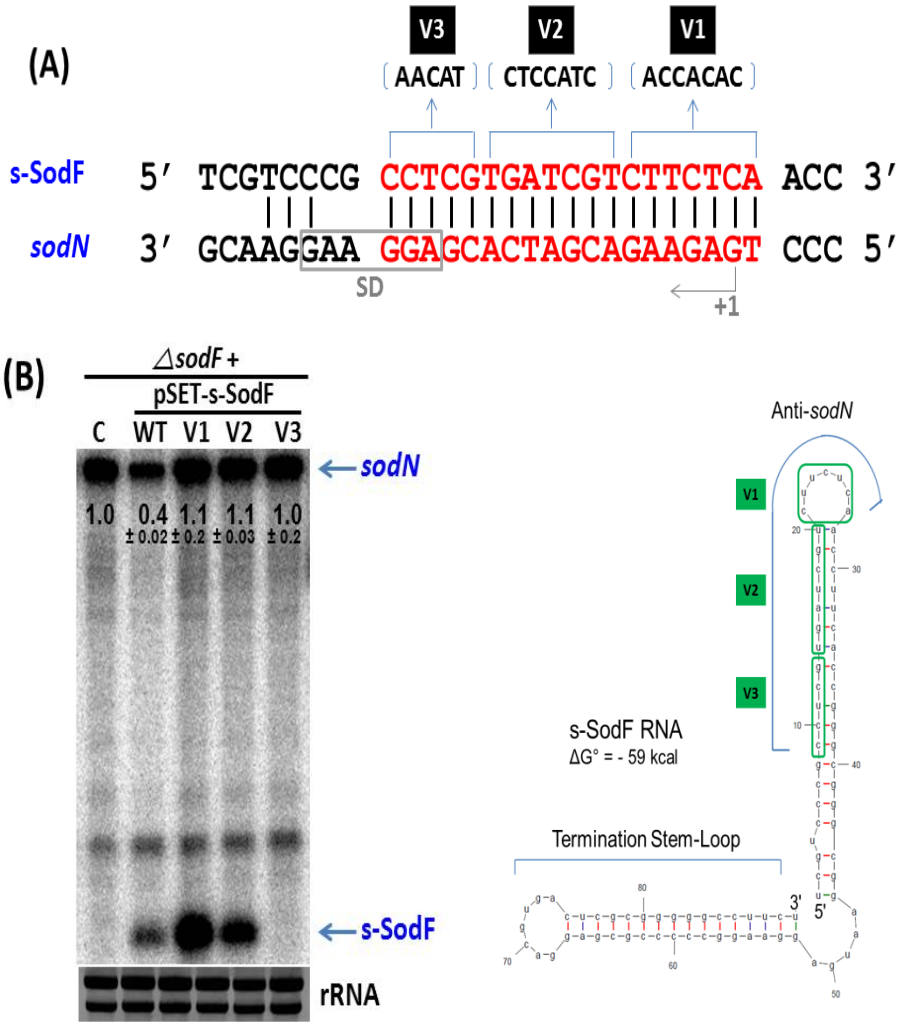
(A)
V3
V2
V1
AACAT
CTCCATC
ACCACAC
s-SodF
5′ TCGTCCCG CCTCGTGATCGTCTTCTCA ACC 3′
sodN
3′ GCAAGGAA GGAGCACTAGCAGAAGAGT CCC 5′
SD
+1
(B)
△sodF +
pSET-s-SodF
C WT V1 V2 V3
sodN
1.0 0.4 ± 0.02 1.1 ± 0.2 1.1 ± 0.03 1.0 ± 0.2
s-SodF
rRNA
Anti-sodN
V1
V2
V3
s-SodF RNA
ΔG° = - 59 kcal
Termination Stem-Loop
3'
5'

(C)

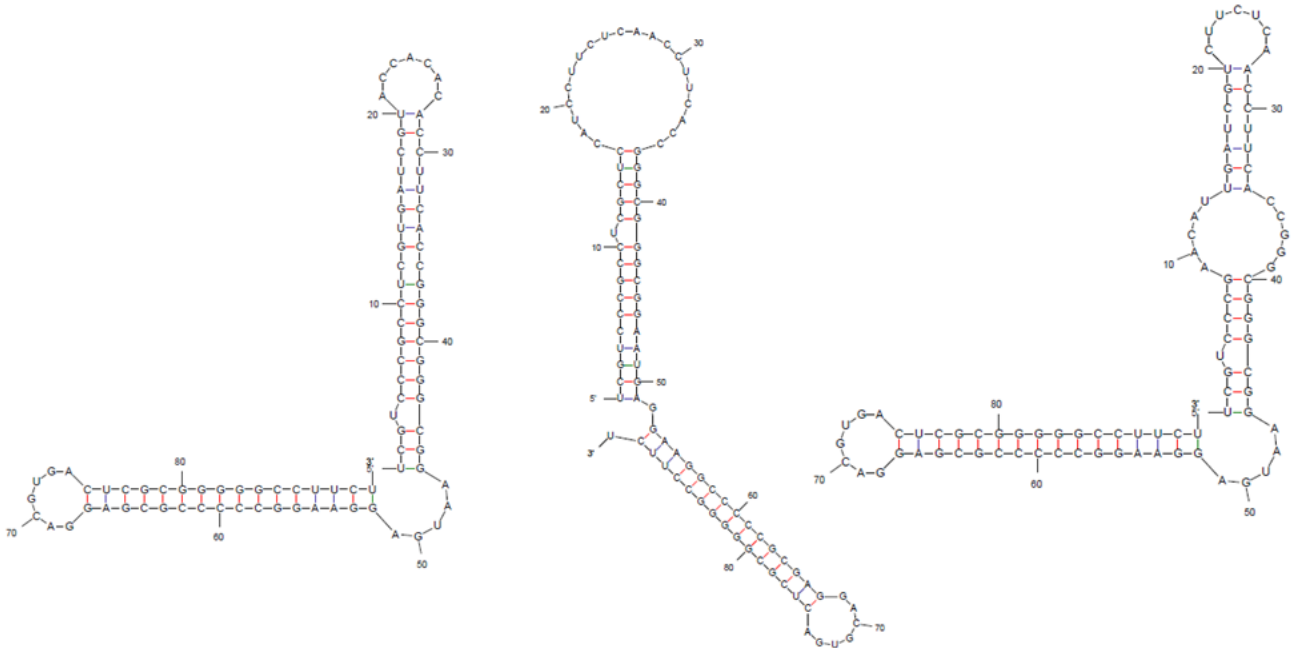

V1
ΔG° = - 59 kcal

V2
ΔG° = - 55 kcal

V3
ΔG° = - 47 kcal

experienced extensive variation. So we measured *sod* genes expression in various growth phase. Interestingly, level of *sodF* mRNA and s-SodF increase and *sodN* mRNA decrease as cell growth proceeded from early to late stages of exponential growth (Fig. III-15B). As expected, this phenomenon was not shown in *sodF* mutant and *sodN* is highly derepressed in all growth phase. In M145, increased *sodF* mRNA slightly decreases up to OD 1.6 but s-SodF increases continuously (Fig. III-15B). In Fig. III-15A, M145 and *sodF* mutant are showed similar growth pattern in YEME and this results suggests that total SOD level may be critical to *S. coelicolor* growth.

III.1.7.2. half life of *sodN* mRNA in various growth phase

At early exponential phase (OD_{600} < 0.5) *sodN* RNA was more prevalent than *sodF* RNA, whereas the relative amount reversed at later growth phase (Fig. III-16). We then measured the half-life of *sodN* mRNA at different OD by rifampicin chase experiment. A representative result presented in Fig. III-17 demonstrated clearly that at later phase of growth, where the amount of *sodF* RNA increased, the half-life of *sodN* mRNA became shorter. We plotted the change in *sodN* mRNA half-life as growth progresses in the exponential phase, along with the relative amount of *sodF* mRNA to *sodN* mRNA. Results in Fig. III-17B coincided well with the proposal that *sodF* transcripts lower the stability of *sodN* mRNA.

That is, in early exponential phase which is nickel abundant condition, *sodF* is repressed by nickel-bound Nur and then level of anti-s*odN* s-SodF is low and *sodN* is increased. When cells growth proceeded to late exponential stage, nickel is depleted and *sodF* is derepressed and then processed s-SodF can binds to s*odN* mRNA and destabilized *sodN* mRNA.

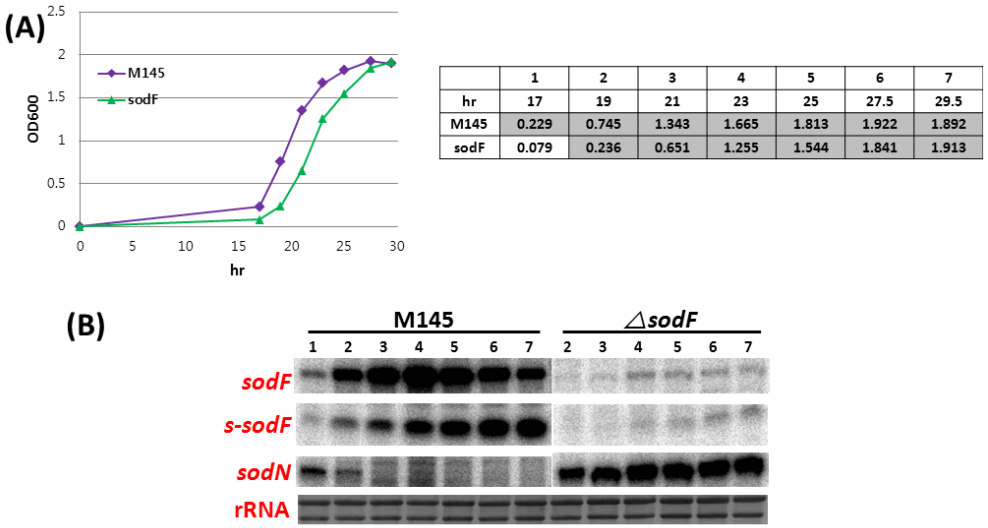

	1	2	3	4	5	6	7
hr	17	19	21	23	25	27.5	29.5
M145	0.229	0.745	1.343	1.665	1.813	1.922	1.892
sodF	0.079	0.236	0.651	1.255	1.544	1.841	1.913

Fig. III-15. *sod* genes expression in growth phase (M145 vs *sodF*)

(A) Growth curve of M145 and *sodF* mutant in YEME. OD600 of harvested sample which uesd in S1 mapping is indicated. (B) *sod* genes expression in various growth phases

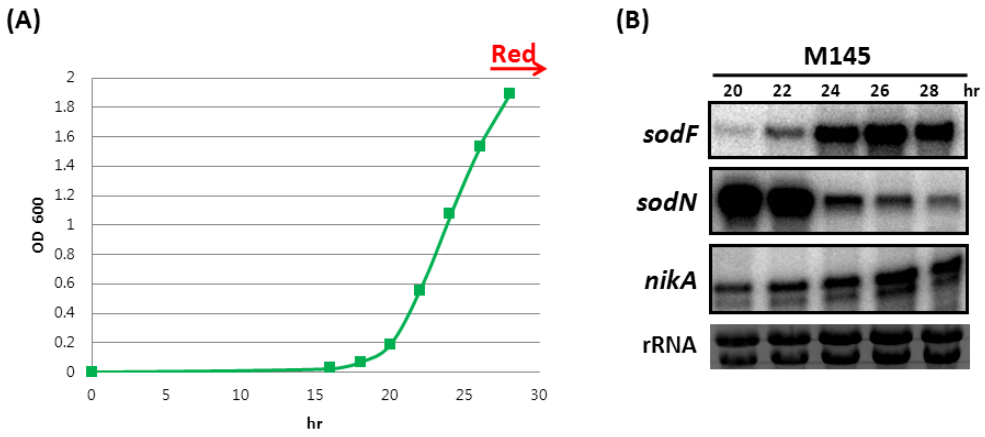

Fig. III-16. Growth-phase dependent expression of *sodF* and *sodN* genes.

(A) A representative growth curve of *S. coelicolor* M145 strain in YEME media. M145 spores ($2x10^7$) were inoculated to 200 mL YEME media and were incubated at 30°C by shaking. Production of red antibiotic (undecyl prodigiosin) is visible between 26 and 28 hr culture when OD_{600} increases above 1.5. (B) S1 mapping of *sodF*, *sodN*, and *nikA* RNAs. RNA samples were prepared from cells grown for different lengths of time.

Fig. III-17. Correlation between *sodF/sodN* ratio and the stability of *sodN* mRNA during growth

(A) Measurement of *sodF* and *sodN* mRNA stability at different growth phases in WT. *S.coelicolor* cells were grown in YEME medium to OD_{600} of 0.2 to 1.0 and treated with rifampicin (300 μg/ml) at specific OD_{600}. At 5, 10, 15, and 20 min after rifampicin treatment, cells were harvested and fixed with methanol. Their RNAs were analysed by S1 mapping with 5′ end-labeled probes for *sodF* and *sodN* RNAs. The radioactivity of the S1-protected bands was quantified by Phosphor Imager (Bio-Rad) and presented as relative values to the untreated sample. Representative results from cells grown to OD_{600} of 0.24, 0.54, and 0.87 were shown. (B) The change in the relative amount of *sodF* and *sodN* mRNA (*sodF/sodN*) during exponential growth was plotted, along with the changing half-lives of *sodN* mRNA, as batch culture proceeds. The *sodF/sodN* ratio was taken from the quantified amount of each mRNA-specific band in untreated samples at specific growth stage, as represented in Fig. 17A.

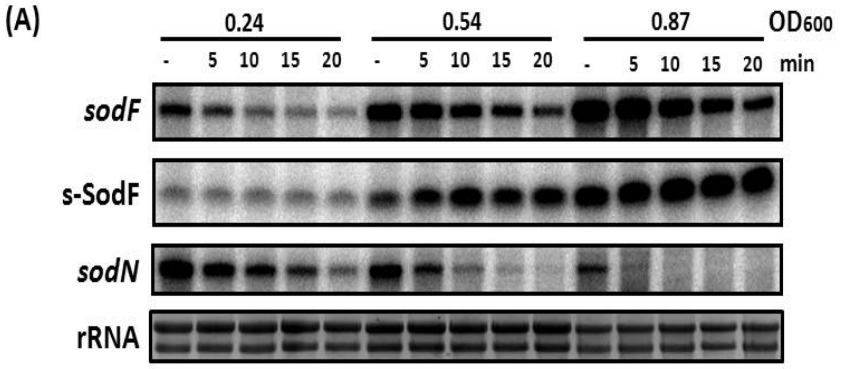
(A)
0.24
0.54
0.87
OD600
- 5 10 15 20 - 5 10 15 20 - 5 10 15 20 min
sodF
s-SodF
sodN
rRNA

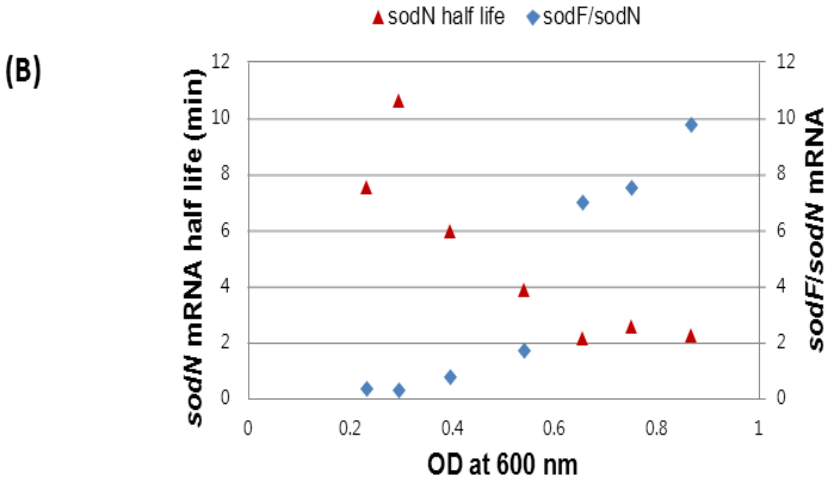
(B)
sodN half life
sodF/sodN
sodN mRNA half life (min)
sodF/sodN mRNA
OD at 600 nm
0
2
4
6
8
10
12
0
0.2
0.4
0.6
0.8
1

III.1.8. Nickel responsiveness of *sod* genes

III.1.8.1. Nickel sensitivity of *sod* mutants

When we tested nickel sensitivity of *sod* mutants in NA plate, interesting phenomenon was observed. *sodF* mutant is more sensitive rather than WT in NA plate without any $NiSO_4$ (Fig. III-18). In *sodF* mutant, *sodN* which nickel-cofactor SOD is highly derepressed because of low level of *sodF*. But nickel level of medium is low and cells can not survive well because they can't use Ni-SOD. As expected, *sodN* mutant is more sensitive in NA plate with 50uM $NiSO_4$ (Fig. III-18). In nickel-repleted condition, *sodF* is repressed but cells can not use efficiently Ni-SOD and cell can not grow well. Growth defect of both *sodF* mutant in NA plate and *sodN* mutant in 50uM nickel treated NA plate results from double mutant effect of *sodF* and *sodN*. These data show that both SOD (Fe-SOD and Ni-SOD) are very important to *S. coeliclor* and if cells can not use both SOD and they can't live well. In addition, this nickel sensitivity test replects that Nur activates *sodN* expression through inhibiting the synthesis of *sodF* mRNA.

III.1.8.2. Responsive level of *sod* transcription to nickel

We tracked change of *sod* transcripts in response to nickel. M145 cells were grown in YEME to mid-exponential phase (OD600 0.614) and we treated 50uM $NiSO_4$. At 0, 10, 20, 30, 40, 50 and 60 min after nickel treatment, cells were harvested and RNA samples were analyzed by S1 mapping. *sodF* mRNA rapidly decrease after 10min and s-SodF more slowly decreased compared to *sodF* mRNA (Fig. III-19). In contrast, *sodN* mRNA increased after 30min nickel treatment (Fig. III-19). *nur* transcript is equal in all the time of experiment (Fig. III-19). This kinetic data reflects regulation order of *sod* genes in *S. coelicolor*. First, *sodF* mRNA is transcribed and s-SodF is processed from long *sodF* mRNA by unknown mechanism and then s-SodF finally binds to 5′ end of *sodN* mRNA and

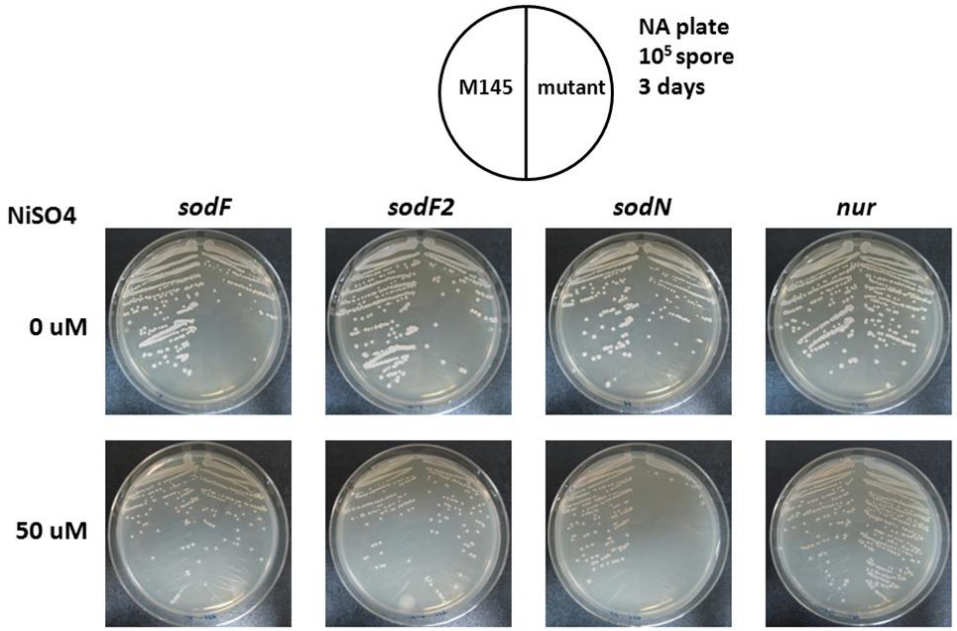

Fig. III-18. Nickel sensitivity test of various mutants in NA plate.

10^5 spores are streaked on NA plate containing either 50uM NiSO4 or not

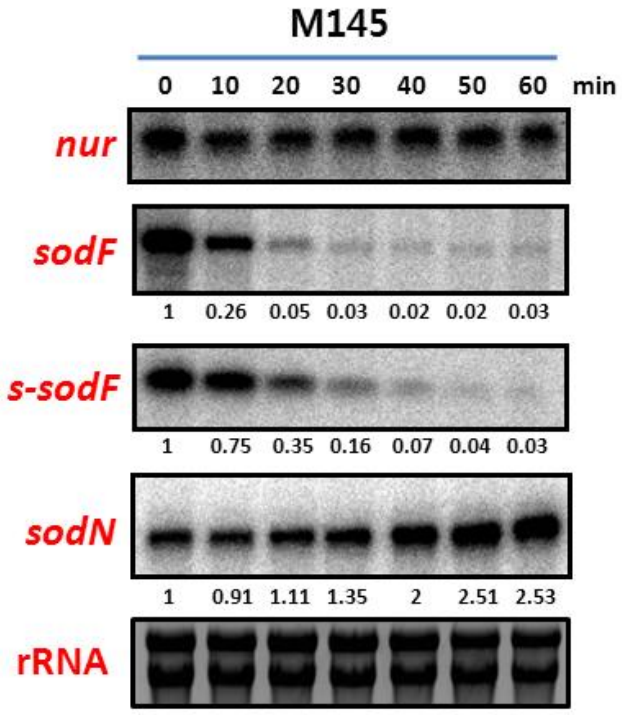

Fig. III-19. Responsive level of SODs transcription to nickel

nur and *sod* genes expression in 10 min time interval after addition of 50uM nickel

Fig. III-20. A model for Nur-dependent inverse regulation of *sodF* and *sodN*

This model describes that the small processed *sodF* RNA negatively regulates the translation and stability of *sodN* mRNA, enabling the antagonistic regulation of *sodN* and *sodF* genes through nickel-specific Nur. Under nickel-limited conditions, Nur without nickel loses its binding activity to *sodF* promoter. Induction of *sodF* gene transcription ensues, producing full length *sodF* mRNA, from which a 90 nt-long 3′ UTR segment that contains anti-*sodN* sequence of 19 nt can be cleaved off to function as a stable small regulatory RNA (s-SodF). The s-SodF RNA is able to form perfect base pairing with the 5′ end segment of *sodN* mRNA by up to 18 bp. The base-pairing can inhibit translation by occluding ribosome binding, and facilitates degradation of *sodN* mRNA, resulting in rapid decrease in the production of Ni-SOD.

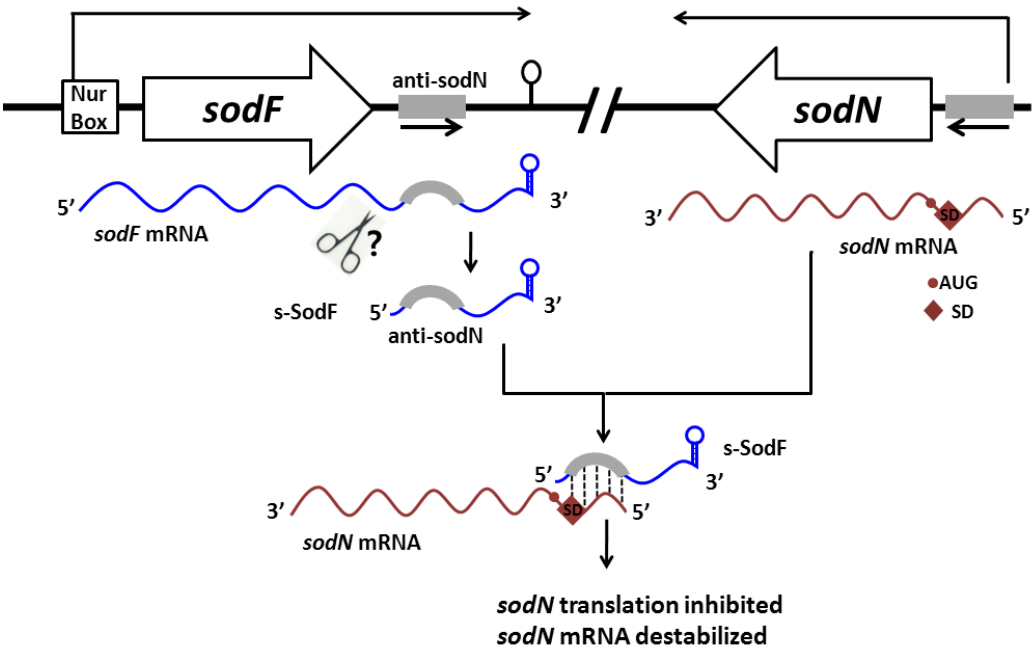
Nur Box
sodF
anti-sodN
sodN
5′
sodF mRNA
3′
?
s-SodF
5′
3′
anti-sodN
3′
SD
5′
sodN mRNA
AUG
SD
s-SodF
5′
3′
3′
SD
5′
sodN mRNA
sodN translation inhibited
sodN mRNA destabilized

regulates *sodN* mRNA stability.

III.2. Determination of critical residues for Nur activity

III.2.1. Prediction of metal coordination ligands of Nur

To predict the metal binding ligands within the Nur protein, phylogenetic relationship among the Nur and other Fur homologues was compared with amino acids (Fig. III-21). 26 representative Fur homologues were selected from BLAST search, using ScoNur, BsuPerR, PaeFur, and MtuFurB as sequence queries. A phylogenetic tree was built by Vector NTITM (Invitrogen) using the Neighbor Joining method (NJ). The distance from the nearest branch point was indicated in parenthesis. The reported name as appears in GenBank was used to designate each protein, whereas uncharacterized homologues were designated as Fur(H). Abbreviations used to indicate source bacteria are: **Sco**, *Streptomyces coelicolor*; **Sav**, *S. avermitilis*; **Ace**, *Acidothermus cellulolyticus*; **Nsp**, *Nocardioides sp*; **Kra**, *Kineococcus radiotolerans*; **Bsu**, *Bacillus subtilis*; **Lin**, *Listeria innocua*; **Sau**, *Staphylococcus aureus*; **Lsa**, *Lactobacillus sakei*; **Pp**e, *Pediococcus pentosaceus*; **Bja**, *Bradyrhizobium japonicum*; **Rle**, *Rhizobium leguminosarum*; **Sme**, *Sinorhizobium meliloti*; **Eco**, *Escherichia coli*; **Ype**, *Yesinia pestis*; **Pae**, *Pseudomonas aeruginosa*; **Xax**, *Xanthomonas axonopodis*; **Mtu**, *Mycobacterium tuberculosis*; **Nfa**, *Nocardia farcinica*; **Rsp**, *Rhodococcus sp*.

To select the appropriate amino acids for metal coordination, multiple sequence alignment of 26 Fur homologues was carried by Clustal W program in Vector NTI package (Fig. III-22). The residue numbers for ScoNur were given on top line, along with an arrangement of secondary structure motifs as described in Fig. III-23. Conserved residues were indicated with different color blocks. Position of residues for Ni-site, M-site and Cys4-Zn site in ScoNur was indicated by filled and open arrowheads, respectively, on top of residue numberings. Position of metal-binding residues for PaeFur, MtuFurB, and apo-PerR whose structures

Fig. III-21. Comparison of subgroups in Fur family members.

Phylogenetic relationship among Nur and other Fur homologues. 26 representative Fur homologues were selected from BLAST search, using ScoNur, BsuPerR, PaeFur, and MtuFurB as sequence queries. A phylogenetic tree was built by Vector NTI™ (Invitrogen) using the Neighbor Joining method (NJ). The distance from the nearest branch point was indicated in parenthesis. The reported name as appears in GenBank was used to designate each protein, whereas uncharacterized homologues were designated as Fur(H). Abbreviations used to indicate source bacteria are: Sco, *Streptomyces coelicolor*; Sav, *S. avermitilis*; Ace, *Acidothermus cellulolyticus*; Nsp, *Nocardioides sp*; Kra, *Kineococcus radiotolerans*; Bsu, *Bacillus subtilis*; Lin, *Listeria innocua*; Sau, *Staphylococcus aureus*; Lsa, *Lactobacillus sakei*; Ppe, *Pediococcus pentosaceus*; Bja, *Bradyrhizobium japonicum*; Rle, *Rhizobium leguminosarum*; Sme, *Sinorhizobium meliloti*; Eco, *Escherichia coli*; Ype, *Yesinia pestis*; Pae, *Pseudomonas aeruginosa*; Xax, *Xanthomonas axonopodis*; Mtu, *Mycobacterium tuberculosis*; Nfa, *Nocardia farcinica*; Rsp, *Rhodococcus sp*.

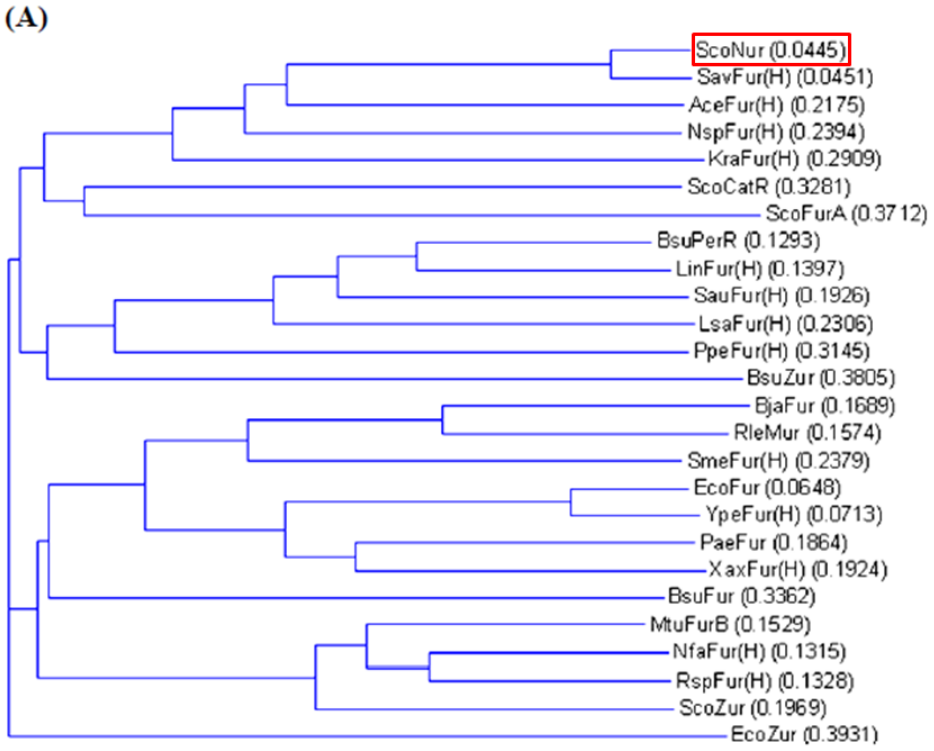
(A)
ScoNur (0.0445)
SavFur(H) (0.0451)
AceFur(H) (0.2175)
NspFur(H) (0.2394)
KraFur(H) (0.2909)
ScoCatR (0.3281)
ScoFurA (0.3712)
BsuPerR (0.1293)
LinFur(H) (0.1397)
SauFur(H) (0.1926)
LsaFur(H) (0.2306)
PpeFur(H) (0.3145)
BsuZur (0.3805)
BjaFur (0.1689)
RleMur (0.1574)
SmeFur(H) (0.2379)
EcoFur (0.0648)
YpeFur(H) (0.0713)
PaeFur (0.1864)
XaxFur(H) (0.1924)
BsuFur (0.3362)
MtuFurB (0.1529)
NfaFur(H) (0.1315)
RspFur(H) (0.1328)
ScoZur (0.1969)
EcoZur (0.3931)

Fig. III-22. Multiple sequence alignment of 26 Fur homologues was carried by Clustal W program in Vector NTI package.

The residue numbers for ScoNur were given on top line, along with an arrangement of secondary structure motifs as described in Fig. III-23. Conserved residues were indicated with different color blocks. Position of residues for Ni-site, M-site and Cys4-Zn site in ScoNur was indicated by filled and open arrowheads, respectively, on top of residue numberings. Position of metal-binding residues for PaeFur, MtuFurB, and apo-PerR whose structures were determined by crystallography was indicated with colored boxes for comparison. Red and blue boxes for PaeFur are for those corresponding to inter-domain M-site (structural □ ; His32, Glu80, His 89 and Glu 100) and Fe-site (regulatory □ ; His86, Asp88, Glu107 and His124), respectively. For MtuFurB, pink box □ marks for M-site I (Asp62, Cys76, His81 and His83), black box for M-site III (His80, 82, Glu101 and His118), and orange box □ for Cys4-Zn site (Cys86, 89, 126 and 129). For apo-PerR, orange boxes mark □ for the Cys4-Zn site (C96, C99, C136, C139).

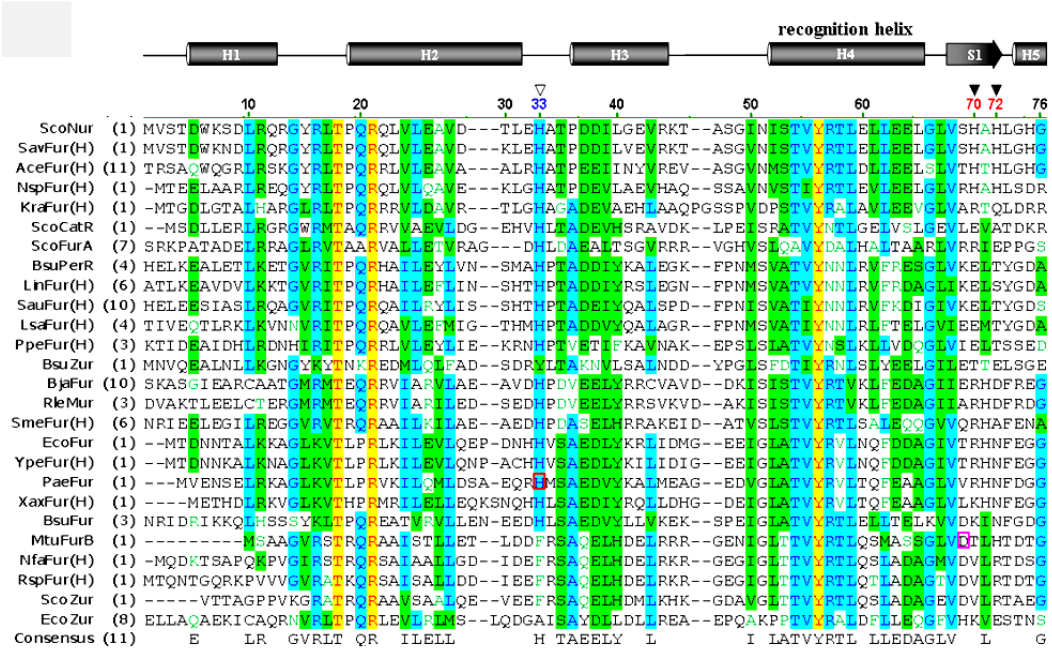
recognition helix
H1
H2
H3
H4
S1
H5
ScoNur (1) MVSTDWKSDLRQRGYRLTPQRQLVLEAVD---TLEHATPDDILGEVRKT--ASGINISTVYRTLELLEELGLVSHAHLGHG
SavFur(H) (1) MVSTDWKNDLRQRGYRLTPQRQLVLEAVD---KLEHATPDDILVEVRKT--ASGVNISTVYRTLELLEELGLVSHAHLGHG
AceFur(H) (11) TRSAQWQGRLRSKGYRLTPQRRLVLEAVA---ALRHATPEEIINYVREV--ASGVNMSTVYRTLDLLEELSLVTHTHLGHG
NspFur(H) (1) -MTEELAARLREQGYRLTPQRQLVLQAVE---KLGHATPDEVLAEVHAQ--SSAVNVSTIYRTLEVLEELGLVRHAHLSDR
KraFur(H) (1) -MTGDLGTALHARGLRLTPQRRVLDAVR---TLGHAGADEVAEHLAAQPGSSPVDPSTVYRALAVLEEVGLVARTQLDRR
ScoCatR (1) --MSDLLERLFGRGWRMTAQRRVVAEVLDG--EHVHLTADEVHSRAVDK--LPEISRATVYNTLGELVSLGEVLEVATDKR
ScoFurA (7) SRKPATADELRRAGLRVTAARVALLETVRAG---DHLDAEALTSGVRRR--VGHVSLQAVYDALHALTAARLVRRIEPPGS
BsuPerR (4) HELKEALETLKETGVRITPQRHAILEYLVN--SMAHPTADDIYKALEGK--FPNMSVATVYNNLRVFRESGLVKEITYGDA
LinFur(H) (6) ATLKEAVDVLKKTGVRITPQRHAILEFLIN--SHTHPTADDIYRSLEGN--FPNMSVATVYNNLRVFRDAGLIKELSYGDA
SauFur(H) (10) HELEESIASLRQAGVRITPQRQAILRYLIS--SHTHPTADEIYQALSPD--FPNISVATIYNNLRVFKDIGIVKELTYGDS
LsaFur(H) (4) TIVEQTLRKLKVNNVRITPQRQAVLEFMIG--THMHPTADDVYQALAGR--FPNMSVATIYNNLRLFTELGVIEEMTYGDA
PpeFur(H) (3) KTIDEAIDHLRDNHIRITPQRRLVLEYLIE--KRNHPTVETIFKAVNAK--EPSLSLATVYNSLKLLVDQGLVIELTSSED
BsuZur (1) MNVQEALNLLKGNGYKYTNKREDMLQLFAD--SDRKLTAKNVLSALNDD--YPGLSFDTIYRNLSLYEELGILETTELSGE
BjaFur (10) SKASGIEARCAATGMRMTEQRRVIARVLAE--AVDHPDVEELYRRCVAVD--DKISISTVYRTVKLFEDAGIIERHDFREG
RleMur (3) DVAKTLEELCTERGMRMTEQRRVIARILED--SEDHPDVEELYRRSVKVD--AKISISTVYRTVKLFEDAGIIARHDFRDG
SmeFur(H) (6) NRIEELEGILREGGVRVTRQRAAILKILAE--AEDHPDASELHRRAKEID--ATVSLSTVYRTLSALEQQGVVQRHAFENA
EcoFur (1) --MTDNNTALKKAGLKVTLPRLKILEVLQEP-DNHHVSAEDLYKRIIDMG--EEIGLATVYRVLNQFDDAGIVTRHNFEGG
YpeFur(H) (1) --MTDNNKALKNAGLKVTLPRLKILEVLQNP-ACHHVSAEDLYKIIIDIG--EEIGLATVYRVLNQFDDAGIVTRHNFEGG
PaeFur (1) ---MVENSELRKAGLKVTLPRVKILQMLDSA-EQRHMSAEDVYKALMEAG--EDVGLATVYRVLTQFEAAGLVVRHNFDGG
XaxFur(H) (1) ----METHDLRKVGLKVTHPRMRILELLEQKSNQHHLSAEDIYRQLLDHG--DEIGLATVYRVLTQFEAAGLVLKHNFEGG
BsuFur (3) NRIDRIKKQLHSSSYKITPQREATVRVLLEN-EEDHLSAEDVYLLVKEK--SPEIGLATVYRTLELLTELKVVDKINFGDG
MtuFurB (1) ----------MSAAGVRSTRQRAAISTLLET--LDDFRSAQELHDELRRR--GENIGLTTVYRTLQSMASSGLVDTLHTDTG
NfaFur(H) (1) -MQDKTSAPQKPVGIRSTRQRSAIAALLGD--IDEFRSAQELHDELRKR--GEGIGLTTVYRTLQSLADAGMVDVLRTDSG
RspFur(H) (1) MTQNTGQRKPVVVGVRATKQRSAISALLDD--IEEFRSAQELHDELRKR--GEGIGLTTVYRTLQTLADAGTVDVLRTDTG
ScoZur (1) -----VTTAGPPVKGRATRQRAAVSAALQE--VEEFRSAQELHDMLKHK--GDAVGLTTVYRTLQSLADAGEVDVLRTAEG
EcoZur (8) ELLAQAEKICAQRNVRLTPQRLEVLRLMS--LQDGAISAYDLLDLLREA--EPQAKPPTVYRALDFLLEQGFVHKVESTNS
Consensus (11) E LR GVRLT QR ILELL H TAEELY L I LATVYRTL LLEDAGLV L G

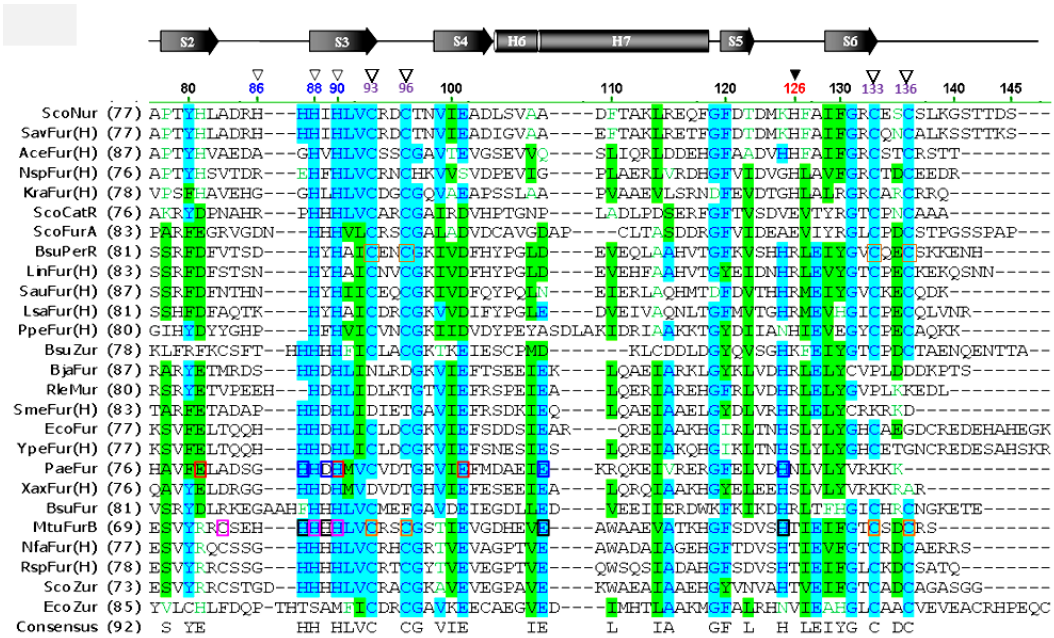
S2
S3
S4
H6
H7
S5
S6
ScoNur (77) APTYHLADRH---HHIHLVCRDCTNVIEADLSVAA----DFTAKLREQFGFDTDMKHFAIFGRCESCSLKGSTTDS---
SavFur(H) (77) APTYHLADRH---HHIHLVCRDCTNVIEADIGVAA----EFTAKLRETFGFDTDMKHFAIFGRCQNCALKSSTTKS---
AceFur(H) (87) APTYHVAEDA---GHVHLVCSSCGAVTEVGSEVVQ----SLIQRLDDEHGFAADVHHFAIFGRCSTCRSTT--------
NspFur(H) (76) APTYHSVTDR---EHFHLVCRNCHKVVSVDPEVIG----PLAERLVRDHGFVIDVGHLAVFGRCTDCEEDR--------
KraFur(H) (78) VPSFHAVEHG---GHLHLVCDGCGQVAEAPSSLAA----PVAAEVLSRNDFEVDTGHLALRGRCARCRRQ---------
ScoCatR (76) AKRYDPNAHR---PHHHLVCARCGAIRDVHPTGNP----LADLPDSERFGFTVSDVEVTYRGTCPNCAAA---------
ScoFurA (83) PARFEGRVGDN---HHHVLCRSCGALADVDCAVGDAP----CLTASDDRGFVIDEAEVIYRGLCPDCSTPGSSPAP---
BsuPerR (81) SSRFDFVTSD----HYHAICENCGKIVDFHYPGLD----EVEQLAAHVTGFKVSHHRLEIYGVCQECSKKENH------
LinFur(H) (83) SSRFDFSTSN----HYHAICNVCGKIVDFHYPGLD----EVEHFAAHVTGYEIDNHRLEVYGTCPECKEKQSNN-----
SauFur(H) (87) SSRFDFNTHN----HYHIICEQCGKIVDFQYPQLN----EIERLAQHMTDFDVTHHRMEIYGVCKECQDK---------
LsaFur(H) (81) SSHFDFAQTK----HYHAICDRCGKVVDIFYPGLE----DVEIVAQNLTGFMVTGHRMEVHGICPECQLVNR-------
PpeFur(H) (80) GIHYDYYGHP----HFHVICVNCGKIIDVDYPEYASDLAKIDRIAAKKTGYDIIANHLEVEGYCPECAQKK--------
BsuZur (78) KLFRFKCSFT--HHHHHFICLACGKTKEIESCPMD--------KLCDDLDGYQVSGHKFEIYGTCPDCTAENQENTTA--
BjaFur (87) RARYETMRDS---HHDHLINLRDGKVIEFTSEEIEK----LQAEIARKLGYKLVDHRLELYCVPLDDDKPTS-------
RleMur (80) RSRYETVPEEH---HDHLIDLKTGTVIEFRSPEIEA----LQERIAREHGFRIVDHRLELYGVPLKKEDL---------
SmeFur(H) (83) TARFETADAP---HHDHLIDIETGAVIEFRSDKIEQ----LQAEIAAELGYDLVRHRLELYCRKRKD------------
EcoFur (77) KSVFELTQQH---HHDHLICLDCGKVIEFSDDSIEAR----QREIAAKHGIRLTNHSLYLYGHCAEGDCREDEHAHEGK
YpeFur(H) (77) KSVFELTQQH---HHDHLICLDCGKVIEFSNESIES----LQREIAKQHGIKLTNHSLYLYGHCETGNCREDESAHSKR
PaeFur (76) HAVEELADSG---EHDHMVCVDTGEVIEFMDAEIE----KRQKEIVRERGFELVDHNLVLYVRKKK-------------
XaxFur(H) (76) QAVYELDRGG---HHDHMVDVDTGHVIEFESEEIEA----LQRQIAAKHGYELEEHSLVLYVRKKRAR-----------
BsuFur (81) VSRYDLRKEGAAHFHHHLVCMEFGAVDEIEGDLLED----VEEIIERDWKFKIKDHRLTFHGICHRCNGKETE------
MtuFurB (69) ESVYRRQSEH---EHEHLVCRSQGSTIEVGDHEVE----AWAAEVATKHGFSDVSHTLEIFGTCSDCRS----------
NfaFur(H) (77) ESVYRQCSSG---HHHHLVCRHCGRTVEVAGPTVE----AWADAIAGEHGFTDVSHTIEVFGTCRDCAERRS-------
RspFur(H) (78) ESVYRRCSSG---HHHHLVCRTCGYTVEVEGPTVE----QWSQSIADAHGFSDVSHTIEIFGLCKDCSATQ--------
ScoZur (73) ESVYRRCSTGD--HHHHLVCRACGKAVEVEGPAVE----KWAEAIAAEHGYVNVAHTVEIFGTCADCAGASGG------
EcoZur (85) YVLCHLFDQP-THTSAMFICDRCGAVKEECAEGVED----IMHTLAAKMGFAIRHNVIEAHGLCAACVEVEACRHPEQC
Consensus (92) S YE HH HLVC CG VIE IE L IA GF L H LEIYG C DC

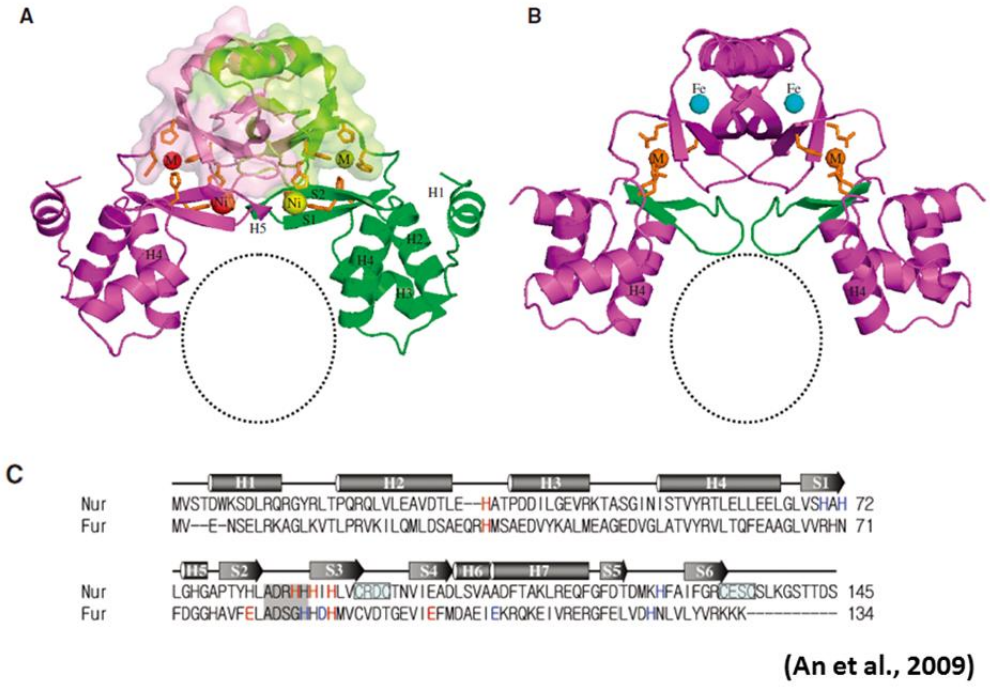

Fig. III-23. Structure of Nur and metal sites.

(A)Ribbon diagram of Nur with the dimeric core veiled by transparent surface. Nickel ions and metal coordinating residues are represented by spheres and sticks, respectively. M and Ni indicate M- and Ni-sites, respectively. A black circle indicates the plausible DNA-binding site. For clarity, secondary structure elements only for DB-domain are labeled. (B)Ribbon diagram of PaFur. M and Fe indicate M- and Fe-sites, respectively. The S1–S2 sheets are in green. Zinc ions and residues of M-site are shown by spheres and sticks, respectively. A black circle indicates the plausible DNA-binding site. (C) A structure-based sequence alignment of Nur with PaFur. Red and blue letters in theNur (PaFur) sequence indicate residues of M- and Ni (Fe)-site, respectively. The hinge region is dark shaded. Two Cys-X-X-Cys motifs are boxed.

were determined by crystallography was indicated with colored boxes for comparison. Red and blue boxes for PaeFur are for those corresponding to inter-domain M-site (structural □ ; His32, Glu80, His 89 and Glu 100) and Fe-site (regulatory □ ; His86, Asp88, Glu107 and His124), respectively. For MtuFurB, pink box □ marks for M-site I (Asp62, Cys76, His81 and His83), black box for M-site III (His80, 82, Glu101 and His118), and orange box □ for Cys4-Zn site (Cys86, 89, 126 and 129). For apo-PerR, orange boxes mark □ for the Cys4-Zn site (C96, C99, C136, C139).

III.2.2. Crystal structure of Nur

We reported the crystal structure of Nur in 2009 (An et al. 2009). Nur is a homodimer like other Fur family members (Fig. III-23A). In crystal structure, two DNA-binding domains (DB-domain) are attached to the dimeric core constructed by two dimerization domains (D-domain). The triangular dimeric conformation of Nur with two closely located DB-domains resembles that of PaFur (Fig. III-23B), and this conformation represents the DNA-binding competent conformation. DB-domain (residues 1–82) consists of four helices and two strands (H1-4 and S1-2; Fig. III-23). Except an N-terminal helix (H1), three helices (H2-H4) form the typical type of the winged helix motif. The last helix (H4), which could make specific contacts with bases in the major groove of DNA, is called a 'recognition helix'(Fig. III-23A). D-domain (residues 88–145) folds as a simple α/β structure (Fig. III-23A) and a loop of residues 83–87 is the hinge region connecting the two domains (Fig. III-23C). The domain structures of Nur are similar to those of PaFur, BsPerR and MtFurB as already predicted from their sequence homology (Fig. I-2, data not shown).

III.2.3. Metal binding sites of Nur

III.2.3.1. Metal-site (M-site)

In previous study, the metal contents of Nur were analyzed by ICP-AES and the result indicates that one molecule of Nur contains one nickel and one zinc atom (data not shown). In crystal structure, Nur has two metal binding sites; one is a metal-binding nonspecific site (M-site) and the other is a nickel-specific metal binding site (Ni-site) in each monomer and both sites were occupied by nickel. M-site is located in the domain interface and is constructed by His33, His86, His88, and His90 (Fig. III-24). Here nickel is coordinated by four nitrogen atoms of the four histidines with a square-planar geometry, one of the preferred coordination geometries for nickel (Rulisek and Vondrasek 1998). Interestingly, M-site seems to be able to accommodate zinc, too. In a zinc MAD data, the zinc position was nearly identical to the nickel position of M-site. This suggests that zinc is compatible with a relatively low nickel-occupancy at M site. Actually, among Nur proteins in crystals, most proteins have nickel but some have zinc at this site. It is probable that the addition of $NiCl_2$ to crystallization conditions might have caused nickel preponderance at M-site in Nur crystals (An et al. 2009). Other Fur family members have a metal site with affinity for various divalent cations whose location is similar to M-site (Giedroc and Arunkumar 2007). Especially, in the crystal structure of PaFur (Pohl et al. 2003), zinc is located at a position that is nearly identical to the nickel position in M-site of Nur (Fig. III-23).

III.2.3.2. Ni-site

In contrast to M-site, Ni-site has never been observed in other Fur family structures, suggesting that this Ni-site is the unique metal site of Nur. Ni-site resides at the domain interface and is constructed His70 and His72 in DB-domain and His126 in D-domain participate in metal coordination at this site (Fig. III-

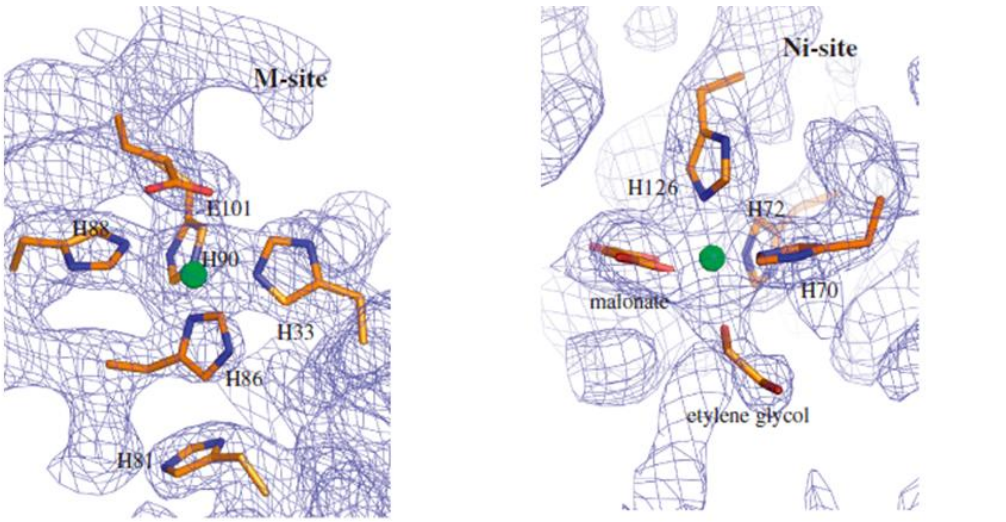

(An et al., 2009)

Fig. III-24. M-site and Ni-site of Nur

Stereo view of the final *2Fo – Fc* electron density maps contoured at 1σ, showing M- and Ni-sites. Ni and Ni-coordinating residues are shown in spheres and sticks, respectively.

23,24). Three nitrogen atoms from the histidines and three oxygen atoms from malonate and ethylene glycol, coordinate a nickel ion with an octahedral geometry (Fig. III-24). The oxygen contributors would be water molecules in vivo. Compared with M-site for an affinity for zinc, Ni-site site probably prefers nickel rather than zinc and this site is highly occupied by nickel in crystal structure. A crystal of Nur was transferred to a crystallization solution containing $ZnCl_2$ instead of $NiCl_2$. We repeated this procedure five times for 4 h, collected a Ni-MAD data set with the transferred crystal and the position of nickel ions was identified using the SOLVE program (An et al. 2009). Interestingly, Ni-site still contains a nickel ion. Nur seems to be exquisitely selective for nickel.

In the Fur superfamily, only Nur orthologs appear to have the horizontal S1–S2 sheets (Fig. III-23A). In addition, three histidine residues constituting Ni-site which is located in S1-S2 sheets are conserved only in Nur orthologs (Fig. III-22), indicating that other Fur family members do not contain metal-binding sites that correspond to Ni-site in Nur. Therefore, the S1–S2 sheets in other Fur subfamilies possibly adopt the slant conformation like PaFur (Fig. III-23B), which allows contact with bases in the central minor groove on complex formation. Nickel specificity of Ni-site, coupled with the affinity of M-site for zinc, strongly suggests that Ni-site is critical for the nickel responsive activation of Nur.

III.2.3.3. Possible Zinc binding site (two Cys-X-X-Cys motif)

There are two Cys-X-X-Cys motifs in the primary structure of Nur (Fig. III-23C) and this could be related to the existence of zinc (Cys4-Zn) the coordinated by four cysteine residues (Lee and Helmann 2006; Traore et al. 2006). In the case of BsuPerR, the zinc coordination by four cysteines in the motifs was suggested to be critical to stabilize their dimerization domain and hence their dimeric structures, indicating the structural role of Cys4-Zn (Traore et al. 2006). However, there is no Cys4-Zn coordinated by four cysteines of two Cys-X-X-Cys motifs in

Nur crystal structure. The absence of Cys4-Zn is not caused by the oxidation of cystein residues because crystals of Nur were grown in reducing conditions. In spite of absence of Cys4-Zn, Nur maintains the dimeric conformation (An et al. 2009)(Fig. III-23). Cys4-Zn seems not to be essential for maintaining the DNA-competent conformation of Nur (Fig. III-23A). Considering the zinc avidity of the Cys-X-X-Cys motif and the abundance of zinc ions, Nur could have zinc ions bound at this site in vivo.

III.2.4. Verification of the various metal binding residues in Nur in vitro

III.2.4.1. Various Nur protein expression in *E. coli*

To verify the various metal binding residues, Nur ORF region was constructed in pET-3a using NdeI/BamHI site. This construct was named as pET3aNur. And then selected target amino acids were exchanged into Ala by site directed mutagenesis, respectively. Mutated clones were checked by sequencing. First of all, to check the in vitro effects of various Nur variants, pET3aNur plasmids were transformed into *E. coli* BL21 (DE3) pLysS cells. And then, overexpression efficiency of various Nur variants was tested by IPTG induction. BL21 harboring pET3aNur were grown in 3ml LB to OD600 of 0.5 and induced with 1mM IPTG (isopropyl-1-thio-β-D-galactopyranoside) for 2hr. After harvest, cells were resuspended in 30ul 1X SDS loading buffer. Resuspended samples were analyzed on 15% SDS-PAGE and protein bands are visualized by coomassie staining (data not shown).

III.2.4.2. The binding activity of Nur variants in vitro

The DNA binding activity of various Nur variants was checked by electrophoretic mobility shift assay with overexpressed *E. coli* crude extracts with

additional 100uM nickel treatment. In Fig. III-25, H88A and H90A mutants showed no DNA binding activity, indicating that His88 and His90 residues are critical in constructing M-site. H33A exhibited significantly reduced binding, whereas H86A did not affect DNA binding greatly. It is possible that the absence of one histidine residue like His86 cannot disrupt M-site. In such a mutant protein, a water molecule or a nearby residue such as His81 could possibly participate in metal coordination (Fig. III-24).

In Fig. III-26, His70, His72 and His126 constructing Ni-site are all essential for the maintenance of Ni-site because their respective mutant proteins (H70A, H72A and H126A) exhibited nearly no DNA-binding activity of *sodF* promoter.

Two Cys-X-X-Cys motifs mutants (C93S, C96S, C133S and C136S) can bind to *sodF* promoter well compared to WT (Fig. III-27). This data shows that Cys4-Zn appears not to be essential for the DNA-binding activity of Nur.

All together, these DNA binding data of three metal binding site (M-site, Ni-site and Cys4-Zn site) greatly match with crystal structure of Nur.

III.2.5. Verification of the various metal binding residues in Nur in vivo

III.2.5.1. Various Nur protein expression in *S. coelicolor*

Various pSET162::p*nur-nur* were constructed by II.7 in method section. These Mutated clones were checked by sequencing. To verify the various metal binding residues in vivo, pSET162::p*nur-nur* were introduced into the *Δnur* mutant cell by conjugal gene transfer. Conjugated single spores were selected on replica plates containing antibiotics and the confirmation of the gene integration into the choromosome was checked by genomic DNA PCR and sequencing (data not shown). Each complemented strains were grown to early exponential phase in YEME medium containing 10.3% sucrose.

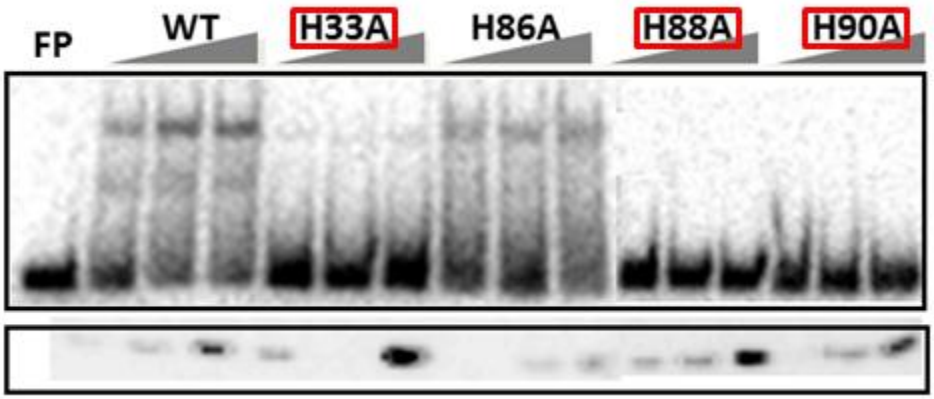

Fig. III-25. DNA-binding activity of Nur variants with substitution mutations of M-site residues.

Electrophoretic mobility shift assay was performed for binding between the *sodF* promoter DNA fragment and cell extracts containing either wild-type or mutant Nur proteins with H33A, H86A, H88A and H90A mutations. For each Nur variant, three separate reactions with increasing amounts of cell extracts were examined, along with the assessment of Nur protein levels by western blot analysis (lower panel). FP indicates a sample with free probe only.

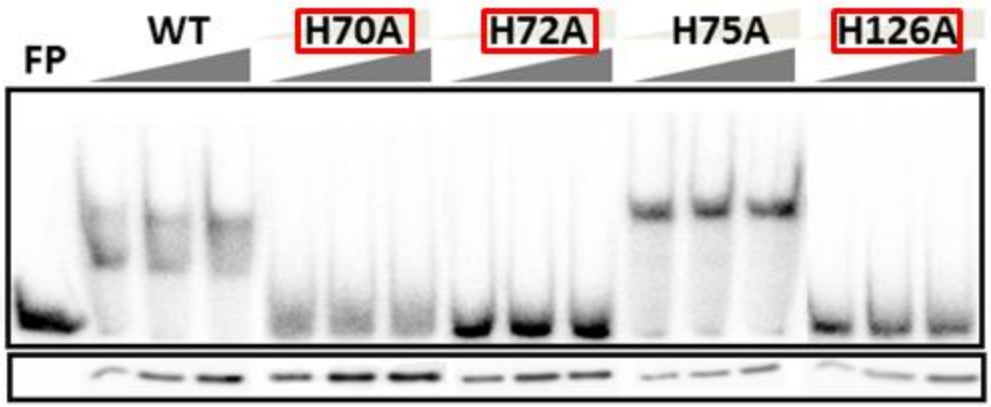

Fig. III-26. DNA-binding activity of Nur variants with substitution mutations of Ni-site residues.

Nur variants with H70A, H72A and H126A mutations were examined as described in Fig. III-25. H75A mutant was examined in parallel for comparison.

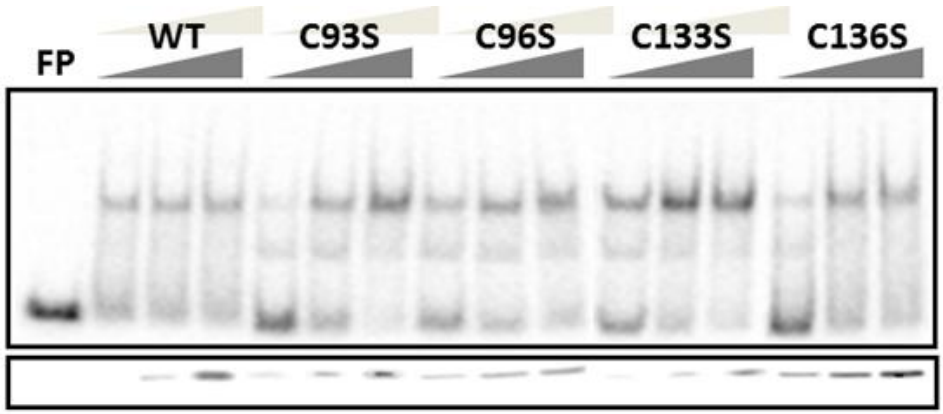

Fig. III-27. DNA-binding activity of Nur variants with substitution mutations of four cystein residues.

Nur variants with C93S, C96S, C133S and C136S mutations were examined as described in Fig. III-25

III.2.5.2. The complementation effects of various Nur variant proteins in vivo

The complementation effects of various Nur variant proteins were analyzed by S1 mapping assay with *sodF* DNA probes. To select the metal coordination residues, repression level of *sodF* gene was compared to WT in nickel-supplement condition. In Fig. III-28, the *sodF* gene expression did not repressed in several Nur variants containing cell; H72A, H126A, C96S, C133S and C136S. In case of H72A and H126A which consist of Ni-site of Nur, these Nur variants did not repressed well *sodF* gene in nickel treated condition and this is the same result with in vitro data. This result shows that these two histidine residues (His72, His126) of Nur are important for appropriate function in vitro and in vivo. That is, nickel coordination to Ni-site is very important for Nur in vitro and in vivo.

Unexpected, H33A, H86A, H88A and H90A which consist of M-site of Nur could repressed *sodF* gene very well compared to WT Nur and this in vivo result indicates that M-site is not critical to repressor function of Nur in vivo.

Furthermore, the C93S, C96S, C133S and C136S mutations did not affect the DNA-binding activity of Nur in vitro (Fig. III-27), but interestingly, in vivo results of four cystein mutants shows the difference result to compare the in vitro results. In S1 data, C96S partially could not repress *sodF* gene and C133S and C136S entirely could not repress *sodF* gene (Fig. III-28). This data indicates that cystein residues (Cys96, Cys133 and C136S) of Nur seems to be important for function of Nur in vivo.

III.2.5.3. The binding activity of Nur variants in vivo

To investigate critical residues for DNA binding activity of Nur in vivo and to explain the difference between in vitro data and in vivo data, we did EMSA

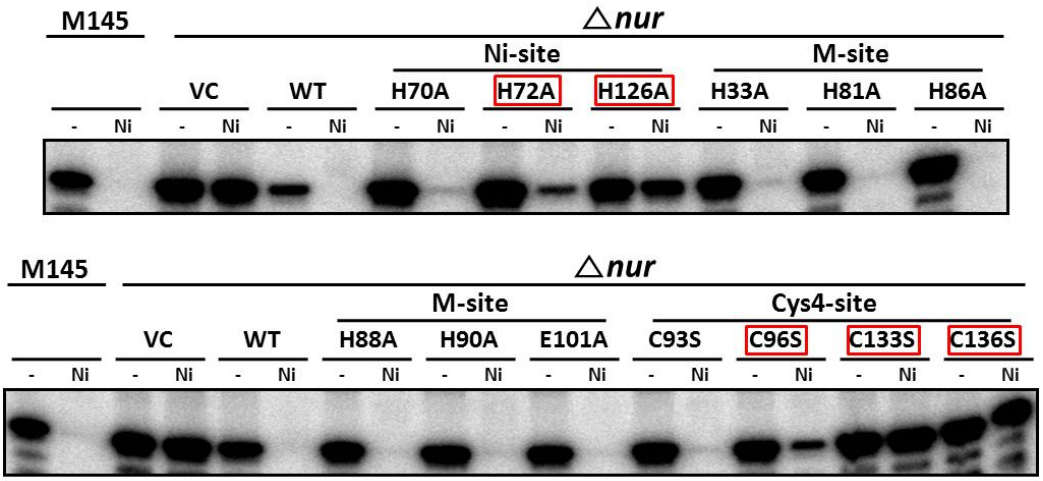

Fig. III-28. Target gene repression activity of Nur variants in vivo.

S1 mapping of *sodF* RNA in Nur variants complementation strains. RNAs were prepared from the wild type (M145) and △*nur::162*::p*nur-nur* strains grown in the presence and absence of 50 μM $NiSO_4$.

using *S. coelicolor* cell extract. *S. coelicolor* cell extracts were obtained in 50uM $NiSO_4$ treated YEME. Unlike in EMSA with *E. coli* cell extract, all binding buffer, gel running buffer were made without EDTA for avoiding metal chelation (Table. III-1).

Interestingly, H86A and H88A which consist of M-site exhibited no binding defect (Fig. III-29). H72A and H126A which construct Ni-site exhibited slightly and significantly reduced binding to *sodF* promoter, respectively (Fig. III-30). C96S, C133S and C136S which seems to be coordinate zinc exhibited significantly reduced binding to *sodF* promoter (Fig. III-31). This difference of binding degree in EMSA among Nur variants greatly matches with repression degree in S1 mapping in vivo and it means that there is a direct correlation between EMSA (in vitro) and S1(in vivo) data in *S.coelicolor*.

These data shows that Ni-site and Cys4-Zn site are both critical for maintenance activity of Nur in vivo.

III.3. Overall prospect about Nur

In this study, we investigated the antagonistic regulation of *sodF* and *sodN* is achieved through Nur and metal binding site of Nur. We found that a small regulatory RNA is produced from *sodF* mRNA by endonucleolytic cleavage of about 90 nt from its 3'UTR. This provides a novel example of small regulatory RNA produced from the 3'UTR of functional mRNA by cleavage. Very recently, the presence of 3'UTR-generated processed small RNAs associated with Hfq in *Salmonella* has been demonstrated (Chao et al. 2012; Kroger et al. 2012). However, their role as regulatory molecules, rather than intermediates in mRNA degradation pathway, awaits experimental validation. We now present the first example of a small regulatory RNA that is generated from the 3'UTR of a functional mRNA without affecting its coding region. These findings led us to

Probe	*sodF* 90bp	*sodF* 90bp
Protein	*E. coli* cell extract (Nur overexpression using PET system)	*S.coelicolor* cell extract (YEME + 50uM NiSO4)
Binding buffer	4mM Tris-HCl , 1mM EDTA, 4mM DTT, 5mM MgCl2. 20mM KCl, 0.3mg/ml BSA, 10% Glycerol	4mM Tris-HCl , 1mM DTT, 5mM MgCl2. 20mM KCl, 0.3mg/ml BSA, 5% Glycerol (no EDTA)
Metal	Ni 100uM	Ni 100uM / Zn 100uM
Gel running	TBE gel/ TBE buffer running	TB gel / TB buffer running

Table III-1. Comparison of EMSA condition

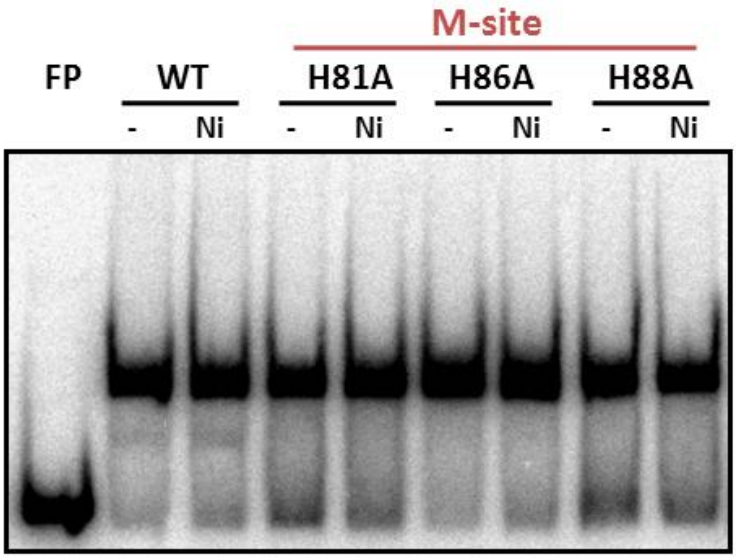

Fig. III-29. DNA-binding activity of Nur variants with substitution mutations of M-site residues.

Electrophoretic mobility shift assay was performed for binding between the *sodF* promoter DNA fragment and *S. coelicolor* cell extracts containing either wild-type or mutant Nur proteins with H81A, H86A and H88A mutations. FP indicates a sample with free probe only.

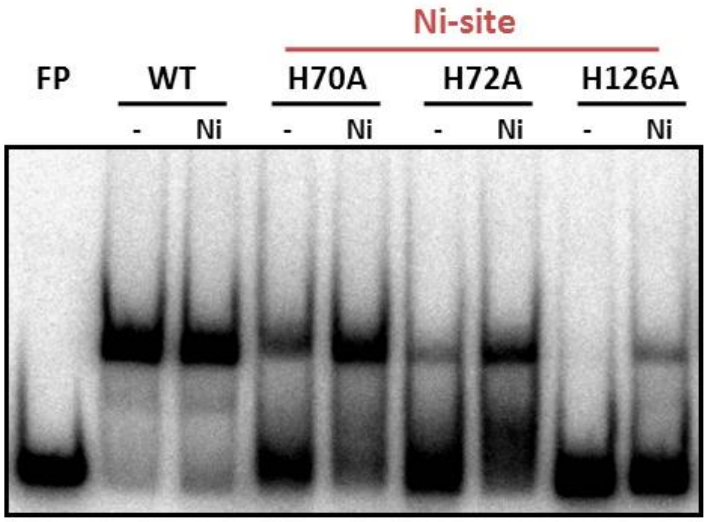

Fig. III-30. DNA-binding activity of Nur variants with substitution mutations of Ni-site residues.

Electrophoretic mobility shift assay was performed for binding between the *sodF* promoter DNA fragment and *S. coelicolor* cell extracts containing either wild-type or mutant Nur proteins with H70A, H72A and H126A mutations. FP indicates a sample with free probe only.

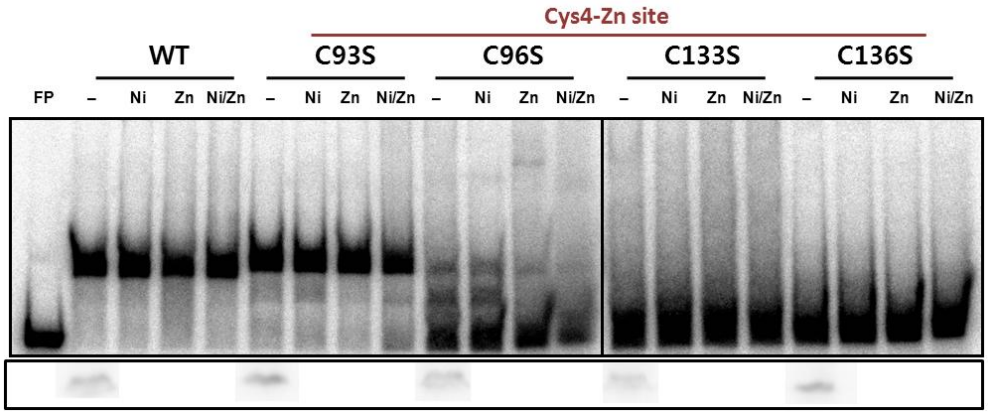

Fig. III-31. DNA-binding activity of Nur variants with substitution mutations of Cys4-Zn site residues.

Electrophoretic mobility shift assay was performed for binding between the *sodF* promoter DNA fragment and *S. coelicolor* cell extracts containing either wild-type or mutant Nur proteins with C93S, C96S, C133S and C136S mutations. FP indicates a sample with free probe only.

propose a conclusive model where Nur activates *sodN* expression by inhibiting the production of small *sodF* RNA, which pairs with *sodN* mRNA, blocks its translation, and facilitates *sodN* mRNA decay. Study about RNA-binding molecule related to processing s-SodF and general application of s-SodF like regulation of other organism are needed.

We also found that Nur is exquisitely selective for nickel in vitro and in vivo. The exclusive activation of Nur by nickel is absolutely related to the Ni-site. We confirmed this Ni-site is essential for Nur in vivo. We also showed the possibility which two Cys-X-X-Cys motif could coordinate a zinc generating Cys4-Zn in vivo like BsuPerR. Critical residues of Nur deduced from in vitro and in vivo data are in indicated in Table III-2. Detail study about metal binding site of Nur is needed in the future.

			Ni-site			M-site						Cys-4 site			
		WT	H70A	H72A	H126A	H33A	H81A	H86A	H88A	H90A	E101A	C93S	C96S	C133S	C136S
EMSA	*E. coli* cell extr		X	X	X	X	X		X	X					
	S. coeli cell extr			X	X	NT				NT	NT		X	X	X
S1	*S. coeli* RNA			X	X								X	X	X

Table III-2. Functionally important residues of Nur in vitro and in vivo.

Loss of binding activity and repressor function are indicated 'X' (inactive Nur). NT means 'Not Tested'.

CHAPTER IV.

DISCUSSION

IV.1. General signification of s-SodF regulation

IV.1.1. Small regulatory RNA produced from a functional mRNA inhibits the expression of an antagonistically regulated gene

Based on sequence complementarity, we were able to identify a unique trans-acting small RNA, a cleaved 3′ UTR product of a functional mRNA, which facilitates the decay of another mRNA and possibly inhibits translation, resulting in antagonistic regulation. The model depicted in Fig. III-20 summarized the antagonistic regulatory mechanism of *sodF* and *sodN* gene expression. According to this model, under nickel-limited conditions as experienced in later phases of growth in batch culture, Nur without co-repressor nickel loses its binding affinity for the Nur-consensus (Nur-box) sequence that overlaps the *sodF* promoter (Ahn et al. 2006). Induction of *sodF* gene transcription ensues, producing full length *sodF* mRNA, from which a 90 nt-long 3′ UTR segment that contains the anti-*sodN* sequence of 19 nt can be cleaved off to function as a stable small regulatory RNA (s-SodF). The s-SodF RNA is able to form perfect base pairing with the 5′ terminal portion of *sodN* mRNA by up to 18 bp. The base-pairing facilitates degradation of *sodN* mRNA and may possibly inhibit translation by occluding ribosome binding, resulting in a rapid decrease in the production of Ni-SOD. In this way, cells can ensure production of the non-nickel enzyme (Fe-SOD) and at the same time rapidly turn off the synthesis of nickel-requiring enzyme (Ni-SOD).

IV.1.2. Predicted occurrence of similar regulation

From public genome databases, it is predicted that several groups of bacteria possess both *sodN* and *sodF* genes. They include most *Streptomyces* spp., some actinomycetes, cyanobacteria, chlamydiae, planctomycetes, gamma-, delta-, and

alpha-proteobacteria (Table IV-1). Except *S. cattleya* which contains only the *sodN* gene, all 10 *Streptomyces* species whose genomes were examined exhibited the complementary sequence between the sense strands of *sodF* and *sodN* genes. They range from 16 to 19 nt of complementarity between *sodF* 3'UTR and *sodN* 5' UTR (Table IV-2). Whether these other streptomycetes produce a similar s-SodF RNA and regulate *sodN* in a similar fashion as in *S. coelicolor* is an interesting question to be investigated. A recent genome-wide analysis of non-coding RNAs in three *Streptomyces* spp. revealed the presence of s-SodF RNA in *S. coelicolor* and its homologs in *S. avermitilis* and *S. venezuelae* (Moody et al. 2013). This supports the possibility that similar regulation will be in action in these organisms. In *S. bingchenggensis* BCW-1, there exist two *sodF* paralog genes as in *S. coelicolor* (Table IV-2). However, unlike the two *sodF* genes (*sodF* and *sodF2*) which encode functional SodF proteins in *S. coelicolor*, only one gene (*sodF*; SBI_02504) in *S. bingchenggensis* encodes a functional SodF, followed by a degenerate anti-*sodN* sequence with 8 nt mismatch, which is unlikely to serve an inhibitory function. On the other hand, the *sodF2* gene (SBI_01257) has a big in-frame deletion of the coding region but maintains a relatively good anti-*sodN* sequence (Table IV-2). If there are no sequencing errors, this suggests that the regulatory pathway with s-SodF may have been maintained throughout the evolution of *Streptomyces* spp. even when the adjacent coding sequence no longer produces a functional SodF protein. Whether there are other gene pairs or regulons that utilize this type of 3'-UTR-generated small regulatory RNA requires further bioinformatic and experimental investigations. Search for complementarity between distant regions in the genome, especially between 3'UTR regions and anywhere around distant coding region, is expected to give fruitful clues. This will facilitate excavating small regulatory RNAs with putative targets.

Table IV-1. Co-occurrence of *sodN* and *sodF* in the bacterial genome.

Homologs of ScoSodF (SCO2633) and ScoSodN (SCO5254) were searched toward prokaryotic protein sequences that were downloaded from NCBI (ftp.ncbi.nih.gov/genomes/Bacteria) on March 25, 2013. Up to five iterations of PSI-BLAST (Altschul et al. 1997) were done with default parameters. Homologous matches with e-values below 0.01 from last iteration were examined for further analysis.

Table III-1. Co-occurrence of sodN and sodF in bacterial genome

Bacterial Strain	phylogenetic class	sodN homologs (e-value)[1]	sodF homologs (e-value)[1]
Actinoplanes sp. SE50/110	Actinobacteria	ACPL_7553 (3e-49)	ACPL_279 (3e-75)
Actinosynnema mirum DSM 43827	Actinobacteria	Amir_6282 (4e-47)	Amir_0492 (3e-72)
Frankia sp. EAN1pec	Actinobacteria	Franean1_0977(6e-42)	Franean1_3497 (7e-73)
Frankia symbiont of Datisca glomerata	Actinobacteria	FsymDg_0982 (2e-42)	FsymDg_2119 (5e-77)
Kitasatospora setae KM-6054	Actinobacteria	KSE_49500 (2e-43)	KSE_35460 (1e-75)
Pseudonocardia dioxanivorans CB1190	Actinobacteria	Psed_5144 (4e-49)	Psed_5669 (1e-77)
Saccharopolyspora erythraea NRRL 2338	Actinobacteria	SACE_6419 (9e-50)	SACE_5364 (3e-74)
			SACE_0619 (1e-74)
Saccharothrix espanaensis DSM 44229	Actinobacteria	BN6_75530 (1e-47)	BN6_05370 (2e-72)
Stackebrandtia nassauensis DSM 44728	Actinobacteria	Snas_5159 (3e-49)	Snas_5819 (5e-78)
Streptomyces avermitilis MA-4680	Actinobacteria	SAV_2988 (9e-47)	SAV_5413 (2e-81)
Streptomyces bingchenggensis BCW-1	Actinobacteria	SBI_03931 (3e-44)	SBI_02504 (1e-69)
			SBI_01257 (2e-04)
Streptomyces coelicolor A3(2)	Actinobacteria	SCO5254 (7e-48)	SCO0999 (6e-81)
			SCO2633 (2e-83)
Streptomyces flavogriseus ATCC 33331	Actinobacteria	Sfla_2028 (1e-48)	Sfla_4244 (2e-81)
Streptomyces griseus subsp. griseus NBRC 13350	Actinobacteria	SGR_2245 (4e-48)	SGR_4906 (1e-81)
Streptomyces hygroscopicus subsp. jinggangensis 5008	Actinobacteria	SHJG_6369 (4e-46)	SHJG_4126 (2e-81)
Streptomyces scabiei 87.22	Actinobacteria	SCAB_29931 (4e-43)	SCAB_59731 (6e-80)
Streptomyces sp. SirexAA-E	Actinobacteria	SACTE_4493 (6e-48)	SACTE_2059 (2e-81)
Streptomyces venezuelae ATCC 10712	Actinobacteria	SVEN_4944 (1e-45)	SVEN_2415 (6e-78)
Streptomyces violaceusniger Tu 4113	Actinobacteria	Strvi_1588 (1e-48)	Strvi_7925 (2e-80)
Streptosporangium roseum DSM 43021	Actinobacteria	Sros_8301 (4e-49)	Sros_8508 (7e-73)
Thermomonospora curvata DSM 43183	Actinobacteria	Tcur_3687 (1e-46)	Tcur_0732 (1e-75)
Psychroflexus torquis ATCC 700755	Bacteroidetes	P700755_000729 (4e-39)	P700755_001967 (2e-79)
			P700755_001787 (2e-44)
Coraliomargarita akajimensis DSM 45221	Verrucomicrobia	Caka_1246 (1e-24)	Caka_1894 (6e-80)
Parachlamydia acanthamoebae UV-7	Chlamydiae	PUV_08330 (2e-22)	PUV_17360 (5e-38)
			PUV_04780 (2e-72)
Anaerolinea thermophila UNI-1	Anaerolineae	ANT_02490 (2e-36)	ANT_21010 (2e-77)
Acaryochloris marina MBIC11017	Oscillatoriophycideae	AM1_0511 (2e-42)	AM1_3669 (1e-69)
			AM1_2962 (3e-80)
Cyanobacterium aponinum PCC 10605	Oscillatoriophycideae	Cyan10605_2224 (2e-41)	Cyan10605_2057 (1e-77)
Dactylococcopsis salina PCC 8305	Oscillatoriophycideae	Dacsa_3081 (1e-38)	Dacsa_2555 (7e-80)
Halothece sp. PCC 7418	Oscillatoriophycideae	PCC7418_2939 (3e-39)	PCC7418_2580 (2e-80)
Rivularia sp. PCC 7116	Nostocales	Riv7116_2711 (4e-42)	Riv7116_6286 (2e-81)
			Riv7116_3634 (1e-78)
Stanieria cyanosphaera PCC 7437	Pleurocapsales	Sta7437_1770 (4e-41)	Sta7437_4025 (5e-79)
			Sta7437_4339 (1e-82)
Trichodesmium erythraeum IMS101	Oscillatoriophycideae	Tery_0891 (2e-42)	Tery_4533 (3e-77)
Rhodopirellula baltica SH 1	Planctomycetia	RB12634 (3e-21)	RB6688 (5e-79)
Alteromonas macleodii ATCC 27126	Gammaproteobacteria	MASE_02360 (2e-40)	MASE_05550 (1e-76)
Alteromonas macleodii str. 'Balearic Sea AD45'	Gammaproteobacteria	AMBAS45_02650 (5e-40)	AMBAS45_05760 (1e-76)
Alteromonas macleodii str. 'English Channel 673'	Gammaproteobacteria	AMEC673_02575 (2e-40)	AMEC673_05625 (1e-76)
Colwellia psychrerythraea 34H	Gammaproteobacteria	CPS_0444 (3e-37)	CPS_3476 (2e-72)
Desulfotalea psychrophila LSv54	delta/epsilon subdivisions	DP2504 (2e-24)	DP0316 (2e-71)
Hirschia baltica ATCC 49814	Alphaproteobacteria	Hbal_3001 (2e-24)	Hbal_1410 (2e-78)
Marinomonas mediterranea MMB-1	Gammaproteobacteria	Marme_3155 (1e-36)	Marme_1961 (1e-74)
Marinomonas posidonica IVIA-Po-181	Gammaproteobacteria	Mar181_2423 (2e-36)	Mar181_1776 (3e-75)
Marinomonas sp. MWYL1	Gammaproteobacteria	Mmwyl1_1415 (2e-36)	Mmwyl1_2180 (1e-72,)
Methylophaga sp. JAM7	Gammaproteobacteria	Q7C_2483 (6e-37)	Q7C_2659 (5e-81)
Shewanella piezotolerans WP3	Gammaproteobacteria	swp_3819 (2e-38)	swp_2754 (1e-77)
Shewanella violacea DSS12	Gammaproteobacteria	SVI_2719 (3e-38)	SVI_1884 (5e-77)
Shewanella woodyi ATCC 51908	Gammaproteobacteria	Swoo_1068 (4e-40)	Swoo_2159 (2e-73)

Bacterial Strain	phylogenetic class	sodN homologs (e-value)[1]	sodF homologs (e-value)[1]
Acidimicrobium ferrooxidans DSM 10331	Actinobacteria	Afer_0355 (2e-43)	
Acidothermus cellulolyticus 11B	Actinobacteria	Acel_0566 (3e-48)	
Actinoplanes missouriensis 431	Actinobacteria	AMIS_51430 (1e-47)	
		AMIS_72860 (1e-49)	
Blastococcus saxobsidens DD2	Actinobacteria	BLASA_3991 (9e-49)	
Catenulispora acidiphila DSM 44928	Actinobacteria	Caci_7706 (7e-48)	
Frankia sp. EuI1c	Actinobacteria	FraEuI1c_0811 (7e-42)	
Geodermatophilus obscurus DSM 43160	Actinobacteria	Gobs_4176 (2e-46)	
Kytococcus sedentarius DSM 20547	Actinobacteria	Ksed_18510 (4e-46)	
Micromonospora aurantiaca ATCC 27029	Actinobacteria	Micau_5235 (9e-45)	
Micromonospora sp. L5	Actinobacteria	ML5_3057 (9e-45)	
Modestobacter marinus BC501	Actinobacteria	MODMU_4573 (2e-47)	
Mycobacterium chubuense NBB4	Actinobacteria	Mycch_5022 (3e-40)	
Mycobacterium gilvum PYR-GCK	Actinobacteria	Mflv_1135 (8e-42)	
Mycobacterium gilvum Spyr1	Actinobacteria	Mspyr1_50520 (8e-42)	
Mycobacterium rhodesiae NBB3	Actinobacteria	MycrhN_1911 (8e-41)	
Mycobacterium smegmatis JS623	Actinobacteria	Mycsm_06220 (2e-42)	
Mycobacterium vanbaalenii PYR-1	Actinobacteria	Mvan_5671 (1e-42)	
Nakamurella multipartita DSM 44233	Actinobacteria	Namu_1016 (3e-48)	
Nocardioides sp. JS614	Actinobacteria	Noca_1725 (4e-48)	
Salinispora arenicola CNS-205	Actinobacteria	Sare_4077 (8e-45)	
Salinispora tropica CNB-440	Actinobacteria	Strop_3697 (5e-44)	
Streptomyces cattleya NRRL 8057 = DSM 46488	Actinobacteria	SCAT_4107 (4e-48)	
Streptomyces cattleya NRRL 8057 = DSM 46488	Actinobacteria	SCATT_40980 (4e-48)	
Thermobispora bispora DSM 43833	Actinobacteria	Tbis_2903 (6e-48)	
Verrucosispora maris AB-18-032	Actinobacteria	VAB18032_30011 (1e-44)	
Leptolyngbya sp. PCC 7376	Oscillatoriophycideae	Lepto7376_0549 (4e-38)	
Prochlorococcus marinus str. AS9601	Prochlorales	A9601_14931 (1e-40)	
Prochlorococcus marinus str. MIT 9211	Prochlorales	P9211_13411 (2e-42)	
Prochlorococcus marinus str. MIT 9215	Prochlorales	P9215_15221 (5e-42)	
Prochlorococcus marinus str. MIT 9301	Prochlorales	P9301_14791 (3e-41)	
Prochlorococcus marinus str. MIT 9303	Prochlorales	P9303_19731 (7e-42)	
Prochlorococcus marinus str. MIT 9312	Prochlorales	PMT9312_1390 (7e-41)	
Prochlorococcus marinus str. MIT 9313	Prochlorales	PMT0340 (5e-41)	
Prochlorococcus marinus str. MIT 9515	Prochlorales	P9515_14551 (5e-42)	
Prochlorococcus marinus str. NATL1A	Prochlorales	NATL1_17141 (3e-41)	
Prochlorococcus marinus str. NATL2A	Prochlorales	PMN2A_0861 (1e-40)	
Prochlorococcus marinus subsp. marinus str. CCMP1375	Prochlorales	Pro1368 (1e-40)	
Prochlorococcus marinus subsp. pastoris str. CCMP1986	Prochlorales	PMM1294 (1e-41)	
Synechococcus sp. CC9311	Oscillatoriophycideae	sync_2434 (3e-23)	
		sync_0755 (4e-40)	
Synechococcus sp. CC9605	Oscillatoriophycideae	Syncc9605_0873(1e-41)	
Synechococcus sp. CC9902	Oscillatoriophycideae	Syncc9902_1525 (6e-40)	
Synechococcus sp. WH 8102	Oscillatoriophycideae	SYNW1626 (1e-39)	
Desulfatibacillum alkenivorans AK-01	delta/epsilon subdivisions	Dalk_0807 (2e-20)	
Desulfobacterium autotrophicum HRM2	delta/epsilon subdivisions	HRM2_28400 (1e-24)	
Desulfovibrio piezophilus	delta/epsilon subdivisions	BN4_10596 (1e-23)	

1. homologs are detected by psi-blast with maximum iteration 5. e-value is parsed from last iteration.

Table IV-2. Presence of complementary sequence between *sodF* and *sodN* genes in Streptomycetes.

To find sequences that match with the 19 nt anti-*sodN* sequence of s-SodF in *S. coelicolor*, fuzznuc in EMBOSS package (Rice et al. 2000) was used toward flanking 100 nt regions of SodF and SodN in *Streptomyces* spp. predicted in Table S1 , allowing up to 3 mismatches. Blastn search of 100 nt flanking sequences of SodN homologs by 100 nt flanking sequences of SodF homologs revealed no significant matches in other genomes beyond Streptomyces genus.

Table III-2 Presence of complementary sequence between sodF and sodN genes in Streptomycetes

	SodN ortholog				SodF ortholog			
Species name	gene id	distance[1]	strand[2]	matching sequence[3]	gene id	distance[4]	strand[2]	anti-sodN sequence[3]
S. coelicolor A3(2)	SCO5254	13	-	TGAGAAGACGATCACGAGG	SCO2633 (sodF)	19	+	CCTCGTGATCGTCTTCTCA
					SCO0999 (sodF2)[5]	24	+	GCTCGTGATCGTCTTCTCA
S. avermitilis MA-4680	SAV_2988	13	-	TGAGAAGACGATCACGAGG	SAV_5413	22	+	GCTCGTGATCGTCTTCTCA
S. bingchenggensis BCW-1	SBI_03931	14	-	TGAGAAGACGATCACTTAG	SBI_01257 (sodF2)	25	+	GCTCGTGATCGTCGTCTCA
					SBI_02504 (sodF)[6]	38	+	GCTCGTGAA-GT-GTGTCG
S. flavogriseus ATCC 33331	Sfla_2028	13	-	TGAGAAGACGATCACGAGG	Sfla_4244	30	+	CCTCGTGATCGTCTTCTCA
S. griseus subsp. griseus NBRC 13350	SGR_2245	12	-	TGAGAAGACGATCACGAGG	SGR_4906	30	+	CCTCGTGATCGTCTTCTCA
S. hygroscopicus subsp. jinggangensis 5008	SHJG_6369	13	-	TGAGAAGACGATCACGAGG	SHJG_4126	11	+	CCTCGTGATCGTCTTCTCA
S. scabiei 87.22	SCAB_29931	13	-	TGAGAAGACGATCACGAGG	SCAB_59731	24	+	GCTCGTGATCGTCTTCTCA
S. sp. SirexAA-E	SACTE_4493	13	-	TGAGAAGACGATCACGAGG	SACTE_2059	19	+	CCTCGTGATCGTCTTCTCA
S. venezuelae ATCC 10712	SVEN_4944	13	-	TGAGAAGACGATCACGAGG	SVEN_2415	13	+	GCTCGTGATCGTCTTCTCA
S. violaceusniger Tu 4113	Strvi_1588	15	-	TGAGAAGACGATCACGAAT	Strvi_7925	27	+	TTGCGTGATCGTCTTCTCA

1. distance from the start codon of SodN
2. strand orientation of the coding gene
3. 19 nt sequence complementary to anti-sodN in sodF gene
4. distnace from the stop codon of SodF
5. paralog of sodF.
6. Anti-sodN sequence downstream of the *sodF* gene is degerate. ClustalW multiple alignment of downstream 100 nt regions of all sodF homologs reveal a weakly matching sequence with six mismatches and two gaps in S. bingchenggensis .
7. red underlined character indicates mismatch to sequences in S. coelicolor sodN and sodF

IV.1.3. Inverse regulation of isoenzymes and antagonistic proteins

Antagonistic regulation between Fe-containing and Ni-containing isoforms of enzymes is not unprecedented. In *Helicobacter mustelae*, a carnivore-colonizing species, Fe-containing urease (UreA2B2) is produced under nickel-depleted condition, whereas Ni-containing urease (UreAB) prevails under nickel-sufficient condition (Stoof et al. 2008). In this case, the nickel-specific regulator NikR regulates both operons, directly repressing and activating *ureA2B2* and *ureAB* transcription, respectively (Stoof et al. 2010). It is interesting to note the existence of inverse regulation between FeSOD and its iso-enzymes with different metals, MnSOD and NiSOD. Since SODs are abundant proteins and are important for air-exposed life, antagonistic regulation in response to the availability of specific preferred metal and oxidative conditions should be beneficial for the economy of the cell. For soil-dwelling streptomycetes, abundant nickel in the aerobic soil environment would fit the evolution of a gene regulatory system where *sodF* is repressed such that nickel is utilized before iron. For facultative *E. coli*, life under anaerobic iron-rich condition could have evolved a gene system where SodB is a preferred enzyme under anaerobic condition, and SodA is induced in the presence of oxygen and oxidative stress.

The observation that the inverse regulation exerted by Fur family regulators involves small regulatory RNAs as mediators is intriguing. RyhB-mediated regulation by Fur in *E. coli*, PrrF1/F2-mediated regulation by Fur in *Pseudomonas*, and FsrA-mediated regulation by Fur in *B. subtilis* all enable inverse regulation of Fe- vs. non-Fe proteins. The discovery of s-SodF in *S. coelicolor* adds to this list of small RNA-coupled regulation by Fur family members. These examples support the presence of an evolutionarily robust regulatory circuit mediated by metal-

specific Fur family regulators and small RNAs in coordinated synthesis of iso-proteins with specific metal cofactors across distantly related bacteria.

IV.2. Prospects for Future Studies

Further analyses are needed and designed to understand more about s-SodF.

Little is known about small RNA in Actinobacteria, but we identified specific small RNA and it's function. From this study, RNase III and RNase E are not involved in s-SodF processing and this means that another unknown RNA binding protein could act on s-SodF. Both RNases also did not regulate *sodN* mRNA stability (data not shown) and PNPase which has a phosphorolytic 3' to 5' exoribonuclease activity might be involved in *sodN* mRNA stability regulation. In *S. coelicolor*, SCO5737 which is polynucleotide phosphorylase (PNPase) can synthesize RNA 3' tails under phosphorolysis condition and it will have implications for the degradation of structured RNAs (Jones and Mackie 2013). A recent genome-wide analysis showed the presence of s-SodF RNA in *S. coelicolor* and its homologs in *S. avermitilis* and *S. venezuelae* (Moody et al. 2013). Screening of of RNA binding protein related to s-SodF processing could serve as a clue for fishing binding protein that participate in the function of sRNA in Actinomycetes. s-SodF is expected to act as siRNA (small interfering RNA) in Streptomyces. s-SodF is stably expressed all the time without sodF ORF. If anti-sodN 19nt is replaced with anti-specific targeting gene (X), s-SodF containing anti-X region may actually repress target X. We should consider many options related to stable sRNA expression because in mutation study in the anti-*sodN* region of s-SodF, overall secondary structure of sRNA could influence the expression. This experiment might provide many information about sRNA stability and required sequence for target repression.

REFERENCES

Ahn BE, Cha J, Lee EJ, Han AR, Thompson CJ, Roe JH. 2006. Nur, a nickel-responsive regulator of the Fur family, regulates superoxide dismutases and nickel transport in Streptomyces coelicolor. *Mol Microbiol* **59**: 1848-1858.

Aiba H. 2007. Mechanism of RNA silencing by Hfq-binding small RNAs. *Curr Opin Microbiol* **10**: 134-139.

Altschul SF, Madden TL, Schaffer AA, Zhang J, Zhang Z, Miller W, Lipman DJ. 1997. Gapped BLAST and PSI-BLAST: a new generation of protein database search programs. *Nucleic Acids Res* **25**: 3389-3402.

An YJ, Ahn BE, Han AR, Kim HM, Chung KM, Shin JH, Cho YB, Roe JH, Cha SS. 2009. Structural basis for the specialization of Nur, a nickel-specific Fur homolog, in metal sensing and DNA recognition. *Nucleic Acids Res* **37**: 3442-3451.

Bagg A, Neilands JB. 1987a. Ferric uptake regulation protein acts as a repressor, employing iron (II) as a cofactor to bind the operator of an iron transport operon in Escherichia coli. *Biochemistry* **26**: 5471-5477.

-. 1987b. Molecular mechanism of regulation of siderophore-mediated iron assimilation. *Microbiological reviews* **51**: 509-518.

Barondeau DP, Kassmann CJ, Bruns CK, Tainer JA, Getzoff ED. 2004. Nickel superoxide dismutase structure and mechanism. *Biochemistry* **43**: 8038-8047.

Bartha R, Ordal EJ. 1965. Nickel-Dependent Chemolithotrophic Growth of Two Hydrogenomonas Strains. *J Bacteriol* **89**: 1015-1019.

Bentley SD, Chater KF, Cerdeno-Tarraga AM, Challis GL, Thomson NR, James KD, Harris DE, Quail MA, Kieser H, Harper D et al. 2002. Complete

genome sequence of the model actinomycete Streptomyces coelicolor A3(2). *Nature* **417**: 141-147.

Bibb MJ, Janssen GR, Ward JM. 1985. Cloning and analysis of the promoter region of the erythromycin resistance gene (ermE) of Streptomyces erythraeus. *Gene* **38**: 215-226.

Braun V. 2003. Iron uptake by Escherichia coli. *Frontiers in bioscience : a journal and virtual library* **8**: s1409-1421.

Brennan RG, Link TM. 2007. Hfq structure, function and ligand binding. *Curr Opin Microbiol* **10**: 125-133.

Celesnik H, Deana A, Belasco JG. 2008. PABLO analysis of RNA: 5'-phosphorylation state and 5'-end mapping. *Methods Enzymol* **447**: 83-98.

Chao Y, Papenfort K, Reinhardt R, Sharma CM, Vogel J. 2012. An atlas of Hfq-bound transcripts reveals 3' UTRs as a genomic reservoir of regulatory small RNAs. *EMBO J* **31**: 4005-4019.

Chung HJ, Choi JH, Kim EJ, Cho YH, Roe JH. 1999a. Negative regulation of the gene for Fe-containing superoxide dismutase by an Ni-responsive factor in Streptomyces coelicolor. *J Bacteriol* **181**: 7381-7384.

Chung HJ, Kim EJ, Suh B, Choi JH, Roe JH. 1999b. Duplicate genes for Fe-containing superoxide dismutase in Streptomyces coelicolor A3(2). *Gene* **231**: 87-93.

Conrad C, Rauhut R. 2002. Ribonuclease III: new sense from nuisance. *Int J Biochem Cell Biol* **34**: 116-129.

Datsenko KA, Wanner BL. 2000. One-step inactivation of chromosomal genes in Escherichia coli K-12 using PCR products. *Proc Natl Acad Sci U S A* **97**: 6640-6645.

Davis BM, Waldor MK. 2007. RNase E-dependent processing stabilizes MicX, a Vibrio cholerae sRNA. *Mol Microbiol* **65**: 373-385.

Denkhaus E, Salnikow K. 2002. Nickel essentiality, toxicity, and carcinogenicity.

Critical reviews in oncology/hematology **42**: 35-56.

Drider D, Condon C. 2004. The continuing story of endoribonuclease III. *J Mol Microbiol Biotechnol* **8**: 195-200.

Dubrac S, Touati D. 2000. Fur positive regulation of iron superoxide dismutase in Escherichia coli: functional analysis of the sodB promoter. *J Bacteriol* **182**: 3802-3808.

Dufresne A, Salanoubat M, Partensky F, Artiguenave F, Axmann IM, Barbe V, Duprat S, Galperin MY, Koonin EV, Le Gall F et al. 2003. Genome sequence of the cyanobacterium Prochlorococcus marinus SS120, a nearly minimal oxyphototrophic genome. *Proc Natl Acad Sci U S A* **100**: 10020-10025.

Dupont CL, Neupane K, Shearer J, Palenik B. 2008. Diversity, function and evolution of genes coding for putative Ni-containing superoxide dismutases. *Environ Microbiol* **10**: 1831-1843.

Eitinger T. 2004. In vivo production of active nickel superoxide dismutase from Prochlorococcus marinus MIT9313 is dependent on its cognate peptidase. *J Bacteriol* **186**: 7821-7825.

Escolar L, Perez-Martin J, de Lorenzo V. 1998. Binding of the fur (ferric uptake regulator) repressor of Escherichia coli to arrays of the GATAAT sequence. *J Mol Biol* **283**: 537-547.

Fridovich I. 1997. Superoxide anion radical (O2-.), superoxide dismutases, and related matters. *J Biol Chem* **272**: 18515-18517.

Gaballa A, Antelmann H, Aguilar C, Khakh SK, Song KB, Smaldone GT, Helmann JD. 2008. The Bacillus subtilis iron-sparing response is mediated by a Fur-regulated small RNA and three small, basic proteins. *Proc Natl Acad Sci U S A* **105**: 11927-11932.

Giedroc DP, Arunkumar AI. 2007. Metal sensor proteins: nature's metalloregulated allosteric switches. *Dalton transactions*: 3107-3120.

Gort AS, Ferber DM, Imlay JA. 1999. The regulation and role of the periplasmic copper, zinc superoxide dismutase of Escherichia coli. *Mol Microbiol* **32**: 179-191.

Han A-R. 2007. Regulation of gene expression by a nickel-responsive transcriptional regulator Nur in Streptomyces coelicolor. graduate school, Seoul National University, Seoul.

Hantke K. 1981. Regulation of ferric iron transport in Escherichia coli K12: isolation of a constitutive mutant. *Mol Gen Genet* **182**: 288-292.

-. 2001. Iron and metal regulation in bacteria. *Curr Opin Microbiol* **4**: 172-177.

Hassan HM, Schrum LW. 1994. Roles of manganese and iron in the regulation of the biosynthesis of manganese-superoxide dismutase in Escherichia coli. *FEMS Microbiol Rev* **14**: 315-323.

Hassett DJ, Howell ML, Ochsner UA, Vasil ML, Johnson Z, Dean GE. 1997. An operon containing fumC and sodA encoding fumarase C and manganese superoxide dismutase is controlled by the ferric uptake regulator in Pseudomonas aeruginosa: fur mutants produce elevated alginate levels. *J Bacteriol* **179**: 1452-1459.

Hausinger RP. 1993. *Biochemistry of nickel* Plenum Press, New York.

Herbig AF, Helmann JD. 2001. Roles of metal ions and hydrogen peroxide in modulating the interaction of the Bacillus subtilis PerR peroxide regulon repressor with operator DNA. *Mol Microbiol* **41**: 849-859.

Jones GH, Mackie GA. 2013. Streptomyces coelicolor polynucleotide phosphorylase can polymerize nucleoside diphosphates under phosphorolysis conditions, with implications for the degradation of structured RNAs. *J Bacteriol* **195**: 5151-5159.

Joseph Sambrook DWR. 2001. *Molecular cloning : a laboratory manual*. Cold spring Harbor Laboratory Press, New York.

Kieser T. 2000. *Practical streptomyces genetics*. John Innes Foundation, Norwich.

Kim EJ, Chung HJ, Suh B, Hah YC, Roe JH. 1998a. Expression and regulation of the sodF gene encoding iron- and zinc-containing superoxide dismutase in Streptomyces coelicolor Muller. *J Bacteriol* **180**: 2014-2020.

-. 1998b. Transcriptional and post-transcriptional regulation by nickel of sodN gene encoding nickel-containing superoxide dismutase from Streptomyces coelicolor Muller. *Mol Microbiol* **27**: 187-195.

Kim MS, Hahn MY, Cho Y, Cho SN, Roe JH. 2009. Positive and negative feedback regulatory loops of thiol-oxidative stress response mediated by an unstable isoform of sigmaR in actinomycetes. *Mol Microbiol* **73**: 815-825.

Kroger C, Dillon SC, Cameron AD, Papenfort K, Sivasankaran SK, Hokamp K, Chao Y, Sittka A, Hebrard M, Handler K et al. 2012. The transcriptional landscape and small RNAs of Salmonella enterica serovar Typhimurium. *Proc Natl Acad Sci U S A* **109**: E1277-1286.

Lee JW, Helmann JD. 2006. The PerR transcription factor senses H2O2 by metal-catalysed histidine oxidation. *Nature* **440**: 363-367.

-. 2007. Functional specialization within the Fur family of metalloregulators. *Biometals* **20**: 485-499.

Lee K, Cohen SN. 2003. A Streptomyces coelicolor functional orthologue of Escherichia coli RNase E shows shuffling of catalytic and PNPase-binding domains. *Mol Microbiol* **48**: 349-360.

Lucarelli D, Russo S, Garman E, Milano A, Meyer-Klaucke W, Pohl E. 2007. Crystal Structure and Function of the Zinc Uptake Regulator FurB from Mycobacterium tuberculosis. *Journal of Biological Chemistry* **282**: 9914-9922.

MacNeil DJ, Gewain KM, Ruby CL, Dezeny G, Gibbons PH, MacNeil T. 1992. Analysis of Streptomyces avermitilis genes required for avermectin biosynthesis utilizing a novel integration vector. *Gene* **111**: 61-68.

Masse E, Gottesman S. 2002. A small RNA regulates the expression of genes

involved in iron metabolism in Escherichia coli. *Proc Natl Acad Sci U S A* **99**: 4620-4625.

Miller AF. 2004. Superoxide dismutases: active sites that save, but a protein that kills. *Current opinion in chemical biology* **8**: 162-168.

-. 2012. Superoxide dismutases: ancient enzymes and new insights. *FEBS Lett* **586**: 585-595.

Mitra A, Angamuthu K, Jayashree HV, Nagaraja V. 2009. Occurrence, divergence and evolution of intrinsic terminators across eubacteria. *Genomics* **94**: 110-116.

Moody MJ, Young RA, Jones SE, Elliot MA. 2013. Comparative analysis of non-coding RNAs in the antibiotic-producing Streptomyces bacteria. *BMC Genomics* **14**: 558.

Mulrooney SB, Hausinger RP. 2003. Nickel uptake and utilization by microorganisms. *FEMS Microbiol Rev* **27**: 239-261.

Navarro C, Wu LF, Mandrand-Berthelot MA. 1993. The nik operon of Escherichia coli encodes a periplasmic binding-protein-dependent transport system for nickel. *Mol Microbiol* **9**: 1181-1191.

Nudler E, Mironov AS. 2004. The riboswitch control of bacterial metabolism. *Trends Biochem Sci* **29**: 11-17.

Palenik B, Brahamsha B, Larimer FW, Land M, Hauser L, Chain P, Lamerdin J, Regala W, Allen EE, McCarren J et al. 2003. The genome of a motile marine Synechococcus. *Nature* **424**: 1037-1042.

Panek J, Bobek J, Mikulik K, Basler M, Vohradsky J. 2008. Biocomputational prediction of small non-coding RNAs in Streptomyces. *BMC Genomics* **9**: 217.

Papenfort K, Said N, Welsink T, Lucchini S, Hinton JC, Vogel J. 2009. Specific and pleiotropic patterns of mRNA regulation by ArcZ, a conserved, Hfq-dependent small RNA. *Mol Microbiol* **74**: 139-158.

Perry JJ, Shin DS, Getzoff ED, Tainer JA. 2010. The structural biochemistry of the superoxide dismutases. *Biochimica et biophysica acta* **1804**: 245-262.

Pohl E, Haller JC, Mijovilovich A, Meyer-Klaucke W, Garman E, Vasil ML. 2003. Architecture of a protein central to iron homeostasis: crystal structure and spectroscopic analysis of the ferric uptake regulator. *Mol Microbiol* **47**: 903-915.

Polack B, Dacheux D, Delic-Attree I, Toussaint B, Vignais PM. 1996. The Pseudomonas aeruginosa fumc and soda genes belong to an iron-responsive operon. *Biochem Biophys Res Commun* **226**: 555-560.

Priya B, Premanandh J, Dhanalakshmi RT, Seethalakshmi T, Uma L, Prabaharan D, Subramanian G. 2007. Comparative analysis of cyanobacterial superoxide dismutases to discriminate canonical forms. *BMC Genomics* **8**: 435.

Redenbach M, Kieser HM, Denapaite D, Eichner A, Cullum J, Kinashi H, Hopwood DA. 1996. A set of ordered cosmids and a detailed genetic and physical map for the 8 Mb Streptomyces coelicolor A3(2) chromosome. *Mol Microbiol* **21**: 77-96.

Rice P, Longden I, Bleasby A. 2000. EMBOSS: the European Molecular Biology Open Software Suite. *Trends in genetics : TIG* **16**: 276-277.

Rocap G, Larimer FW, Lamerdin J, Malfatti S, Chain P, Ahlgren NA, Arellano A, Coleman M, Hauser L, Hess WR et al. 2003. Genome divergence in two Prochlorococcus ecotypes reflects oceanic niche differentiation. *Nature* **424**: 1042-1047.

Rulisek L, Vondrasek J. 1998. Coordination geometries of selected transition metal ions (Co2+, Ni2+, Cu2+, Zn2+, Cd2+, and Hg2+) in metalloproteins. *J Inorg Biochem* **71**: 115-127.

Schmidt A, Gube M, Kothe E. 2009. In silico analysis of nickel containing superoxide dismutase evolution and regulation. *J Basic Microbiol* **49**: 109-

118.

Sharma CM, Vogel J. 2009. Experimental approaches for the discovery and characterization of regulatory small RNA. *Curr Opin Microbiol* **12**: 536-546.

Stohs SJ, Bagchi D. 1995. Oxidative mechanisms in the toxicity of metal ions. *Free Radic Biol Med* **18**: 321-336.

Stoof J, Breijer S, Pot RGJ, van der Neut D, Kuipers EJ, Kusters JG, van Vliet AHM. 2008. Inverse nickel-responsive regulation of two urease enzymes in the gastric pathogenHelicobacter mustelae. *Environmental Microbiology* **10**: 2586-2597.

Stoof J, Kuipers EJ, van Vliet AH. 2010. Characterization of NikR-responsive promoters of urease and metal transport genes of Helicobacter mustelae. *Biometals* **23**: 145-159.

Storz G, Hengge R. 2011. Bacterial stress responses. pp. 1 online resource (xv, 506 p.). ASM Press, Washington, DC.

Storz G, Imlay JA. 1999. Oxidative stress. *Current opinion in microbiology* **2**: 188-194.

Storz G, Vogel J, Wassarman KM. 2011. Regulation by small RNAs in bacteria: expanding frontiers. *Mol Cell* **43**: 880-891.

Sun X, Zhulin I, Wartell RM. 2002. Predicted structure and phyletic distribution of the RNA-binding protein Hfq. *Nucleic Acids Res* **30**: 3662-3671.

Swiercz JP, Hindra, Bobek J, Haiser HJ, Di Berardo C, Tjaden B, Elliot MA. 2008. Small non-coding RNAs in Streptomyces coelicolor. *Nucleic Acids Res* **36**: 7240-7251.

Tardat B, Touati D. 1991. Two global regulators repress the anaerobic expression of MnSOD in Escherichia coli::Fur (ferric uptake regulation) and Arc (aerobic respiration control). *Molecular Microbiology* **5**: 455-465.

Tezuka T, Hara H, Ohnishi Y, Horinouchi S. 2009. Identification and gene disruption of small noncoding RNAs in Streptomyces griseus. *J Bacteriol*

191: 4896-4904.

Traore DA, El Ghazouani A, Ilango S, Dupuy J, Jacquamet L, Ferrer JL, Caux-Thang C, Duarte V, Latour JM. 2006. Crystal structure of the apo-PerR-Zn protein from Bacillus subtilis. *Mol Microbiol* **61**: 1211-1219.

Venter JC, Remington K, Heidelberg JF, Halpern AL, Rusch D, Eisen JA, Wu D, Paulsen I, Nelson KE, Nelson W et al. 2004. Environmental genome shotgun sequencing of the Sargasso Sea. *Science* **304**: 66-74.

Vockenhuber MP, Sharma CM, Statt MG, Schmidt D, Xu Z, Dietrich S, Liesegang H, Mathews DH, Suess B. 2011. Deep sequencing-based identification of small non-coding RNAs in Streptomyces coelicolor. *RNA Biol* **8**: 468-477.

Vockenhuber MP, Suess B. 2012. Streptomyces coelicolor sRNA scr5239 inhibits agarase expression by direct base pairing to the dagA coding region. *Microbiology* **158**: 424-435.

Wassarman KM, Saecker RM. 2006. Synthesis-mediated release of a small RNA inhibitor of RNA polymerase. *Science* **314**: 1601-1603.

Waters LS, Storz G. 2009. Regulatory RNAs in bacteria. *Cell* **136**: 615-628.

Wilderman PJ, Sowa NA, FitzGerald DJ, FitzGerald PC, Gottesman S, Ochsner UA, Vasil ML. 2004. Identification of tandem duplicate regulatory small RNAs in Pseudomonas aeruginosa involved in iron homeostasis. *Proc Natl Acad Sci U S A* **101**: 9792-9797.

Wuerges J, Lee JW, Yim YI, Yim HS, Kang SO, Djinovic Carugo K. 2004. Crystal structure of nickel-containing superoxide dismutase reveals another type of active site. *P Natl Acad Sci USA* **101**: 8569-8574.

Xu W, Huang J, Lin R, Shi J, Cohen SN. 2010. Regulation of morphological differentiation in S. coelicolor by RNase III (AbsB) cleavage of mRNA encoding the AdpA transcription factor. *Mol Microbiol* **75**: 781-791.

Youn HD, Kim EJ, Roe JH, Hah YC, Kang SO. 1996. A novel nickel-containing superoxide dismutase from Streptomyces spp. *The Biochemical journal*

318 (Pt 3): 889-896.

Zuker M. 2003. Mfold web server for nucleic acid folding and hybridization prediction. *Nucleic Acids Res* **31**: 3406-3415.

국문초록

슈퍼옥사이드 디스뮤타제는 여러 금속 보조인자를 가지고 슈퍼옥사이드를 과산화 수소와 산소 분자로 전환시키는 효소이다. 많은 방선균들은 철을 보조인자로 가지는 슈퍼옥사이드를 암호화하는 *sodF* 유전자와 니켈을 보조인자로 가지는 슈퍼옥사이드를 암호화하는 *sodN* 유전자를 동시에 가지고 있다.

Nur 는 nickel uptake regulator 의 약자로 니켈에 특이적인 Fur 계열의 조절자이며 *S. coelicolor* 에서 니켈의 항상성과 항산화 작용을 조절하는 니켈 반응 전사조절자이다. 또한 Nur는. *S. coelicolor*에서 Nur 는 철과 니켈을 각각의 보조인자로 가지는 슈퍼옥사이드 디스뮤타제 발현을 서로 정반대로 조절한다. 니켈이 충분한 조건에서 Nur는 *sodF* 유전자의 전사를 직접적으로 억제함과 동시에 *sodN* 유전자를 간접적으로 활성화시킨다. 생물정보학을 이용하여 *sodN* 유전자의 upstream 과 *sodF* 유전자의 downstream 사이에 완벽하게 결합할 수 있고 잘 보존되어 있는 19개의 뉴클레오타이드가 존재함을 확인하였다. Nur 가 *sodN* 을 간접적으로 활성화시키는 과정에 *sodF* 전사체가 관여할 수 있다는 가설 아래 우리는 먼저 anti-*sodN* 전사체가 발현이 되는지 S1 mapping과 northern blot 통하여 확인을 하였다. 그 결과 *sodN*의 전사체의 5'쪽의 리보솜 결합 자리로부터 결합할 수 있는 anti-*sodN* 서열을 가진 약 90 뉴클레오타이드의 small 전사체가 *sodF* 유전자로부터 안정적으로 발현됨을 확인하였다. 이 small 전사체는 s-SodF 라 명명되었다. s-SodF 가 5'-monophosphate-specific exonuclease에 sensitive 한 결과를 토대로 우리는 s-SodF가 5'-monophosphorylation 되어 있음을 확인 하였다. 이 결과는 s-SodF 가 새롭게 합성된 것이 아니라 *sodF* mRNA의 3'UTR로부터 잘라져서 생성된 것임을 알게 하였다. 또한 s-SodF 가 실제로 세포내에서 *sodN* 유전자를 조절하는지 알기 위하여 s-SodF를 과량발현 시킬 수 있는 프로모터에

클로닝 하여 *sodF* 돌연변이 균주의 게놈에 삽입하였다. 야생형 균주에서 *sodN* mRNA half-life는 3분대임에 반해 *sodF* 돌연변이 균주에서는 16분대로 증가함을 확인하였고, *sodF* 돌연변이 균주에 s-SodF 만을 과량발현 시킨 균주에서는 증가한 *sodN* mRNA half-life가 다시 7분대로 회복됨을 확인하였다. 따라서 s-SodF가 실질적으로 세포내에서 *sodN* mRNA의 half-life를 두드러지게 감소시킴을 알 수 있었다. 이 결과들을 토대로 Nur는 *sodF* mRNA로부터 억제적 s-SodF 의 합성을 저지함으로써 *sodN* 활성을 촉진시킴을 알게 되었다. 또한 이러한 기작은 하나의 전사조절인자에 의해 조절되는 두개의 target 유전자 중 하나의 유전자의 3'UTR로부터 나오는 small 전사체에 의해 또 다른 하나의 유전자가 조절되는 새로운 조절 기작이다.

Nur 가 어떻게 니켈을 인지하고 자기 자신의 형태를 조절하는지는 아직 밝혀지지 않은 문제이다. 최근 우리는 DNA 결합 competent 이합체인 Nur 의 구조를 결정하였다. 각각의 단량체는 니켈에 특이적인 금속 결합자리 (Ni-ste)와 비특이적 금속 결합자리 (M-site)를 각각 하나씩 가지고 있다. 또한 Nur는 두개의 Cys-X-X-Cys motif를 가지고 있지만 다른 Fur family 와 같이 아연이 결합되어 있지는 않는 형태로 결정되었다. *E. coli* 에서 Nur를 발현시킨 세포추출물을 가지고 EMSA를 수행한 결과, Ni-site와 M-site가 Nur 의 DNA 결합 능력에 중요함을 확인하였고, 이 결과는 결정된 Nur 구조로부터 예상된 결과이다. 또한 Nur 의 여러 금속 결합 자리의 돌연변이의 영향을 세포 내에서 *sodF* 유전자의 전사 억제 능력으로 S1 mapping를 통하여 확인하였다. 그 결과 Ni-site 와 Cys-4 site (96번, 133번, 136번 시스테인) 이 Nur 의 활성에 결정적임을 확인하였다. *S. coelicolor* 의 세포추출물을 가지고 동일하게 수행한 EMSA 결과에서 또한 이를 확인하였다. 따라서 니켈이 있는 조건에서 결정된 Nur의 구조는 *S. coelicolor* 의 실제적 Nur 의 구조를 보여주지 못할 수도 있다. 이 결과는 Nur 두개의 Cys-X-X-Cys motif 가 Bacillus subtilis의 PerR처럼 세포내에서 아연과 결합하여 Nur의 구조와 기능에 중요한 역할을 할 것임을 시사하는 결과이다. 이 차이점을 실험적으로

설명하는 것은 앞으로 밝혀야 할 과제이다.

주요단어들 : 방선균, Fur, Nur, 니켈, 구조, 금속 결합자리, small RNA, 슈퍼옥사이드 디스뮤타제

감사의 글

2007년 1월 눈이 많이 내렸던 겨울, 설레이고도 두근거리는 마음으로 서울로 올라왔던 그때가 기억납니다. 그로부터 7년 이라는 시간이 흘렀습니다. 그 7년이라는 시간 동안 이곳에서 참 울기도 많이 울고, 웃기도 많이 웃었던 것 같습니다. 생각보다 힘들었고, 생각보다 많이 행복했고, 생각보다 짧은 시간이었습니다. 박사 졸업을 한달 정도 앞둔 지금, 여전히 7년전처럼 기대되고 조금은 두렵기도 하고 설레입니다.

항상 지켜봐 주시고, 용기를 북돋아 주시는 노정혜 선생님, 선생님의 삶을 보면서 과학자로서 또 한 사람으로서 어떻게 살아야 할지 또 살고 싶은지 알게 해 주셔서 너무 감사합니다. 바쁘신 와중에도 부족한 논문을 심사해 주시고, 항상 따뜻하게 안부 물어 주시는 석영재 선생님, 많은 조언을 해 주신 김빛내리 선생님, 이강석 선생님, 차선신 선생님께 감사의 말씀을 드립니다. 앞으로 더 멋진 과학자가 되도록 노력하겠습니다.

그리고 여러 실험실 선배님들, 6개월의 짧은 시간이었지만 저에게 언제나 좋은 사수인 보은언니, 맛있는 음식으로, 따뜻한 이야기로 함께 해주었던 소영언니, 언제나 냉철한 조언을 해 주셨던 민식오빠, 신중함과 침착함을 배울 수 있었던 주홍오빠, 여전히 도움을 많이 받고 있는 용준오빠, 실험실의 영원한 얼굴 시영오빠, 제게 실험이 무엇인지 가르쳐준 사랑하는 정호오빠, 신앙적으로 늘 응원해 주신 경동오빠, 시크한 유복오빠, 늘 잘 챙겨주시는 경창오빠, 여러 고민들을 함께 고민해준 은경언니, 곁에만 있어도 힘이 되는 효섭오빠, 언제나 도움만 받아서 미안한, 그리고 고마운 강록오빠, 그리고 늘 함께 웃어주고 울어주고 함께 해준 사랑하는 지윤언니, 언니, 오빠들이 있기에 든든했습니다. 감사합니다.

나보다 더 한국 사람 같은 아툴, 삶 속에서 배우고 싶은 게 많은 효진언니,

쇼핑메이트이자 스트렙토 팀을 이끌 든든한 지선이, 실험에 대한 집중력을 배우고 싶은 수진이, 앞으로가 더 멋질 동갑내기 승환이, 후배지만 든든하고 더정이 가는 지은이, 스타일을 이해해주는 파리지앵 은정이, 세심하게 챙겨주는 연범이, 뉴욕리의 프리함을 보여주는 영대, 후배로 받게 되어 오히려 고맙고 감사한 주형이, 그리고 앞으로 즐겁고 열정적으로 실험실 생활을 해나가길 바라는 준선, 경석, 수연이. 후배들에게 해 준 것보다 받은 게 더 많은 것 같습니다. 감사합니다.

초등학교 때부터 지금까지 함께 한 미경, 보현이, 자주보진 못해도 늘 마음에 있는 미리, 서울에서 만난 소중한 친구 상희, 생각만 해도 든든한 우리 독수리 오자매, 언제나 나의 길을 지지해 주고 잘 챙기지도 못하는 제 곁에 있어 주셔서 너무 고맙습니다.

사랑하는 나의 가족. 언제나 큰 사랑과 기도로 지켜봐 주시는, 너무너무 사랑하는 엄마, 아빠. 앞으로 오래도록 효도할 수 있게 제 곁에 있어 주세요. 엄마, 아빠가 있었기에 여기까지 행복하게 올 수 있었습니다. 늘 격려와 응원을 전해주셨던 친척 분들. 받은 사랑보다 더 베풀며 살겠습니다.

그리고 마지막으로 이곳까지 굽이굽이 인도해주시고 사랑해 주신, 앞으로도 영원한 나의 힘이 되신 주님, 사랑합니다.